Spin-Crossover Systems based on 1,3,4-Thiadiazoles

Dissertation

zur Erlangung des Grades

"Doktor der Naturwissenschaften"

im Promotionsfach Chemie

am Fachbereich Chemie, Pharmazie und Geowissenschaften

der Johannes Gutenberg-Universität

in Mainz

Christian Herold

geboren in Koblenz

Mainz, 2016

Die vorliegende Arbeit wurde in der Zeit vom Februar 2013 bis Februar 2016 im Institut für Anorganische Chemie und Analytische Chemie der Johannes Gutenberg-Universität Mainz unter Anleitung von ■■■■■■■ angefertigt.

Ich versichere, dass ich diese Arbeit selbstständig verfasst und keine anderen als die angegebenen Quellen und Hilfsmittel benutzt habe.

Mainz, den 11.02.2016

Dekan:

Erster Berichterstatter:

Zweiter Berichterstatter:

D77

Kurzzusammenfassung

Spin-Crossover Systeme sind Komplexverbindungen, die durch äußere Einflüsse zwischen zwei oder mehr elektronischen Zuständen wechseln können. Ein Spin-Crossover beschreibt einen Wechsel zwischen dem *high-spin* und *low-spin* Zustand. Hierfür können externe Stimuli wie Temperatur, Druck und Licht gezielt genutzt werden, wodurch diese Materialien für verschiedene Anwendungsbereiche relevant sind. Die Nutzung von molekularen Schaltern auf der Basis von Spin-Crossover Verbindungen ist für Speichermedien und Displays denkbar, allerdings ist eine Verwendung als Temperatur-, Druck- oder Chemosensoren von besonderem Interesse.

In der vorliegenden Arbeit wird dieses Phänomen diskutiert und die Synthese und Charakterisierung von neuen zweikernigen Eisen(II)-Spin-Crossover Komplexen beschrieben. In den letzten Jahren stieg das Interesse an mehrkernigen Spin-Crossover Verbindungen. Der Grund ist der Einfluss von intramolekulen Wechselwirkungen auf den Spin-Crossover und die damit einhergehende Optimierung dieser Eigenschaften. Zweikernige Spin-Crossover Verbindungen werden intensiv untersucht, da diese Wechselwirkungen und Einflüsse bei der geringeren Komplexität leichter zu verstehen sind. Darüber hinaus können die Metallzentren in dinuklearen Spin-Crossover Verbindungen prinzipiell getrennt voneinander 'schalten', wodurch die drei unterschiedlichen Zustände ([LS-LS], [HS-LS] und [HS-HS]) gezielt angesteuert werden können.

Die in der vorliegenden Arbeit vorgestellten Komplexe wurden mit Brückenliganden auf Basis des 1,3,4-Thiadiazol-Heterozyklus synthetisiert und stellen die ersten zweikernigen Eisen(II)-Komplexe mit solchen 1,3,4-Thiadiazol-Brückenliganden dar. Es wurde zunächst ein bekanntes und intensiv erforschtes System durch das Einbringen des Thiadiazols in den Liganden verändert und der Einfluss auf die magnetischen Eigenschaften untersucht. Ausgehend von diesen ersten Ergebnissen wurde das Ligandensystem vielfältig variiert und die Eigenschaften der Verbindungen dadurch signifikant verändert. Darüber hinaus wurde der Einfluss von koordinierenden und nicht-koordinierenden Gegenionen erforscht und starke Festkörper- und Lösungsmittel-Effekte auf die magnetischen Eigenschaften beobachtet.

Dies führte zu mehreren neuen Spin-Crossover Verbindungen mit 1,3,4-Thiadiazol-Brückenliganden.

Abstract

Spin-crossover compounds are transition metal complexes that are able to switch between different electronic states as a reaction on an external perturbation. Spin-crossover complexes respond with a change of the spin state from the *high-spin* to the *low-spin* state. This conversion can be triggered by external stimuli, such as temperature, pressure or light, leading to a relevance of these compounds for future applications. A usage of these molecular switches for data storage or display devices would be possible, but the application of these compounds for temperature, pressure or chemosensors is of special interest.

A detailed discussion of the phenomenon and characterization of new dinuclear iron(II) spin-crossover complexes can be found in this work. The interest in polynuclear compounds increased in the last years. The importance of intramolecular interactions between the spin-crossover centers can result in an improvement of the magnetic properties and is the main reason for this interest. Dinuclear spin-crossover complexes are intensively studied, because they are a perfect model system to investigate the interactions and understand their influence on the magnetic properties. Furthermore, the metal centers in dinuclear spin-crossover compounds can switch separately, enabling the access to a third distinguishable magnetic state.

The complexes presented in this work have been synthesized with bridging ligands based on the 1,3,4-thiadiazole heterocycle and represent the first reported dinuclear iron(II) spin-crossover complexes with 1,3,4-thiadiazole bridging ligands. At first, a well known and studied system was varied by the incorporation of a 1,3,4-thiadiazole into the ligand to investigate the influence of this variation on the magnetic properties. Further studies were based on this system and included different modifications of the ligand system. This resulted in significant changes of the magnetic behavior. Furthermore, the influence of coordinating and non-coordinating anions, solid state interactions and solvent effects on the magnetic properties have been investigated in this work.

As a result, various new spin-crossover complexes have been synthesized with 1,3,4-thiadiazole bridging ligands.

Acknowledgement

Contents

1. Introduction

1.1. Molecular Switches

Molecular switches are molecules that can switch between different states as a responce to an external stimuli.[1] These molecules can respond to a variety of pertubations like light, temperature, electric field, pressure, tunneling electrons, pH or exposure to certain chemicals. If a molecule can switch between two or more stable states these materials are of great interest for future applications.[2] Molecular switches are discussed as key building blocks in data storage devices,[3] optoelectronic devices,[4,5] molecular sensors,[6] or even for controlled release of molecules in medical applications.[7,8]

In the early 1990's the Mn_{12}-acetate ($[Mn_{12}O_{12}(MeCOO)_{16}(H_2O)_4]$) was discovered and kicked off a great interest in single-molecule magnets (SMMs). This dodecametallic transition metal compound retained a magnetization in the absence of an external magnetic field for a long period of time, thus being a potential candidate for data storage on a molecular level. In the following years, a lot of SMMs were designed, but the main problem for a possible application of this class of molecular switches - the low working temperature of liquid helium - still persists.[9-13]

A different, very promising attempt is the use of photochromic compounds that can be triggered with light to switch between two different states. This switching process is mainly accompanied by a photoisomerization, photocleavage or photodimerization. Molecules that respond to an excitation with light of a specific wavelength with a photoisomerization are very common examples for molecular switches. One important advantage is their controllability and fast response time after an excitation[7,14,15] Nature's *cis/trans*-isomerization of retinal in the vision process can be seen as a role model for this field.[16-18]

The best-known light-responsive switch on a molecular transition metal complex basis is probably a Nickel(II)-tetrakis(pentafluorophenyl)porphyrin which has been functionalized with an azopyridine (figure 1.1), better known as the 'record player molecule',

designed by Herges *et al.*[19] An excitation with light induces a *cis/trans* switching of the azopyridine arm and a coordination of the pyridine to the nickel(II) when the molecule remains in the *cis* form (figure 1.1, right). The molecular geometry and coordination number of the nickel(II)-ion changes during the switching process and effects the spin state of the system. This cylce is called 'light-driven coordination-induced spin-state switching' (LD-CISSS). Here, the nickel(II) ion in the *trans*-form is in the low-spin (LS) state (diamagnetic, $S = 0$) and in the *cis*-form it is in the high-spin (HS) state (paramagnetic, $S = 1$). The switching process can be performed in solution at room temperature and under aerobic conditions. The excited *cis*-form has a long lifetime and there is no sign of decomposition even after more than 100.000 cycles, which shows that this is a very promising research topic for future applications.[20–23]
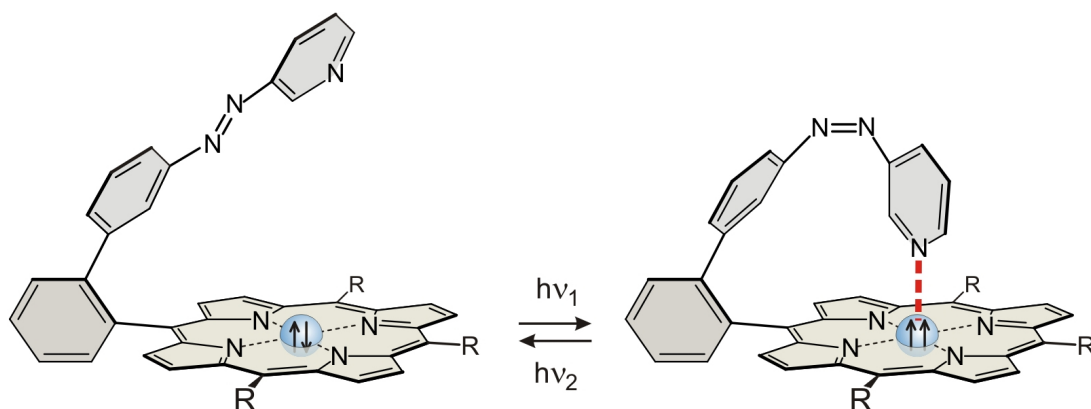
Figure 1.1.: Nickel(II)-tetrakis(pentafluorophenyl)porphyrin functionalized with an azopyridine in the *trans* (left) and *cis* (right) form (record player molecule).[19]

Another attractive research area, aiming towards the realization of molecular switches, can be seen in the research in coordination complexes with spin-crossover (SCO) properties.[24]

The work presented here will focus exclusively on the topic of the spin-crossover phenomenon and the possibility to use this compound class as switchable molecular systems.

1.2. Spin-Crossover

One very interesting and important magnetic property is the spin-crossover in octahedral complexes of $3d^4$-$3d^7$ transition metal ions. Molecular switches based on SCO compounds can be switched in several ways by external stimuli like temperature, light or pressure. Thus such compounds could be used in a number of possible applications like temperature or pressure sensors, data storage and display devices.[6,25,26]

Iron(III) dithiocarbamate complexes have been the first discovered compounds for which SCO behavior was observed. These compounds were reported in 1931 by Cambi *et al.* Although the first explanation was a shift of electrons from the ligand into the 3d orbitals of the iron(III) ion and not a spin transition from the iron(III)-HS to iron(III)-LS state, this discovery attracted many researches to investigate this magnetic behavior.[27–29]

In the early 1960's several groups started to pursue these investigations, reported the first iron(II) and cobalt(II) SCO complexes and described a change of the spin state as the reason for the change of the magnetic moment. These results initiated the interest in spin-crossover compounds ongoing for more than 50 years now.[30–34]

1.2.1. Occurence of the Spin-Crossover Phenomenon

A spin-crossover is theoretically possible for all transition metal ions with a d^4-d^7 configuration in an octahedral coordination environment. The ions can be stabilized in a low-spin or high-spin form (see figure 1.2, illustrated for the case of an $3d^6$ iron(II) ion). The size of the ligand field splitting (Δ) and spin pairing energy (P) determine if the ground state is the LS or HS state. In weak fields, with P being large compared to Δ, the electrons are distributed over the e_g and t_{2g} orbitals following the Hund's rule. This results in the maximal spin multiplicity and a HS ground state (figure 1.2, left). If the ligand field splitting is larger than the spin pairing energy, the complex exists in the LS ground state (figure 1.2, right).[35,36]
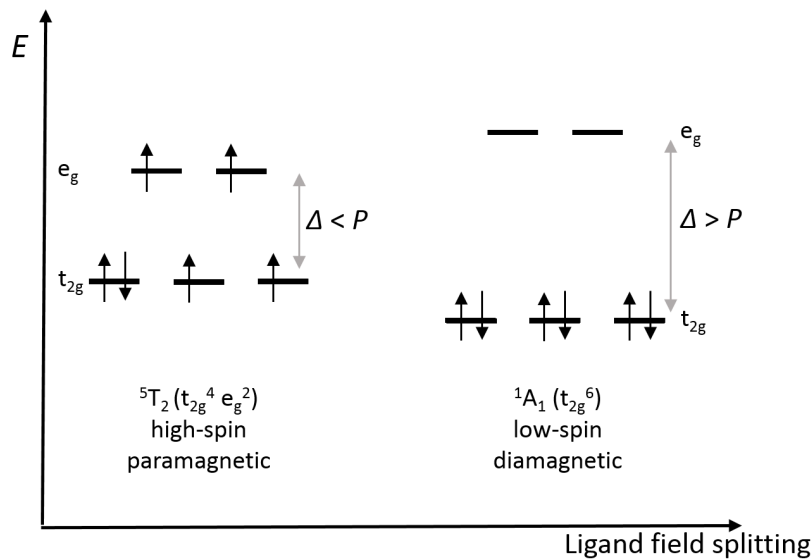
Figure 1.2.: Representation of the two possible electronic configurations for a $3d^6$ iron(II) ion in an octahedral coordination environment. Adapted from[36].

The dependency of the ground state from the ligand field splitting can also be found in the Tanabe-Sugano diagramm (figure 1.3), which shows how the electronic states of a free ion split under the influence of an octahedral ligand field. The ligand field splitting is given on the x axis with a value of 10 Dq and at a value of zero Dq the ground state of a free d^6-ion is the ^5D state. When Δ becomes larger than zero this ^5D state splits into the ^5E and $^5T_2$ state, with the latter being the ground state now. An increasing ligand field results in the stabilization of the LS $^1A_1$ ground state, which has its origin in the ^1I ground state of the free ion. This means the LS state is sta-

Figure 1.3.: Tanabe-sugano diagram for a d^6 transition metal ion in an octahedral complex.[37]

bilized beyond a critical ligand field splitting Δ_{crit} where the spin pairing energy P is equal to the ligand field splitting Δ. The ligand field splitting strongly depends on the metal-ligand distance r (equation (1.1), with the dipole moment of the ligand μ) and an

increasing distance *r* results in a decreasing $\triangle$, favoring a stabilization of the HS state. It is possible to estimate potentials for the HS and LS state depending of the distance r.[35,36,38]

$$10\ Dq\ \approx\ \mu\ /r^6 \tag{1.1}$$

This results in two potential wells for the HS and LS state of a spin-crossover complex along the nuclear coordinate *r(Fe-L)* (figure 1.4), where the minima of the potential wells are displaced vertically and horizontally to each other. The shift of the HS potential well to a higher metal-ligand distance is the result of the population of anti-bonding eg orbitals in the high-spin state. This leads to a stronger repulsion between the metal center and the donor atoms. With increasing temperature, a population of excited vibrational levels of the LS state takes place up to the crossing point of the LS and HS potenti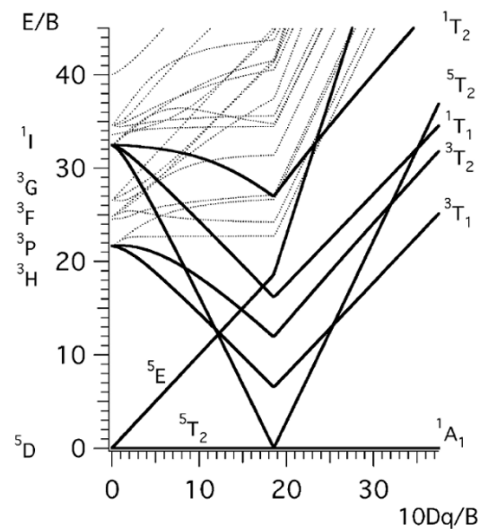al wells. If this crossing point is reached a LS to HS transformation takes place. The scheme of the potential wells of a spin-crossover complex in figure 1.4 displays the zero-point energy difference of the LS and HS state ΔE^0_{HL}, which is the most important factor for the realization of a thermal SCO. For complexes with suitable ligands, the ΔE^0_{HL} is in the order of magnitude of the thermal energy $k_B T$ and a thermally induced SCO can be achieved. In this case the complex is in the LS state at low temperatures and in the HS state at elevated temperatures.

During the spin transition, the difference in Gibbs free energy ΔG is equal to zero at the transition temperature $T_{1/2}$ and depends on the enthalpy difference ΔH and the entropy difference ΔS. The order of ΔH is usually 10-20 kJ mol^{-1} and of ΔS between 50 and 80 kJ mol^{-1} during the spin transition. It can be seen in equation (1.2), that the temperature dependent SCO is an entropy-driven phenomenon. At high temperatures, above $T_{1/2}$, where the complex switches into the HS state, the product $T\Delta S$ dominates.

$$\Delta G = \Delta H - T\Delta S \tag{1.2}$$

There are two contributions to the entropy change during the spin transition. There is the minor contribution of the electronic change (switching from the LS (S = 0) to the HS (S = 2) state) and the major contribution arising from the increasing intramolecular stretching modes and intramolecular deformation modes. This increasing intramolecular entropy is a result of the elongated metal-ligand distance.[24,35,38–40]
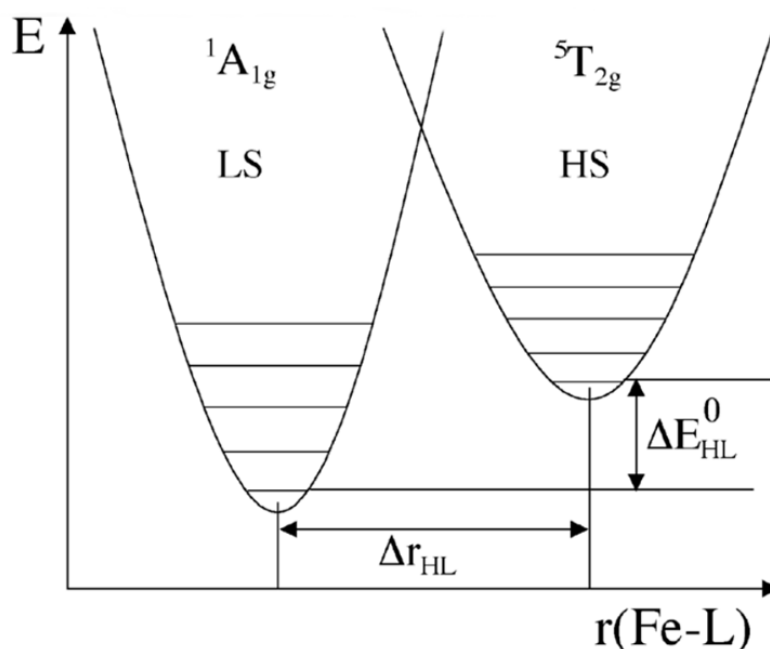
Figure 1.4.: Representative scheme of the potential wells for the low-spin and high-spin state of an iron(II) spin-crossover complex.[37]

As mentioned earlier, another external stimuli that can result in a spin transition is the use of pressure. The reason for the sensitivity of SCO complexes to pressure lies in the different metal-ligand distances and the related volume difference between the two states. This means, that an applied higher external pressure stabilizes the low-spin state, and thus increases the transition temperature $T_{1/2}$ of a spin-crossover complex, which has been investigated in various pressure effect studies on SCO compounds.[37,41,42]

As indicated previously, a thermally induced spin-crossover is theoretically possible for all d^4-d^7 transition metal ions in an octahedral coordination environment. But because of the higher ligand field splitting Δ of 4d and 5d transition metals and equal spin pairing energy P, octahedral 4d and 5d complexes have a strong tendency to stabilize the low-spin form. Thus, most SCO complexes have been synthesized with iron(II), cobalt(II) and iron(III) and a few with chromium(II) and manganese(III).[37,40,43,44]

1.2.2. Light-Induced Excited Spin-State Trapping

Another possibility to achieve a spin transition is using the irradiation with light. This phenomenon is called 'Light-Induced Excited Spin-State Trapping' (LIESST).[45,46] The LIESST phenomenon describes the possibility to switch a complex at temperatures below 100 K from the LS state into a metastable HS state by irradiation with light and was first reported in the early 1980's for iron(II) and iron(III) spin-crossover complexes.[47,48]
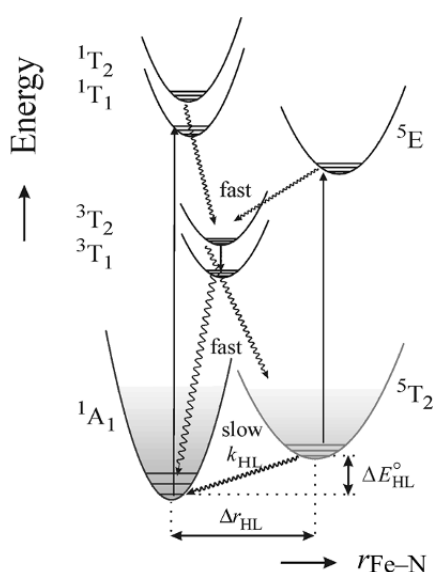
Figure 1.5.: Illustration of the LIESST and reverse LIESST phenomenon of a d^6 spin-crossover complex.[36]

The scheme in figure 1.5 shows the potential wells of the LS ground state ($^1A_1$), the HS state ($^5T_2$) with the respective higher excited states and illustrates the mechanism of the LIESST effect. Irradiation of a sample in the LS ground state at low temperatures with light of appropiate energy leads to the spin-allowed population of the $^1T_1$ state. The next steps are an intersystem crossing decay into the triplet states $^3T_2$ or $^3T_1$ and a second intersystem crossing decay into the metastable $^5T_2$ state. The radiative relaxation into the LS ground state is forbidden and a thermal tunneling into the $^1A_1$ state is very slow at low temperatures. As a consequence, the metastable $^5T_2$ state can have a long lifetime at low temperatures. Interestingly a second irradiation of a complex in the metastable

$^5T_2$ state with light of a different wavelength can lead to the relaxation back into the $^1A_1$ ground state, which is called reverse LIESST. These light-induced switching processes LIESST and reverse LIESST intensified the interest to use these SCO compounds for technical applications.[39,45,49]

1.2.3. Characterization of SCO Complexes

There are many methods to detect a spin transition, for example magnetic susceptibility, Mössbauer spectroscopy, X-ray diffraction, optical and Raman/FT-IR spectroscopy and heat capacity measurements. These techniques can be used to study the temperature dependence of the spin state and provide the characteristic spin transition (ST) curve displaying the HS fraction versus the temperature. The spin transition curves (see figure 1.6) provide a lot of information including the transition temperature ($T_{1/2}$) and first indications about cooperative interactions, which will be discussed in detail in section 1.2.5.[37,38]

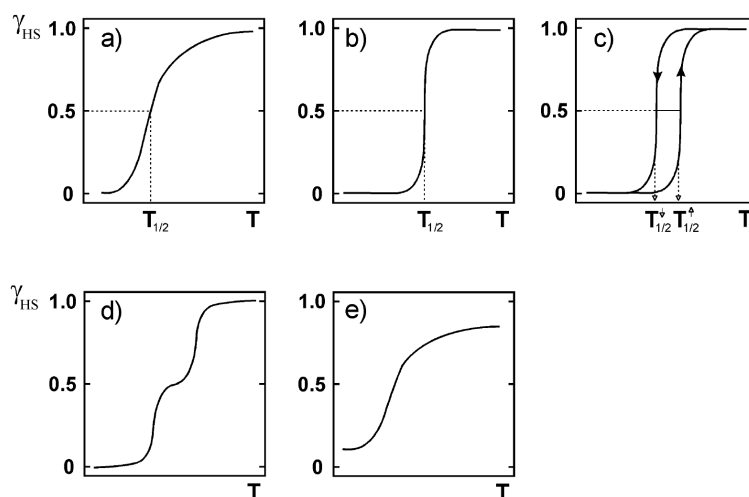Figure 1.6.: Schematic representation of the possible occurence of a SCO. Displaying the high-spin fraction (γ_{HS}) vs. the temperature (T) for a gradual ST (a), abrupt ST (b), ST with hysteresis (c), two-step ST (d) and incomplete ST (e).[37]

The spin transition behavior can be very different, as shown in figure 1.6. The hysteretic behavior (c) is the most desirable form as it reflects a possible bistability for

the application as molecular switches. For a hysteretic or abrupt (b) ST a high co-operativity in the solid state is essential. The strong interactions between the complexes result in a communication in the solid state and a simultaneous spin transition. On the contrary, the cooperativity is usually weak in the case of SCO complexes displaying a gradual ST (a). The two-step ST (e) plays a very important role in dinuclear SCO complexes, where the two SCO-active transition metal centers can switch independently. This results in three possible spin states ([LS-LS], [HS-LS] and [HS-HS]) and will be explained in detail in section 1.2.7.

The most common technique for the detection of a spin-crossover is the measurement of the magnetic susceptibility as a function of the temperature $\chi(T)$. Solid samples of SCO compounds can be investigated using SQUID (*Superconducting QUantum Interference Device*) magnetometers, that have a high sensitivity towards a change in the magnetic susceptibility. The change in the magnetic susceptibility is very pronounced in spin-crossover compounds, especially in the case for iron(II) ions where the paramagnetic high-spin state consists of four unpaired electrons (S = 2) and the diamagnetic low-spin state has no unpaired electrons (S = 0).

An additional advantage of SQUID magnetometers is the possibility to measure the magnetic moment with external perturbations, such as hydrostatic pressure for pressure effect studies or light irradiation to observe the LIESST effect.[37,43,50–52]

As previously stated, the bond lengths change during a spin transition, which makes it possible to monitor the SCO by temperature dependent X-ray diffraction studies. The largest change of the metal - donor atom distance can be measured for iron(II) SCO complexes, because of a large difference of the total spin (ΔS = 2) that goes along with a change in the occupancy of the antibonding e_g in the high-spin state. This results in a change of the distances of approximately 10 % with extended bond lengths in the high-spin state, which can be detected in single-crystal X-ray diffraction measurements. Furthermore, this technique is very important for the investigation of intermolecular interactions in the solid state, such as π-π stacking, classical and non-classical hydrogen bonding or halogen bonding interactions. These short- and long-range interactions have a big influence on the spin transition behavior of SCO complexes and play a crucial role in the understanding of the spin-crossover phenomenon.[53–57]

Another very important technique for the investigation of iron SCO compounds is the

Mössbauer spectroscopy, which has been used by König *et al.* in 1966 to deliver the final proof for a temperature dependent spin state equilibrium in the mononuclear iron(II) complex [Fe(phen)$_2$(NCS)$_2$].[58] After this discovery the Mössbauer spectroscopy became a crucial tool for the characterization of iron SCO compounds. The two important values, that can be obtained from a Mössbauer spectrum, are the isomer shift δ and the quadrupole splitting ΔE_Q, which differ significantly for the HS and LS state in iron(II) and iron(III) complexes. The isomer shift provides information about the oxidation and spin state and the quadrupole splitting about the molecular symmetry, especially the electronic environment of the Mössbauer active element.

Figure 1.7 shows an example for the changes in the Mössbauer spectrum going from a HS doublet at high temperatures (300 K) to a LS doublet at low temperatures (77 K) for the mononuclear spin-crossover complex [Fe(phen)$_2$(NCS)$_2$]. It clearly displays the spin-crossover of the complex around 185 K. Mössbauer spectra at different temperatures can be used to determine the HS and LS fractions by fitting the area fractions of the resonance lines with a Lorentzian fit. Similar to magnetic measurements, it is also possible to include external perturbations like pressure and light irradiation into Mössbauer measurements, enforcing further the value of this technique.[26,37,59,60]

Figure 1.7.: Mössbauer spectra of [Fe(phen)$_2$(NCS)$_2$] at different temperatures.[59]

Differential scanning calorimetry (DSC) is a method to investigate changes in the heat capacity of a sample and can be used to calculate enthalpy and entropy changes during phase transitions. Having in mind, that a spin transition is connected to an enthalpy and entropy change (see section 1.2.1), a DSC measurement can be used to determine the transition temperature. This method was used by Sorai *et al.* in 1972 for the first time to investigate the [Fe(phen)$_2$(NCX)$_2$] (X = S and Se) SCO complexes. It provides infor-

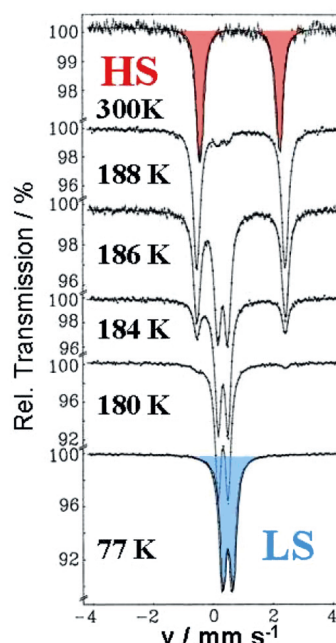mation about the enthalpy and entropy changes and became a reliable technique for the characterization of SCO compounds. An integration of the excess heat capacity during the cooling or heating process leads to the value of ΔH and since $\Delta G = 0$ at the transition temperature, ΔS can be calculated at $T_{1/2}$.[61–65]

A method to investigate the spin transition, based on the very often accompanied color change of SCO compounds (thermochromism), is the electronic (UV/Vis) spectroscopy. If the color of an iron(II) SCO compound has its main origin in the d-d transitions, the compound will be nearly colorless in the HS state due to spin-forbidden transitions and intensely colored in the LS state. This color change can be monitored via variable-temperature UV/Vis spectroscopy, with the detection of a d-d transition in the near infrared at high temperatures, corresponding to the spin allowed $^5T_2$ - ^5E transition. This transition disappears upon cooling, and two d-d transitions in the visible region can be measured, corresponding to the two spin allowed $^1A_1$ - $^1T_1$ and $^1A_1$ - $^1T_2$ transitions of the iron(II) low-spin species.[37,49,66]

It is also possible to track a spin transition with vibrational spectroscopy, such as Raman- and FT/IR-spectroscopy. The change of the metal-donor atom bond lengths can be observed in the different metal-donor atom stretching frequency, which is usually found in the range from 500 cm^{-1} to 250 cm^{-1} for a nitrogen donor atom coordinated to an iron(II) center. Another way to monitor the spin transition is by observing vibrational modes in coordinating ligands, that show a high sensitivity towards the spin state of the metal ion. The best example is the C-N stretching mode of the N-coordinating thiocyanate anion (NCS$^-$). This can be used as a marker in the temperature dependent Raman spectroscopy to monitor the spin transition of the complex. The Raman
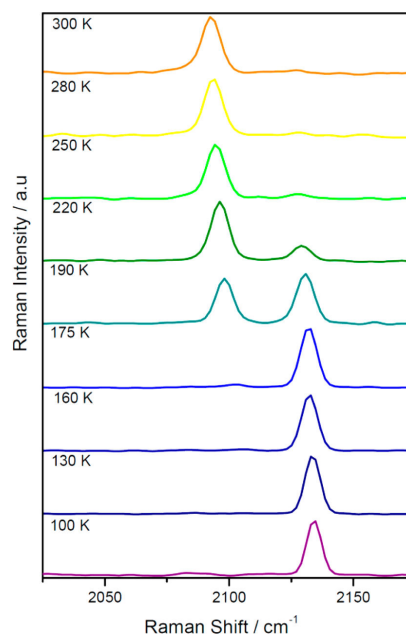

Figure 1.8.: Raman spectra of [Fe(padpt)$_2$(SCN)$_2$] between 300 and 100 K.[65]

shift of this C-N stretch changes significantly during the spin transition, which can be seen in figure 1.8 for a mononuclear iron(II) SCO complex with two *trans*-coordinated thiocyanate anions and a transition temperature of 182 K.[37,65,67]

1.2.4. Spin-Crossover in Iron(II) Complexes

Although the first discovered SCO compound by Cambi *et al.* was an iron(III) complex, the research shifted quickly towards the investigation of iron(II) complexes. There are several reasons for the large interest in iron(II) SCO compounds compared to iron(III) and cobalt(II) SCO compounds, which will be discussed briefly in this section.

All essential techniques for the characterization are based on magnetic, optical, vibrational and structural changes and show a better resolution and provide more information for iron(II) SCO compounds than for iron(III) or cobalt(II) SCO complexes. This was especially important in the early years of the research field. Iron(II) SCO compounds are the only ones switching between a completely diamagnetic low-spin state ($S = 0$) and a paramagnetic high-spin state ($S = 2$) and show the strongest color change during the spin transition. Iron(II) SCO complexes show the largest change in the metal-ligand distance between the high-spin and low-spin state, leading to additional possibilities to characterize and investigate the spin transition. Furthermore, the LIESST effect (section 1.2.2) is interesting in the perspective of photo-switchable molecular magnetic materials and is mainly observed for iron(II) complexes and only for a small number of iron(III) complexes.[43,45,50,68,69]

These advantages of iron(II) SCO complexes and the possibility to synthesize complexes showing a very pronounced thermochromism in combination with a magnetic bistability around room temperature result in the still continuing interest to incorporate these materials in future applications. This task has already been accomplished for model systems as display devices or thermosensors in gels (see figure 1.9) and shows the large potential of these materials. But even after several decades of research, the properties of SCO compounds cannot easily be predicted due to the large influence of solid state interactions. This represents the main challenge of this research area and will be discussed later on.[43,68]
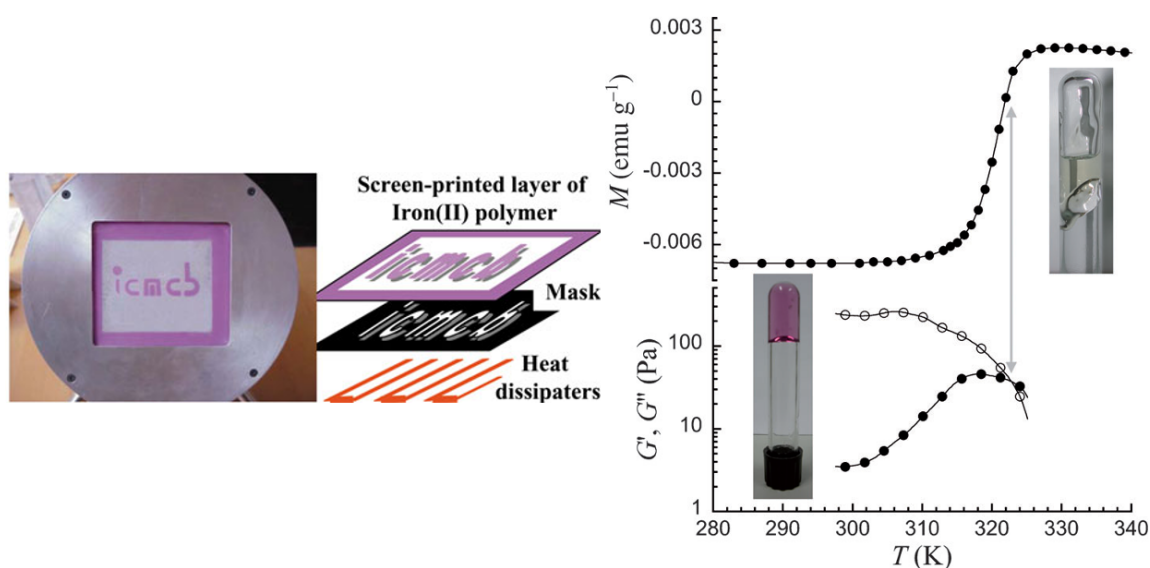
Figure 1.9.: Two examples for the possible applications of SCO compounds. The left picture shows an iron(II) SCO complex used as a display device[70] and the right picture an iron(II) SCO complex integrated into a gel.[71]

1.2.4.1. Ligand Design

The most common coordination environment for iron(II) SCO systems is the FeN_6 type, which covers approximately 90 % of the iron(II) SCO compounds.[72] The second most popular coordination environment for iron(II) is the N_4O_2[73–76] donor set, typically with salen-type ligands. Finally, there are even examples for SCO complexes with a N_4C_2 environment for the iron(II) ion.[77] In my thesis I will focus on the FeN_6 type further on since this is the only one used in this work.

However, the SCO properties of these iron(II) complexes do not solely depend on the type of donor atom sets. Another very important factor is the steric hindrance in the complex.

As indicated previously, the ligand field splitting correlates to the Fe-donor atom distance (equation (1.1)). A larger distance results in a lower ligand field splitting and the stabilization of the HS state. Iron(II) systems with nitrogen donor atoms show the largest bond length change during the spin transition, with an average value of 2.2 Å for the HS state and 2.0 Å for the LS state. This large difference is a result of the occupa-

tion of the antibonding e_g orbitals, which leads to a stronger repulsion. The knowledge about the influence of the bond length on the properties can be used for the synthesis of SCO compounds. Incorporation of substituents in the meta-position of the donor atoms leads to a steric hindrance between the metal center and the ligand. This strategy can be used to change the spin state of a system from the LS to the HS state.[37,78,79]

In general, a spin transition is accompanied with a second structural change in the coordination environment of the SCO center. The distortion of the octahedral coordination sphere increases significantly during a SCO from the LS to the HS state and is displayed in the octahedral distortion parameter Σ. This parameter is a summation of the *cis*-N-Fe-N angle deviations from $90°$, resulting in higher Σ values for complexes in the HS state.[56,78]

The first reported iron(II) SCO compounds are still very interesting examples regarding the ligand design, because they combine two basic concepts to achieve SCO properties. The LS complex $[Fe(phen)_3]^{2+}$ (phen = 1,10-phenanthroline) can be varied in two ways to obtain a SCO complex. Ligand substitution of one phen ligand or a modification of the phen ligands to add steric hindrance in the cation can result in SCO properties.

The 1st strategy is a substitution of one bidentate phen ligand by two N-coordinating anions (for example SCN^- in $[Fe(phen)_2(SCN)_2]$) and results in a complex with SCO properties. These coordinating anions have a lower ligand field strength and thus directly influence the properties of the metal center. This was the first known iron(II) SCO complex. It has been studied in detail due to its versatile magnetic properties, including abrupt and hysteretic SCO behavior with LIESST effect and pressure dependency of the transition temperature. This complex has also been the starting point for several structural investigations and further SCO complexes, aiming towards an improvement of the properties.[30,37,58,80–82]

The 2nd strategy is via functionalization in the 2-position of the phenanthroline ligands. Substitution of one hydrogen atom per ligand by a methyl- or methoxy-group leads to a larger steric hindrance in the complex cation and SCO behavior. The enlargement of the bond length leads to a lower ligand field strength and a stabilization of the HS state at elevated temperatures, which was accomplished here with the steric effect of the additional group in the 2-position.[83–85]

A 3rd strategy to influence SCO properties is the fine tuning with coordinating anions, such as SCN^-, $SeCN^-$, H_3BCN^-, CN^-, OCN^- or $(CN)_2N^-$. As described before, a ligand substitution by an anion with a different ligand field strength has a direct influence on the ligand field splitting of the complex. An exchange of the anion with an anion having a different ligand field strength has an effect as well. There are many studies where the XCN^- anion series has been used and a clear shift of the transition temperature of the SCO complex has been found. The shift of $T_{1/2}$ of the complexes to higher transition temperatures is in agreement with an increasing ligand field strength of the anion ($SCN^- < SeCN^- < H_3BCN^-$).[62,82,84,86–91]

All these considerations regarding the 'ligand design' can only be seen as a guideline for the successful synthesis of SCO complexes. Cooperative interactions in the solid state have a big influence on the magnetic properties and can - in most cases - not be predicted or controlled.

1.2.5. Cooperativity in SCO Complexes

It has been confirmed by DSC measurements, that a spin transition can be seen as a first-order phase transition that propagates through a bulk or crystalline material. The propagation of the ST in the solid has to be mediated with intermolecular interaction. This explains the importance of cooperative interactions in these bulk or crystalline materials and why intermolecular interactions have such an influence on the type of spin transition. The shape of the ST curve depends largely on the strength of the cooperative interactions. Low cooperativity mainly results in an incomplete or gradual spin transition and thus, an enhancement of the cooperative interactions can lead to an abrupt or even hysteretic SCO.[43,51,92,93]
The best way to clarify the importance of cooperativity is by studying the magnetic behavior for cases where the intermolecular interactions are suppressed.

This can be achieved by metal dilution with other transition metals (zinc(II), nickel(II), manganese(II) or cobalt(II)).

There have been several studies where an iron(II) SCO complex has also been synthesized as mixed crystals with an unchanged crystal structure, but with different contents of other metal ions instead of iron(II). The study of the magnetic behavior (for example figure 1.10) showed, that the shape of the spin transition curve changes to a more gradual form with a decreasing amount of iron(II) in the mixed crystal due to the suppression of the interactions in the solid state.[38,94–97]
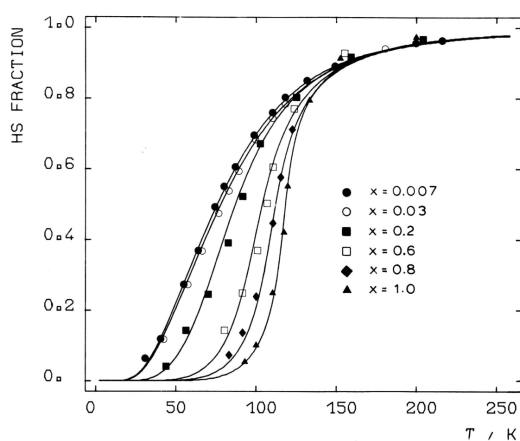

Figure 1.10.: γ_{HS} vs. T of [Fe$_x$Zn$_{1-x}$(2-pic)$_3$]Cl$_2$ · EtOH for different iron(II) fractions x.[43]

Another way is to study the magnetic behavior of SCO compounds in solution. The interactions are completely canceled out in solutions and the spin transition curve of complexes showing an abrupt ST in the solid state is possibly only gradual.[40,98]

There are different types of intermolecular interactions in the solid state, that are of interest in SCO complexes. The main interaction pathways are through classical and non-classical hydrogen bonding and π-π-stacking interactions. There are also a few examples for lone pair-π and halogen bonding interactions.[67,99–103]

The knowledge about the importance of these interactions led to modifications of the ligand systems to enhance the cooperative interactions. These modifications of the ligand systems include the incorporation of amine (N-H) and hydroxy (O-H) groups for the development of hydrogen bonding networks between the complex cations, the enlargement of the aromatic system for stronger π-π-interactions, or the replacement of hydrogen atoms by halogen atoms.[56,57,73,103–105]

1.2.5.1. Anion and Solvent Effect on the SCO

The intermolecular interactions in the solid state are often mediated through non-coordinating anions or solvent molecules and not directly between the complex cations. The incorporation of the anions in the crystal lattice often leads to short contacts with

the complex cation and the formation of intermolecular interaction pathways. Furthermore, a shift of electron density between the anion and the complex cation can influence the electronic structure of the complex cation as well. This can result in a shift of the transition temperature, a different type of spin transition or even a suppression of the SCO properties.
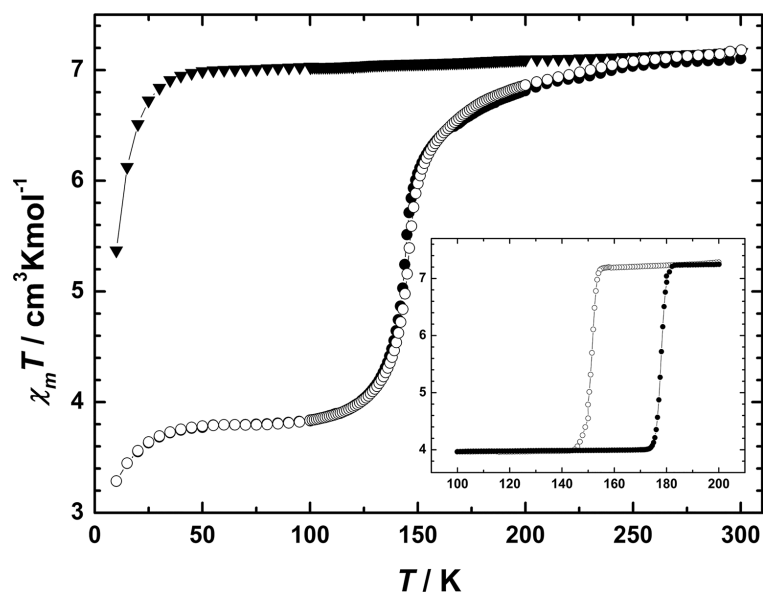

Figure 1.11.: χ_MT vs T for a dinuclear iron(II) complex with different anions (triangles: BF_4^-, circles: ClO_4^-, inset: $F_3CSO_3^-$).[106]

Figure 1.11 shows the magnetic properties of dinuclear SCO complexes with a 1,3,4-oxadiazole bridging ligand, which are clearly influenced by the anions. Depending on the anion, the dinuclear complex cations are differently connected in the solid state. This results in one SCO-inactive (BF_4^-) and two SCO-active (ClO_4^- and $F_3CSO_3^-$) complexes with a different $T_{1/2}$ and in one case hysteretic SCO behavior. The well-pronounced hysteresis of the triflate compound has been explained with the formation of a linear chain of the complex cations. These are connected through the anions and lead to a very high intermolecular interaction. In this case, the interactions between the complex cations are exclusively mediated through classical and non-classical hydrogen bonding interaction with the non-coordinating anions.[79,106–109]

An analog influence on the spin transition can be observed for non-coordinating sol-

vents. The solvent effects include a shift of the transition temperature[110–112], a change of the hysteresis width[113] and the spin state[114] of the complexes.

The differences are based on the incorporation of the molecules in the crystal lattice and thus mediation of intermolecular interactions. These solvent effects can sometimes be reversibly triggered by desolvation and resolvation of the appropiate solvent, leading to a possibility to use these compounds as chemosensors.[115–117]

Figure 1.12 shows the effect of the solvent in the solid state in the case of a dinuclear iron(II) complex by Murray *et al.*[111] The transition temperature and type of spin transition depends on the amount of solvent in the compound (a and b). A complete desolvation (d) suppresses the ST, but it is possible to regain the SCO properties by resolvation (c).
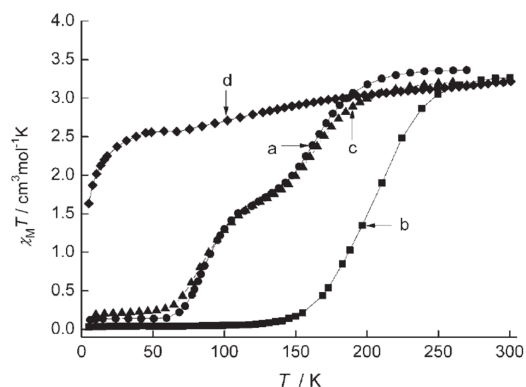

Figure 1.12.: χ_MT vs T for a dinuclear iron(II) complex and different solvent content (a: with four DCM, b: with one DCM, c: re-solvated and d: without solvent).[111]

1.2.6. Polynuclear SCO Complexes

Another strategy to improve the cooperativity is the addition of intramolecular interactions. This can be accomplished with polynuclear complexes where the SCO centers are connected via aromatic ligands or anionic linkers. This led to a rising interest in polynuclear SCO complexes in the 1980's. A large number of SCO complexes where the SCO-active centers are integrated in polymeric structures or even in metal-organic frameworks have been published since then.[101,102,118–120]

Coordination polymers of iron(II) with three 1,2,4-triazole bridges between the iron(II) centers are probably the most important class of polymeric SCO compounds. These 1D chains often show a very abrupt and hysteretic spin transition. A few examples have a wide hysteresis around room temperature and display thermochromism, which

makes them suitable for applications (see figure 1.9, section 1.2.4). The incorporation of these complexes into substrates, such as gels, has been successful as well, but they have never been used for commercial applications. The main difficulty of this class of compounds is the complete structural characterization of the complexes, which is not possible due to crystallization problems. In many cases, the structures cannot be obtained from single-crystal X-ray diffraction measurements, making it impossible to discuss the interactions in the solid state. Therefore, the investigation of discrete polynuclear systems has found an increasing interest. SCO complexes with defined nuclearity can combine the advantages of 1D chains and the possibility to be characterized with all fundamental methods.[68,71,121–123]

1.2.7. Dinuclear SCO Complexes

The simplest model for the investigation of magnetic and cooperative effects between two bridged SCO centers is a dinuclear complex, which raised this class to the most extensively studied type of discrete polynuclear compounds. The first reported complex was an iron(III) compound with aromatic bridging ligands by Ohta *et al.* in 1986, followed by the first iron(II) species by Real *et al.* in 1987 with a bipyrimidine bridging ligand. It showed a two-step spin transition, which is characteristic for dinuclear SCO complexes.[114,124–126]

A key feature of dinuclear SCO complexes is the possibility that the two metal centers switch separately, although there should be a high probability of the two centers to behave identical. Beside the direct spin transition from the [HS-HS] to the [LS-LS] state, the spin transition can occur in two steps ([HS-HS] → '[HS-LS]' → [LS-LS]), resulting in a transition curve with a '[HS-LS]' plateau region. It is also possible that the complexes remain in this mixed spin state without stabilizing the diamagnetic [LS-LS] state at low temperatures. Furthermore, the intermediate '[HS-LS]' state can display either isolated molecules with one center in the HS and the other in the LS state or it can be a 1:1 mixture of molecules in the [HS-HS] and [LS-LS] state. The type and origin of the intermediate spin state led to an increased interest in dinuclear SCO complexes and several studies focusing on the '[HS-LS]' state.[126–128]

The first dinuclear iron(II) SCO complexes exhibiting a two-step transition led to the

postulation of isolated [HS-LS] molecules in a few cases. It was suggested that a synergistic effect between the strength of inter- and intramolecular interactions would be the determining factor whether discrete [HS-LS] molecules or a mixture of [HS-HS] and [LS-LS] molecules are present during the measurements around the plateau region of the 'half-SCO'. Without having an absolute evidence, Real *et al.* stated in 1992 that their complex was an isolated [HS-LS] species, based on calorimetric and Mössbauer measurements. This was confirmed by Ksenofontov *et al.* with applied field Mössbauer measurements. The applied field during the Mössbauer experiment results in two distinguishable signals for the iron(II) centers in the HS state in either [HS-HS] or [HS-LS] molecules.[128–131]

It took nearly twenty years, after the discovery of the first dinuclear SCO complexes, until Brooker *et al.* reported the final proof for the existence of the mixed [HS-LS] state with the first X-ray crystal structure of a trapped [HS-LS] species (figure 1.13). Crystal structures in previous studies only showed average bond lengths in the complexes. But here two crystallographically independent iron(II) centers with different bond lengths, corresponding to the HS and LS state, were measured. Unfortunately, strain in the [HS-LS] species leads to this trapped species, making it impossible to achieve the [LS-LS] state at lower temperatures.[41,78,111]
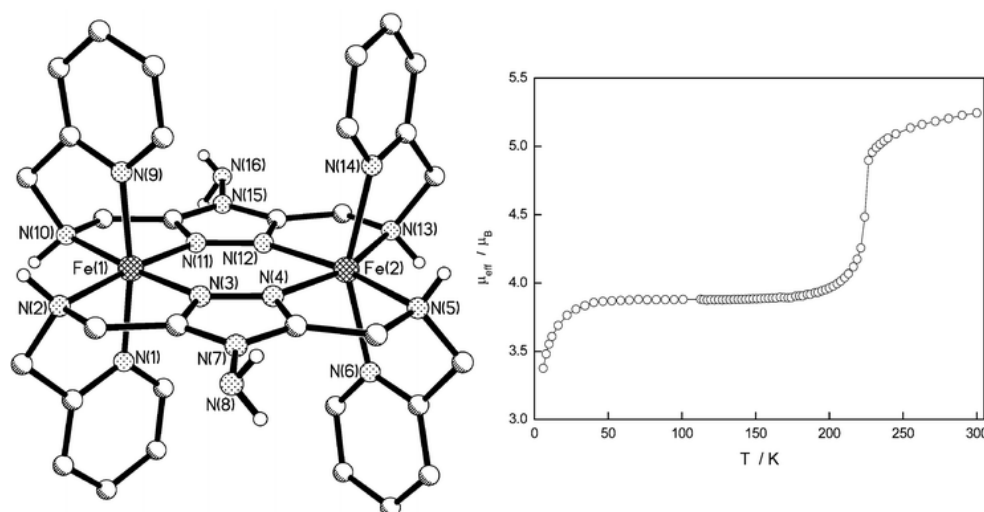

Figure 1.13.: Crystal structure of the trapped [HS-LS] species (left)[132] and the temperature dependent effective magnetic moment (right)[78] of $[Fe_2(PMAT)_2](BF_4)_4$*DMF.

Based on this system it was also possible to demonstrate that the mixed spin state can be detected with Mössbauer measurement without an applied field. In many cases, an increased linewidth of the HS doublet in the region of the spin transition is a clear sign for a coexistence and superposition of iron(II) HS doublets from the [HS-HS] and [HS-LS] molecules.[132]

It is worth mentioning that these results do not propose that all dinuclear SCO complexes feature the mixed spin state if they show a two-step spin transition. There has also been crystallographic evidence for complexes coexisting in their [HS-HS] and [LS-LS] form in the plateau region.[133]

Different studies and spectroscopic data resulted in the explanation, that strong intramolecular interactions lead to a favored [HS-LS] formation and strong intermolecular interactions lead to the formation of a [HS-HS]/[LS-LS] mixture. The spin transition of one SCO center influences the ligand field splitting of the second metal center, if the intramolecular interactions are large in a dinuclear complex. This results in a shift of the transition temperature, which leads to the two-step ST. Strong intermolecular interactions have the same effect between neighboring dinuclear complexes. These findings are in agreement with the initially stated synergism between the inter- and intramolecular interactions by Real *et al.* being responsible for the type of spin state.[129,133,134]

2. Aim of this Work

The description of the advantages and special properties of dinuclear spin-crossover complexes in section 1.2.7 shows the potential in this research area. Although the field rapidly developed in the last thirty years, there are still uncertainties concerning the interactions in the solid state (section 1.2.5). It is still not possible to predict the influence of changes in the ligand environment on the magnetic properties, due to major effects on the spin states resulting from inter- and intramolecular solid state interactions.

The aim of this work was the synthesis of new dinuclear iron(II) spin-crossover complexes and the investigation of interactions in the solid state in regard to the magnetic properties to develop a better understanding of these effects.

The most important part of dinuclear systems is an appropriate bridging ligand, which needs multiple donor atoms to chelate two transition metal ions. The goal is the synthesis of dinuclear iron(II) SCO complexes, being able to stabilize the three spin states [HS-HS], [HS-LS] and [LS-LS]. Therefore, the bridging ligand needs a central unit capable of mediating strong intramolecular interactions between the two iron(II) centers (see section 1.2.7). Also, the usage of nitrogen donor atoms has been proven to be ideal for iron(II) SCO systems. Therefore, an aromatic ring system as a bridging unit is a common option and we focused on the 1,3,4-thiadiazole heterocycle in this work.

The 1,3,4-thiadiazole heterocycle can be synthesized in different ways and it can be used as a central unit for symmetrical and unsymmetrical ligands. Previous work in our group with unsymmetrical 1,3,4-thiadiazole bridging ligands showed the good coordination behavior in transition metal complexes. Here we focus on symmetrically substituted ligand systems for iron(II) SCO complexes.[135–138]
The central 1,3,4-thiadiazole heterocyle contains an azo-bridge to coordinate two metal centers and the aromatic nitrogen donor atoms should have a suitable ligand field strength for the synthesis of iron(II) SCO systems. The first reported iron(II) SCO com-

plexes with 1,3,4-thiadiazole ligands are in agreement with this and show the potential for the synthesis of iron(II) SCO compounds.[139] However, the previously reported complexes are mononuclear and the 1,3,4-thiadiazole coordinates with only one nitrogen donor atom. Prior to this work, there have been no reports of dinuclear iron(II) SCO complexes with 1,3,4-thiadiazole bridging ligands.

The essential goal of this work was the synthesis of the first dinuclear iron(II) complexes with a 1,3,4-thiadiazole bridging ligand showing a spin transition. The compounds were inspired by a known system, which has been synthesized with a 1,2,4-triazole bridging ligand by Brooker *et al.* This system has been discussed earlier (section 1.2.7), the large strain in the complex prevented the ST into the [LS-LS] state. Having in mind that the bond lengths and angles change significantly during a spin transition, the key factor in these systems is the ligand flexibility. Thus, the incorporation of the 1,3,4-thiadiazole with a larger sulfur atom should reduce the strain and result in the [LS-LS] state at low temperatures. The aim was to investigate the effect of the new central motif on the SCO properties.

In further studies the influence of different solvents in the solid state on the spin-crossover properties and thus the importance of intermolecular interactions was investigated.

Based on first results, a series of new ligands was synthesized in order to influence the magnetic properties of the iron(II) complexes. These new ligands deal with the importance of steric and electronic effects on the spin state of the iron(II) centers and with the suppression of the short range interactions in the solid state.

3. A Family of Dinuclear Iron(II) SCO Compounds Based on a 1,3,4-Thiadiazole Bridging Ligand

3.1. Introduction

We were able to synthesize a new family of dinuclear SCO complexes containing a new 1,3,4-thiadiazole based bridging ligand **L1** (2,5-bis[(2-pyridylmethyl)amino]methyl-1,3,4-thiadiazole).

Previous studies by Brooker *et al.* discussed the analog 1,2,4-triazole based ligand PMAT, which provided the final proof that dinuclear SCO complexes can exist in a trapped [HS-LS] state via X-ray diffraction studies of this species (section 1.2.7).[78,132] The dinuclear SCO complexes showed a very interesting and versatile magnetic behavior with strong influences of the solvents, counterions or substituents on the triazoles[105,108,140]. These results led to further studies on the effect of pressure on the SCO[41] and the effect of the scan-rate dependence on the hysteretic SCO behavior[64]. It is a very important system for the understanding of spin transitions in dinuclear SCO complexes. However, for this system the diamagnetic [LS-LS] state cannot be achieved and the system can only switch between the paramagnetic [HS-HS] and trapped [HS-LS] state. The reported reason is the highly constrained nature of the trapped [HS-LS] state and the rigidity of the 1,2,4-triazole based PMAT ligand.[78] The group also reported the analog pyrazolate based ligand PMAP, which showed no spin transition and is in the [HS-LS] state in the range from 1.8 to 300 K. The pyrazolate heterocycle has a higher ligand field strength and the [HS-HS] state cannot be reached at room temperature. At the same time, the strain in the cation prevents the stabilization of the [LS-LS] state at low temperatures, leading to a loss of the SCO properties.[141]

The first reported SCO complexes with a 1,3,4-thiadiazole moiety, the potentially bis-(bidentate) bridging ligand 2,5-di-(2-pyridyl)-1,3,4-thiadiazole, by Klingele *et al.* indicated the potential of this heterocycle for the use in SCO compounds. The mononu-
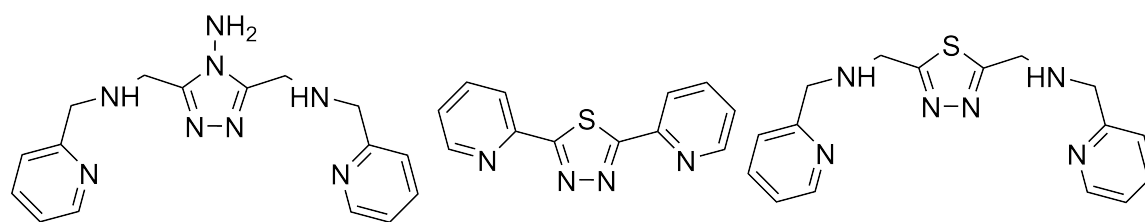
Figure 3.1.: The three discussed ligand systems. The 1,2,4-triazole based
PMAT ligand (*left*, 4-amino-3,5-bis{[(2-pyridylmethyl)amino]methyl}-4H-1,2,4-triazole)
of the Brooker's group, the 1,3,4-thiadiazole ligand (*middle*, 2,5-di-(2-pyridyl)-1,3,4-
thiadiazole) of Klingele *et al.* and the synthesized 1,3,4-thiadiazole bridging ligand **L1**
(*right*, 2,5-bis[(2-pyridylmethyl)amino]methyl-1,3,4-thiadiazole)

clear iron(II) complexes of the [Fe(L)$_2$X$_2$]-type (with X = SCN$^-$, SeCN$^-$ and H$_3$BCN$^-$)
showed a SCO with the transition temperature being influenced by the different coor-
dinating counterions.[87,139] The usage of this 1,3,4-thiadiazole bridging ligand for the
synthesis of dinuclear iron(II) complexes was not successful. This was only possible
with the analog pyrazolate and triazolate bridging ligands where the central heterocy-
cles are negatively charged in their deprotonated forms.[142,143]

The idea for the first ligand system **L1** was the incorporation of the 1,3,4-thiadiazole
moiety into the bis(tridentate) PMAT ligand of the Brooker's group and replacement of
the central 1,2,4-triazole. This sulfur atom should reduce the rigidity in the ligand sys-
tem and with that the high strain in the complex cation. The aim for this ligand system
was the realization and stabilization of the previously elusive [LS-LS] state in dinuclear
iron(II) complexes of analog ligands. The retained nitrogen donor atoms in the 1,3,4-
thiadiazole heterocycle suggest that the ligand field strength in iron(II) complexes with
the new ligand **L1** should be in a similar range, compared to the complexes with the
PMAT ligand.

In comparison to the reported 1,3,4-thiadiazole ligand of Klingele *et al.* this new ligand
should have an improved geometry for the synthesis of dinuclear complexes. The angle
between the aliphatic nitrogen donor atoms and the azole bridge in **L1** is closer to 180°,
resulting in a lower strain in a possible dinuclear complex.

'A Family of Dinuclear Iron(II) SCO Compounds Based on a 1,3,4-Thiadiazole Bridging Ligand'
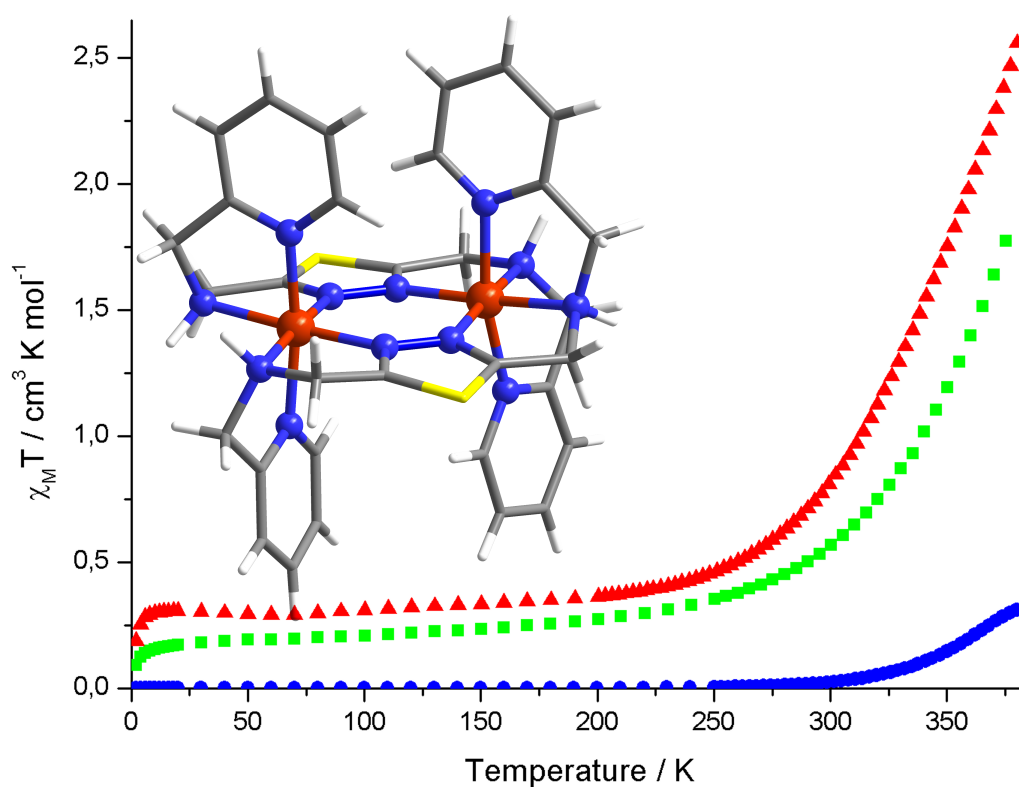
Christian F. Herold, Luca M. Carrella, and Eva Rentschler

3.2. Abstract

A new family of dinuclear iron(II) spin-crossover (SCO) compounds with the formula
$[Fe_2(\mu\text{-L1})_2]X_4$, with three different counteranions [X = BF_4^- (**1**), ClO_4^- (**2**) and $F_3CSO_3^-$
(**3**)], was prepared and characterized by single-crystal X-ray diffraction, variable-tem-
perature magnetic susceptibility and Mössbauer measurements. These are the first din-
uclear iron(II) SCO complexes with a 1,3,4-thiadiazole bridging ligand L1 (with L1 = 2,5-
bis[(2-pyridylmethyl)amino]methyl-1,3,4-thiadiazole). The magnetic measurements re-
veal a gradual and incomplete SCO of the three compounds around room temperature,
starting from a diamagnetic [LS-LS] state. The diamagnetic ground state is in agree-
ment with the singlecrystal X-ray diffraction and Mössbauer data.

3.3. Introduction

The thermally induced spin-crossover (SCO) in octahedral complexes of $3d^4$-$3d^7$ transi-
tion metal ions plays a very important role in the field of advanced molecular materials.[1]
These SCO materials can be switched by external stimuli such as temperature, light or
pressure and can be used for applications like temperature or pressure sensors, data
storage and display devices.[2] The special interest in the SCO in iron(II) materials has
several reasons. They can switch between a diamagnetic LS and paramagnetic HS
state, can be characterised with all fundamental methods, and the spin transition can
also be accompanied by an intensive colour change.[3]
The SCO in the solid state strongly depends on the cooperative interactions between
the metal centers. A higher cooperativity in the solid state can be achieved with in-
termolecular contacts between mononuclear complex molecules, mostly due to hydro-
gen bonding or π-π interactions between aromatic moieties of the ligand system.[4]
Another way to increase the communication between the metal centers is the synthesis
of polynuclear SCO systems. In the past this led to a number of coordination polymers
and 3D frameworks with abrupt SCO and wide thermal hysteresis around room temper-
ature, important for possible applications.[5] However, over recent years the research
into discrete polynuclear and especially dinuclear SCO systems increased. The rea-

sons are the much better crystallisation of the complexes and this being the simplest
model for the interactions between SCO centers. Furthermore, the sometimes addi-
tional, and very interesting, mixed "[HS-LS]" spin state in dinuclear SCO compounds
leads to a possible third state beside the diamagnetic [LS-LS] and the paramagnetic
[HS-HS] state.[6]

Herein, we present the synthesis and characterisation of a new family of dinuclear
iron(II) spin-crossover compounds with a 1,3,4-thiadiazole bridging ligand. This new
1,3,4-thiadiazole ligand L1 is related to the analogous 1,2,4-triazole ligand from Broo-
ker's group.[7] The dinuclear iron(II) SCO complex with the PMAT ligand provided the
first X-ray crystal structure of a trapped [HS-LS] species, followed by extensive Möss-
bauer and pressure effect studies.[7] Further modifications of the ligand system led to a
range of SCO compounds with abrupt spin transition and even thermal hysteresis. But
a result of the highly constrained bridging ligand is that the compounds remain in the
[HS-LS] state and do not switch to the fully diamagnetic [LS-LS] state.[8] Replacing
one nitrogen atom in the five-membered heterocycle by a larger sulfur atom results in
a higher flexibility in the ligand and the complex cation, and the electron-deficient nature
of the 1,3,4-thiadiazole heterocycle causes a larger ligand-field splitting.[9]

3.4. Results and Discussion

3.4.1. Synthesis

The ligand L1 (2,5-bis[(2-pyridylmethyl)amino]methyl-1,3,4-thiadiazole) represents a
new bis(tridentate) bridging ligand with a 1,3,4-thiadiazole heterocycle as a central mo-
tif. The ligand can be synthesized in two steps by starting from 1,2-bis(chloroacetyl)-
hydrazine. The first step is the thionation of the 1,2-bis(chloroacetyl)hydrazine with
Lawesson reagent, followed by a cyclisation to the desired 2,5-bis(chloromethyl)-1,3,4-
thiadiazole (TDA) under release of hydrogen sulfide.[10] The second step is a nucle-
ophilic substitution reaction between TDA and 2-(aminomethyl)pyridine, leading to the
final ligand 2,5-bis[(2-pyridylmethyl)-amino]methyl-1,3,4-thiadiazole (L1) (figure 3.2).[7e]
The dinuclear iron(II) complexes $1 \cdot 0.75MeOH \cdot 0.5H_2O$ (**1a**), $2 \cdot 0.75MeOH \cdot 0.5H_2O$ (**2a**)
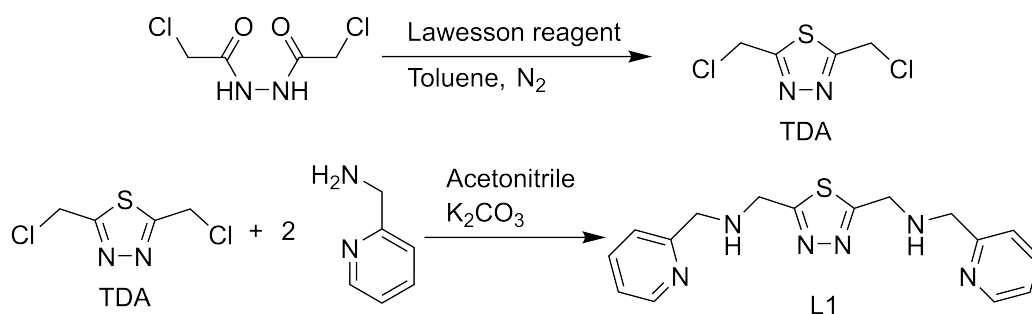
Figure 3.2.: Synthesis of the 1,3,4-thiadiazole precursor TDA and the ligand L1.

and $\mathbf{3}\cdot$1.5MeOH$\cdot$0.5CH$_2$Cl$_2$($\mathbf{3a}$) were obtained by layering a dichloromethane solution of the ligand L1 with a DCM/MeOH (1:1) separation layer and a methanolic solution of the respective iron(II) salt. Single crystals of $\mathbf{1a}$, $\mathbf{2a}$ and $\mathbf{3a}$, suitable for X-ray diffraction experiments, were isolated after 2-3 weeks and complete diffusion of the solutions.

3.4.2. Crystal Structures

All three compounds ($\mathbf{1a}$, $\mathbf{2a}$ and $\mathbf{3a}$) were obtained as single crystals from diffusion experiments of the ligand and the corresponding iron(II) salt.

The complexes $\mathbf{1a}$ and $\mathbf{2a}$ crystallise in the monoclinic space group $P2_1/n$, and complex $\mathbf{3a}$ crystallises in the orthorhombic space group $Pbca$, with the entire complex in the asymmetric unit in all three cases. The complex cation (figure 3.3) has the same structure in all three compounds and consists of two iron(II) ions brigded by two ligand molecules. This results in the desired dinuclear iron(II) complexes in which the two ligand molecules provide the 12 nitrogen donor atoms for the 2 octahedral FeN6 coordination spheres. In contrast to the analogous 1,2,4-triazole ligand, here the 1,3,4-thiadiazole ligand binds with one sidearm up and one down, in all three cases.[7b]

Beside the two iron(II) ions and the two ligand molecules, the crystal structures of the complexes also include four non-coordinating counteranions per complex cation ($\mathbf{1}$: BF$_4^-$; $\mathbf{2}$: ClO$_4^-$; $\mathbf{3}$: F$_3$CSO$_3^-$) and solvent molecules. Complexes $\mathbf{1a}$ and $\mathbf{2a}$ both crystallise with 0.5 water and 0.75 methanol molecules, whereas complex $\mathbf{3a}$ crystallises with 0.5 dichloromethane and 1.5 methanol molecules. The counteranions and

solvent molecules surround the complex cations in the crystal and mediate between neighbouring complex cations through hydrogen-bonding interactions. There is no evidence of π-π stacking interactions between the aromatic rings of the ligand systems of neighbouring complex cations. The average Fe-N bond lengths for the iron(II) centers
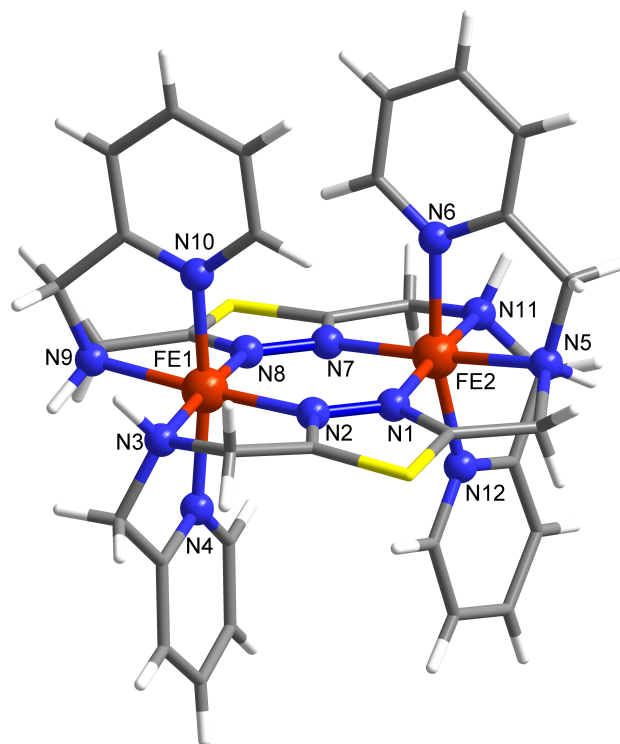

Figure 3.3.: Representative view of the complex cation $[Fe_2(\mu\text{-}L1)_2]_4^+$ from **1a**. Exclusively nitrogen and iron atoms have been highlighted and labeled. Sulfur atoms are yellow, carbon atoms are grey, and hydrogen atoms are white.

in compounds **1a**, **2a** and **3a** at 173 K (table 3.1) are between 1.985 Å and 1.997 Å, typical for Fe-N bonds with iron(II) in the LS state.[11,1,2b] Another way to obtain information on the spin state of the iron(II) ion is by using the octahedral distortion parameter Σ, which is the sum of the deviations from 90° of the 12 *cis*-N-Fe-N angles. A high Σ value indicates that the metal ion is in the high-spin state. The octahedral distortion parameter Σ values of the reported compounds (table 3.1) are in the range between 57.59° and 66.09°, which is also evidence for the iron(II) centers being in the LS state. This represents a clear difference compared to the previously reported 1,2,4-triazole system of Brooker's group (Σ(Fe[LS]) = 65.0° and Σ(Fe[HS]) = 133.1°).[7b]

Table 3.1.: Selected Fe-N bond lengths Å and N-Fe-N bond angles ° for compounds **1a**, **2a**, **3a** and $[Fe_2(PMAT)_2](BF_4)_4\cdot$ DMF (at 123 K; Fe1: LS; Fe2: HS).[7b]

	1a	2a	3a	$[Fe_2(PMAT)_2](BF_4)_4\cdot$ DMF
Fe-N$_{TDA/TZ}$[a]	1.936(2),	1.935(3),	1.940(2),	1.934(3),
	1.941(2)/	1.938(3)/	1.944(2)/	1.946(3)/
	1.938(2),	1.940(3),	1.932(2),	2.131(3),
	1.946(2)	1.949(3)	1.941(2)	2.136(3)
Fe-N$_{pyr}$[a]	1.986(3),	1.988(3),	1.990(2),	1.987(4),
	1.990(2)/	1.995(3)/	1.991(2)/	1.986(4)/
	1.995(3),	1.994(3),	1.983(2),	2.155(4),
	2.007(3)	2.011(3)	1.988(3)	2.159(4)
Fe-N$_{NH}$[a]	2.033(2),	2.034(3),	2.025(2),	2.066(4),
	2.037(2)/	2.038(3)/	2.027(2)/	2.071(4)/
	2.034(3),	2.042(3),	2.031(2),	2.319(4),
	2.037(2)	2.043(3)	2.034(2)	2.312(4)
av. Fe-N[a]	1.987/1.993	1.988/1.997	1.986/1.985	1.998/2.202
av. *cis*-N-Fe-N[a]	90.02/90.06	90.02/90.06	90.00/90.02	90.07/90.98
av. *trans*-N-Fe-N[a]	174.81/172.74	174.69/172.78	174.09/173.84	174.1/160.0
Σ [a,b]	58.36/65.40	59.16/66.09	61.39/57.59	65.0/133.1
av. N$_{TDA/TZ}$-N$_{TDA/TZ}$-N$_{NH}$[c]	174.62	175.43	178.08	174.37/170.23[a]

[a] Fe1/Fe2. [b] Octahedral distortion parameter Σ (sum of the deviation from 90° of the 12 cis-N-Fe-N angles in the FeN6 coordination sphere). [c] Angle between the two thiadiazole/triazole nitrogen donor atoms and the secondary amine nitrogen atoms.

Interestingly, the average *cis*- and *trans*-N-Fe-N angles of **1a**, **2a** and **3a** are in the range between 90.00° and 90.06° (for *cis*) and 172.74° and 174.81° (for *trans*) and correspond to the values of the LS iron(II) centre in the analogous triazole compound (*cis*: 90.07°; *trans*: 174.37°). The main difference between the structures with the 1,3,4-thiadiazole and the 1,2,4-triazole ligands, however, can be seen in the angle between the two thiadiazole/triazole nitrogen donor atoms and the amine nitrogen atoms ($N_{TDA/TZ}$-$N_{TDA/TZ}$-N_{NH} angle; see table 3.1). Thus, the incorporation of the sulfur atom into the heterocycle leads to a higher flexibility, a nearly linear alignment of the donor atoms and the ability to achieve an angle closer to 180°. These structural changes result - according to the X-ray diffraction data - in the achievement of the fully diamagnetic [LS-LS] state.[7e,8a,12]

3.4.3. Magnetic Properties and Mössbauer Measurements

The magnetic susceptibilities of crystalline samples of **1**·2H$_2$O (**1b**), **2**·0.5H$_2$O (**2b**) and **3**·1.5MeOH·0.5CH$_2$Cl$_2$ (**3b**) (Figure 2) were measured with an external field of 10 kOe in a temperature range from 2 to 380 K (compounds **1b** and **3b**) and from 2 to 375 K (compound **2b**), respectively.

The magnetic susceptibility data of the three dinuclear iron(II) compounds **1b**, **2b** and **3b** (figure 3.4) show a diamagnetic ground state at low temperatures. This is in agreement with the information obtained from the Fe-N bond lengths and the octahedral distortion parameters Σ (as mentioned above). The increasing χ_MT value at higher temperatures is a result of a spin transition to high-spin iron(II). The χ_MT value of compounds **1b** and **2b** increases gradual starting around 250 K and reaches values of 2.62 cm^3 K mol^{-1} (for **1b** at 380 K) and cm^3 K mol^{-1} (for **2b** at 375 K). The spin transition of compound **3b** starts above 300 K and represents the most gradual SCO of these three compounds, resulting in a χ_MT value of 0.33 cm^3 K mol^{-1} at 380 K. It can be seen, that the χ_MT values of the three compounds do not reach the expected value for a mixed [HS-LS] state, not to mention the complete [HS-HS] state. But the targeted fully diamagnetic [LS-LS] ground state and a spin transition at temperatures above 250 K could be observed for all three reported compounds.

As expected, the combination of the counteranion and solvents in the solid state have
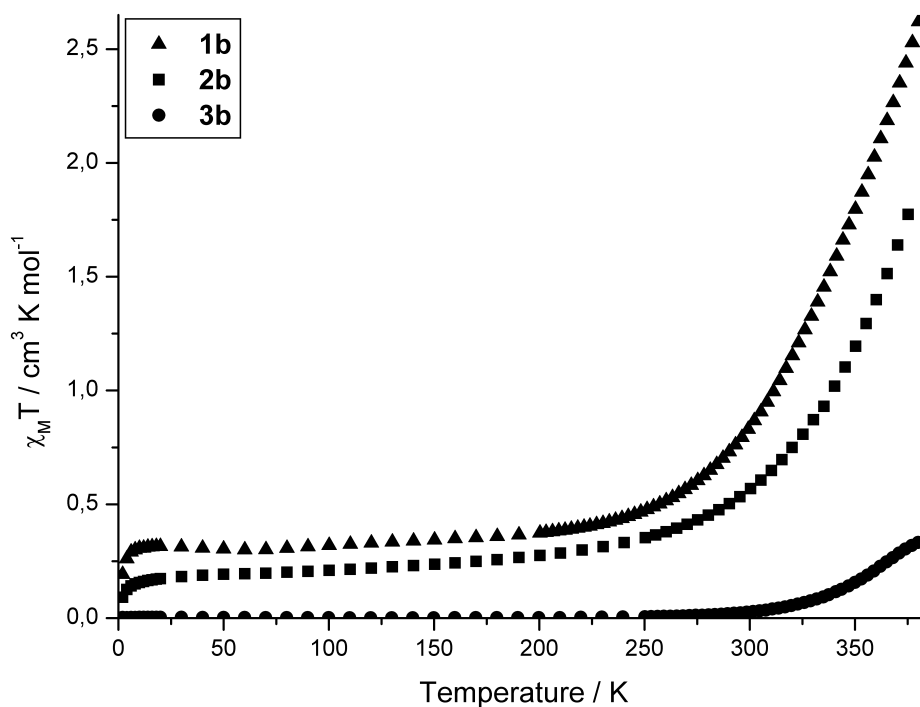
Figure 3.4.: χ_MT vs. T data for the compounds **1b** (triangles), **2b** (squares) and **3b** (dots). Data per dinuclear complex molecule.

an effect on the transition temperature of the systems, and the χ_MT values differ as a result. This is mainly related to the crystal packing of the complexes in this series. Compounds **1b** and **2b** with the smaller tetrafluoroborate and perchlorate counteranions crystallise in the same space group $P2_1/n$ with the same solvents in the crystal structure and show a similar magnetic behaviour, with **1** showing a slightly steeper spin transition and a higher χ_MT value. The compound with the larger triflate counteranion **3b** crystallises in the space group *Pbca* with different lattice solvent molecules, which leads to a different behaviour with a higher transition temperature and a more gradual spin transition. However, due to solvent loss in the time between the sample preparation and measurement of the magnetic data, the samples used for the magnetic studies have a slightly different solvent content compared to the X-ray crystal structures. Microanalysis of the compounds confirmed the expected loss of methanol during the short drying process and incorporation of water in one case.

The higher transition temperature of **3b** might also be a result of the shorter Fe-N bonds and the lower octahedral distortion parameters Σ for the two iron(II) centers. Compound

3a is, in comparison to **1a** and **2a**, structurally less distorted from the expected geometry of iron(II) in the low-spin state.

In this series the tetrafluoroborate complex **1b** shows the most promising magnetic behaviour, with the highest $\chi_M T$ value and the steepest spin transition.

Compound **1b** has been further investigated by using ^{57}Fe Mössbauer spectroscopy. The spectra were recorded at 80 K and 307 K (figure 3.12 and figure 3.13) and show a singlet at both temperatures. The isomer shifts δ of 0.45 mm/s at 80 K and of 0.37 mm/s at 307 K are in the characteristic range for iron(II) in the low-spin state. The result at 80 K is in agreement with the magnetic measurements and X-ray crystal structure. Also, the Mössbauer spectrum at 307 K does not show a doublet characteristic for iron(II) in the high-spin state. The reason is the low fraction of iron(II) ions that switched into the high-spin form at this temperature and the broad background, normal for Mössbauer spectra at elevated temperatures.[3d,13]

3.5. Conclusion

We were able to synthesize and characterize the first dinuclear iron(II) SCO compounds with a new 1,3,4-thiadiazole bridging ligand. All three reported compounds in this series have a [LS-LS] ground state at low temperatures, and the magnetic measurements reveal a gradual and incomplete spin transition around room temperature. Clearly, the reason for the achieved diamagnetic [LS-LS] ground state has to be the sulfur atom in the five-membered 1,3,4-thiadiazole heterocycle, which resulted in a lower strain in the ligand system and finally also in the complex molecules. Even though the SCO occurs at temperatures above 250 K and is of a gradual nature, this system represents a good basis for further work with dinuclear SCO systems with 1,3,4-thiadiazole bridging ligands. We are currently investigating the intermolecular interactions in the solid state and modifying the ligand system to obtain the [HS-HS] state at room temperature.

3.6. Experimental Section

General Methods and Materials: All chemicals were purchased from Alfa Aesar, Deutero, Fisher Chemicals, Sigma-Aldrich and Acros Organics and used without further purification. The NMR spectra were recorded at room temperature by using a Bruker DRX 400 spectrometer and analysed with the program MestReNova.[14] Magnetic susceptibility data was collected with a Quantum Design SQUID magnetometer MPMSXL in a temperature range of 2-380 K or 2-375 K with an applied field of 10 kOe. ^{57}Fe Mössbauer spectra were recorded at the Johannes Gutenberg University Mainz by Dr. Vadim Ksenofontov. ESI mass spectra, FD mass spectra and elemental analyses (C, H, N and S) were measured at the microanalytical laboratories of the Johannes Gutenberg University Mainz. X-ray diffraction data were collected at 173 K with a Bruker SMART diffractometer at the Johannes Gutenberg University Mainz. The structures were solved with SIR 97 and refined with SHELX 2013 with the program Olex2.[15] CCDC-1062666 (for **1**·0.75MeOH·0.5H$_2$O), -1062665 (for **2**·0.75MeOH·0.5H$_2$O) and -1062667 (for **3**·1.5MeOH·0.5CH$_2$Cl$_2$) contain the supplementary crystallographic data for this paper. These data can be obtained free of charge from The Cambridge Crystallographic Data Centre via `www.ccdc.cam.ac.uk/data_request/cif`.

Caution! The prepared perchlorate complexes are potentially explosive. Even though no explosions occurred, only small amounts should be prepared and handled with care.

Ligand Synthesis: 1,2-Bis(chloroacetyl)hydrazine was prepared as described previously,[16] 2,5-bis(chloromethyl)-1,3,4-thiadiazole was prepared according to a modified literature procedure for the general synthesis of 1,3,4-thiadiazoles[10] and 2,5-bis[(2-pyridylmethyl)amino]methyl-1,3,4-thiadiazole (L1) was synthesized according to a modified literature procedure for the analogous 1,2,4-triazole ligand.[7e]

2,5-Bis(chloromethyl)-1,3,4-thiadiazole (TDA): 1,2-Bis(chloroacetyl)hydrazine (6.00 g, 32.43 mmol) and 1.2 equiv. of Lawesson reagent (15.74 g, 38.92 mmol) were suspended in dry toluene (750 mL) and heated under nitrogen at reflux for 16 h. The toluene was evaporated under reduced pressure to give a yellow solid. The crude product was purified by column chromatography (silica); first 2,4,6-tris(4-methoxyphenyl)-

1,3,5,2,4,6-trioxatriphosphoran 2,4,6-trisulfide was eluted with dichloromethane, and then the product was eluted with a dichloromethane/diethylether (9:1) mixture to give the pure compound as a yellow oil.

Yield: 5.58 g (30.48 mmol, 94%)

^{1}H NMR (400 MHz, CDCl$_3$, 25 °C): (figure 3.5)

δ = 4.95 (s, 4 H, CH$_2$) ppm.

^{13}C NMR (100 MHz, CDCl$_3$, 25 °C): (figure 3.6)

δ = 169.30 (C, TDA), 38.27 (CH$_2$) ppm.

ESI-MS (MeOH): m/z (%) = 182.94 (100) [TDA + H$^+$].

Elemental Analysis: C$_4$H$_4$Cl$_2$N$_2$S (TDA) (183.06): calcd. C 26.24, H 2.20, N 15.30, S 17.52; found C 26.29, H 2.41, N 15.56, S 17.30.

2,5-Bis[(2-pyridylmethyl)amino]methyl-1,3,4-thiadiazole (L1): A suspension of 2-(aminomethyl)pyridine (1.622 g, 15.00 mmol) and potassium carbonate (3.455 g, 25.00 mmol) in acetonitrile (600 mL) was heated at 70 °C. A solution of 2,5-bis(chloromethyl)-1,3,4-thiadiazole (0.915 g, 5.00 mmol) in acetonitrile (100 mL) was added dropwise over a period of 30 min. After complete addition, the suspension was heated for further 16 h. The mixture was cooled to room temperature, the white precipitate filtered, and the filtrate concentrated to dryness under reduced pressure. The resulting brown oil was purified by column chromatography (aluminium oxide; chloroform/methanol, 99:1) to give the pure product as an orange oil.

Yield: 1.21 g (3.71 mmol, 74%)

^{1}H NMR(400 MHz, CDCl$_3$, 25 °C): (figure 3.7)

δ = 8.56 (d, $^3J_{H,H}$ = 4.8 Hz, 2 H, H5, Py), 7.65 (td, $^3J_{H,H}$ = 7.7, 1.8 Hz, 2 H, H4, Py), 7.29 (d, $^3J_{H,H}$ = 8.3 Hz, 2 H, H2, Py), 7.18 (ddd, $^3J_{H,H}$ = 7.4, 4.9 Hz, 1.0 Hz, 2 H, H3, Py), 4.23 (s, 4 H, CH$_2$, TDA), 3.98 (s, 4 H, CH$_2$, Py), 2.67 (s, 2 H, NH) ppm.

^{13}C NMR (100 MHz, CDCl3, 25°C): (figure 3.8)

δ = 172.14 (C, TDA), 158.68 (C1, Py), 149.43 (C5, Py), 136.54 (C4, Py), 122.40 (C2, Py), 122.21 (C3, Py), 54.24 (CH$_2$, Py), 47.84 (CH$_2$, TDA) ppm.

FD-MS (DMSO): m/z (%) = 327.16 (100) [L1 + H$^+$], 328.15 (20) [L1 + H$^+$].

Elemental Analysis: C$_{16.5}$H$_{20}$N$_6$SO$_{0.5}$ (L1·0.5MeOH) (342.44): calcd. C 57.87, H 5.89, N 24.54, S 9.36; found C 58.23, H 6.21, N 24.27, S 9.34.

Synthesis of Complexes [Fe$_2$(μ-L1)$_2$]X$_4$:

An orange solution of 2,5-bis[(2-pyridylmethyl)amino]methyl-1,3,4-thiadiazole (L1) (82 mg, 0.25 mmol) in dichloromethane (7 mL) was layered with a dichloromethane/ methanol (1:1) separation layer (5 mL). This was layered with a methanolic solution (7 mL) of the corresponding iron(II) salt [0.25 mmol; Fe(BF$_4$)$_2$·6 H$_2$O, Fe(ClO$_4$)$_2$·xH$_2$O or Fe(F$_3$CSO$_3$)$_2$]. After 2-3 weeks, single crystals of the desired product in X-ray diffraction quality could be obtained.

[Fe$_2$(μ-L1)$_2$](BF$_4$)$_4$·0.75 MeOH·0.5H$_2$O (1): Fe(BF$_4$)$_2$·6 H$_2$O (84 mg) was used to obtain **1** (73 mg, 51%) as dark red single crystals suitable for X-ray diffraction.

Elemental Analysis: C$_{32}$H$_{40}$B$_4$F$_{16}$Fe$_2$ N$_{12}$O$_2$S$_2$ ([Fe$_2$(μ-L1)$_2$](BF$_4$)$_4$·2H$_2$O) (1147.78): calcd. C 33.49, H 3.51, N 14.64, S 5.59; found C 33.32, H 3.53, N 14.34, S 5.75.

[Fe$_2$(μ-L1)$_2$](ClO$_4$)$_4$·0.75 MeOH·0.5H$_2$O (2): Fe(ClO$_4$)$_2$·xH$_2$O (73 mg) was used to obtain **2** (79 mg, 53%) as dark red single crystals suitable for X-ray diffraction.

Elemental Analysis: C$_{32}$H$_{37}$Cl$_4$ Fe$_2$N$_{12}$O$_{16.5}$S$_2$ ([Fe$_2$(μ-L1)$_2$](ClO$_4$)$_4$·0.5H$_2$O) (1171.34): calcd. C 32.81, H 3.18, N 14.35, S 5.47; found C 32.66, H 3.20, N 14.31, S 5.76.

[Fe$_2$(μ-L1)$_2$](F$_3$CSO$_3$)$_4$·1.5MeOH·0.5CH$_2$Cl$_2$ (3): Fe(F$_3$CSO$_3$)$_2$ (89 mg) was used to obtain **3** (82 mg, 45%) as red single crystals suitable for X-ray diffraction.

Elemental Analysis: C$_{38}$H$_{43}$Cl$_1$F$_{12}$Fe$_2$ N$_{12}$O$_{13.5}$S$_6$ ([Fe$_2$(μ-L1)$_2$](F$_3$CSO$_3$)$_4$·1.5MeOH ·0.5CH$_2$Cl$_2$) (1451.32): calcd. C 31.45, H 2.99, N 11.58, S 13.26; found C 31.38, H 2.77, N 11.70, S 13.30.

Acknowledgments

3.7. References

[1] P. Gütlich, H. A. Goodwin, *Top. Curr. Chem.* **2004**, *233*, 1-47.

[2] a) S. Brooker, J. A. Kitchen, *Dalton Trans.* **2009**, 7331-7340

b) P. Gütlich, A. B. Gaspar, Y. Garcia, *Beilstein J. Org. Chem.* **2013**, *9*, 342-391

c) P. Gütlich, Y. Garcia, H. A. Goodwin, *Chem. Soc. Rev.* **2000**, *29*, 419-427

d) M. Seredyuk, M. C. Muñoz, V. Ksenofontov, P. Gütlich, Y. Galyametdinov,
J. A. Real, *Inorg. Chem.* **2014**, *53*, 8442-8454

e) O. Kahn, C. J. Martinez, *Science* **1998**, *279*, 44-48

f) G. Agustí, S. Cobo, A. B. Gaspar, G. Molnár, N. O. Moussa, P. Á. Szilágyi,
V. Pálfi, C. Vieu, M. C. Muñoz, J. A. Real, A. Bousseksou, *Chem. Mater.*
2008, *20*, 6721-6732

g) O. Roubeau, A. Colin, V. Schmitt, R. Clérac, *Angew. Chem. Int. Ed.*
2004, *43*, 3283-3286; *Angew. Chem.* **2004**, *116*, 3345

[3] a) M. A. Halcrow, *Chem. Commun.* **2013**, *49*, 10890-10892

b) C. Carbonera, J. S. Costa, V. A. Money, J. Elhaïk, J. A. K. Howard,
M. A. Halcrow, J.-F. Létard, *Dalton Trans.* **2006**, 3058-3066

c) S. Decurtins, P. Gütlich, C. P. Köhler, H. Spiering, A. Hauser, *Chem. Phys.
Lett.* **1984**, *105*, 1-4

d) P. Gütlich, *Z. Anorg. Allg. Chem.* **2012**, 15-43

[4] a) L. A. Barrios, E. Peyrecave-Lleixà, G. A. Craig, O. Roubeau, S. J. Teat,
G. Aromi, Eur. J. *Inorg. Chem.* **2014**, *35*, 6013-6021

b) O. Kahn, C. J. Martinez, *Science* **1998**, *279*, 44-48

c) M. A. Halcrow, *Chem. Soc. Rev.* **2011**, *40*, 4119-4142

d) P. Gütlich, H. A. Goodwin, *Top. Curr. Chem.* **2004**, *233*, 1-47

e) S. Schlamp, K. Dankhoff, B. Weber, *New J. Chem.* **2014**, *38*, 1965-1972

f) T. D. Roberts, M. A. Little, L. J. K. Cook, M. A. Halcrow, *Dalton Trans.*
2014, *43*, 7577-7588

g) W. Bauer, C. Lochenie, B. Weber, *Dalton Trans.* **2014**, *43*, 1990-1999

[5] a) J. Kröber, E. Codjovi, O. Kahn, F. Groliìre, C. Jay, *J. Am. Chem. Soc.* **1993**,
115, 9810-9811

[5] b) Y. Garcia, P. J. van Koningsbruggen, R. Lapouyade, L. Rabardel, O. Kahn, M. Wieczorek, R. Bronisz, Z. Ciunik, M. F. Rudolf, *C. R. Acad. Sci., Ser. IIc: Chim.* **1998**, *1*, 523-532

c) V. Niel, J. M. Martinez-Agudo, M. C. Muñoz, A. B. Gaspar, J. A. Real, *Inorg. Chem.* **2001**, *40*, 3838-3839

d) M. M. Dîrtu, C. Neuhausen, A. D. Naik, A. Rotaru, L. Spinu, Y. Garcia, *Inorg. Chem.* **2010**, *49*, 5723-5736

[6] a) M. A. Halcrow, *Spin-Crossover Materials*, Wiley-VCH, Weinheim, **2013**

b) J. A. Real, A. B. Gaspar, M. C. Muñoz, *Dalton Trans.* **2005**, 2062-2079

c) J. A. Real, A. B. Gaspar, V. Niel, M. C. Muñoz, *Coord. Chem. Rev.* **2003**, *236*, 121-141

[7] a) M. H. Klingele, B. Moubaraki, K. S. Murray, S. Brooker, *Chem. Eur. J.* **2005**, *11*, 6962-6973

b) M. H. Klingele, B. Moubaraki, J. D. Cashion, K. S. Murray, S. Brooker, *Chem. Commun.* **2005**, 987-989

c) C. M. Grunert, S. Reiman, H. Spiering, J. A. Kitchen, S. Brooker, P. Gütlich, *Angew. Chem. Int. Ed.* **2008**, *47*, 2997-2999; *Angew. Chem.* **2008**, *120*, 3039

d) A. Bhattacharjee, V. Ksenofontov, J. A. Kitchen, N. G. White, S. Brooker, P. Gütlich, *Appl. Phys. Lett.* **2008**, *92*, 174104

e) J. A. Kitchen, N. G. White, G. N. L. Jameson, J. L. Tallon, S. Brooker, *Inorg. Chem.* **2011**, *50*, 4586-4597

[8] a) J. A. Kitchen, J. Oluín, R. Kulmaczewski, N. G. White, V. A. Milway, G. N. L. Jameson, J. L. Tallon, S. Brooker, *Inorg. Chem.* **2013**, *52*, 11185-11199

b) R. Kulmaczewski, J. Olguín, J. A. Kitchen, H. L. C. Feltham, G. N. L. Jameson, J. L. Tallon, S. Brooker, *J. Am. Chem. Soc.* **2014**, *136*, 878-881

[9] a) A. Kurowska, A. S. Kostyuchenko, P. Zassowski, L. Skorka, V. L. Yurpalov, A. S. Fisyuk, A. Pron, W. Domagala, *J. Phys. Chem. C* **2014**, *118*, 25176-25189

b) S. U.-D. Khan, A. Mahmood, U. A. Rana, S. Haider, *Theor. Chem. Acc.* **2015**, *134*, 1596

c) Y. Hu, C.-Y. Li, X.-M. Wang, Y.-H. Yang, H.-L. Zhu, *Chem. Rev.* **2014**, *114*, 5572-5610

[10] B. Gierczyk, M. Zalas, *Org. Prep. Proceed. Int.* **2005**, *37*, 213-222

[11]   a) E. König, *Struct. Bonding (Berlin)* **1991**, *76*, 51-152

b) D. L. Reger, C. A. Little, M. D. Smith, A. L. Rheingold, K.-C. Lam, T. L.
Concolino, G. J. Long, R. P. Hermann, F. Grandjean, *Eur. J. Inorg. Chem.*
2002, 1190-1197

c) J. D. Oliver, D. F. Mullica, B. B. Hutchinson, W. O. Milligan, *Inorg. Chem.*
1980, *19*, 165-169

[12]   a) P. Guionneau, C. Brigouleix, Y. Barrans, A. E. Goeta, J.-F. Létard, J. A. K.
Howard, J. Gaultier, D. Chasseau, *C. R. Acad. Sci., Ser. IIc: Chim.* **2001**
4, 161-171

b) B. Moubaraki, B. A. Leita, G. J. Halder, S. R. Batten, P. Jensen, J. P. Smith,
J. D. Cashion, C. J. Kepert, J.-F. Létard, K. Murray, *Dalton Trans.* **2007**,
4413-4426.

[13]   a) G. Psomas, N. Bréfuel, F. Dahan, J.-P. Tuchagues, *Inorg. Chem.* **2004**, *43*,
4590-4594

b) R. J. Dosser, W. J. Eilbeck, A. E. Underhill, P. R. Edwards, C. E. Johnson,
J. Chem. Soc. A **1969**, 810-816

[14]   J. C. Cobas, F. J. Sardina, *Concepts Magn. Reson., Part A* **2003**, *19*, 80-96.

[15]   a) A. Altomare, M. C. Burla, M. Camalli, G. Cascarano, C. Giacovazzo, A.
Guagliardi, G. Moliterni, G. Polidori, R. Spagna, *J. Appl. Crystallogr., Sect. C*
1999, *32*, 115-119

b) G. M. Sheldrick, *Acta Crystallogr.* **2015**, *C71*, 3-8

c) O. V. Dolomanov, L. J. Bourhis, R. J. Gildea, J. A. K. Howard, H.
v *J. Appl. Crystallogr.* **2009**, *42*, 339-341

[16]   R. Zhang, R. Jordan, O. Nuyken, *Macromol. Rapid Commun.* **2003**, *24*,
246-250.

3.8. Supporting Information

3.8.1. NMR-Spectroscopy
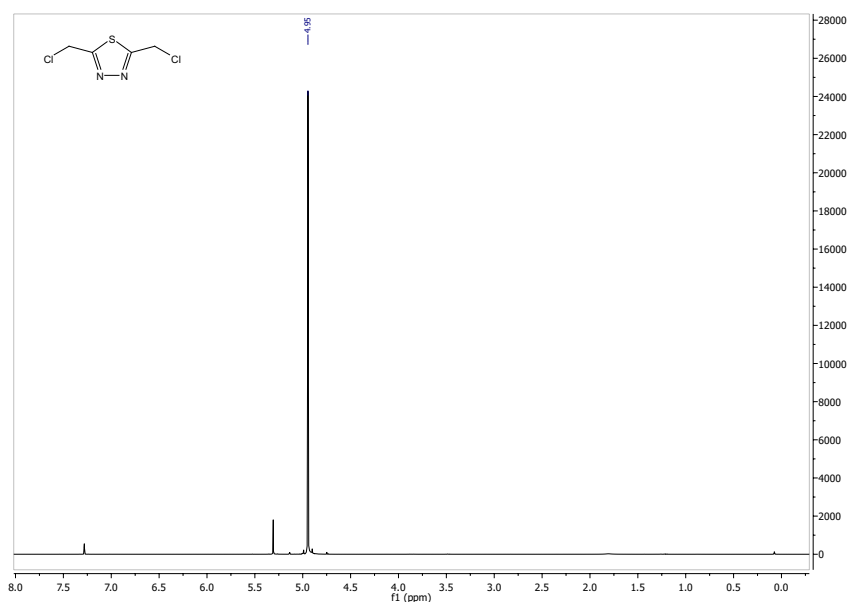
Figure 3.5.: ^{1}H NMR spectrum of 2,5-Bis(chloromethyl)-1,3,4-thiadiazole (**TDA**).
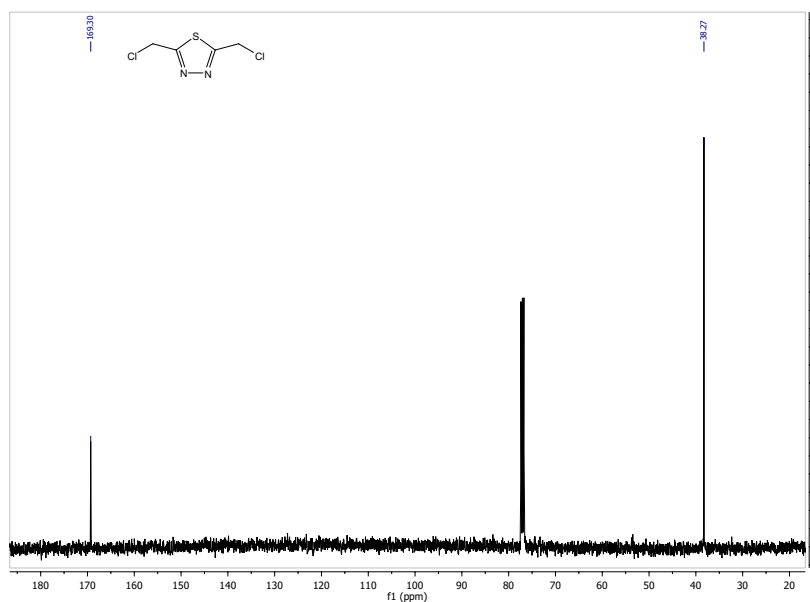
Figure 3.6.: ^{13}C NMR spectrum of 2,5-Bis(chloromethyl)-1,3,4-thiadiazole (**TDA**).
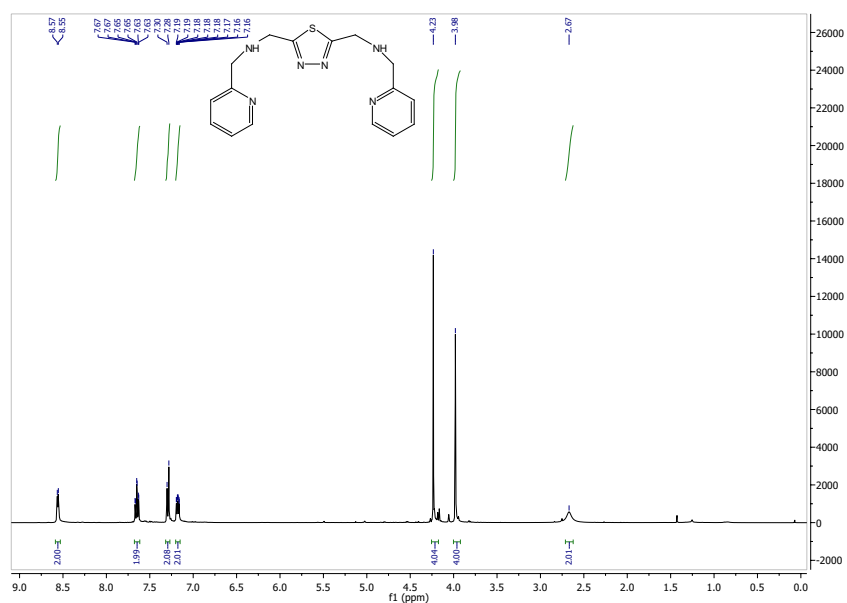
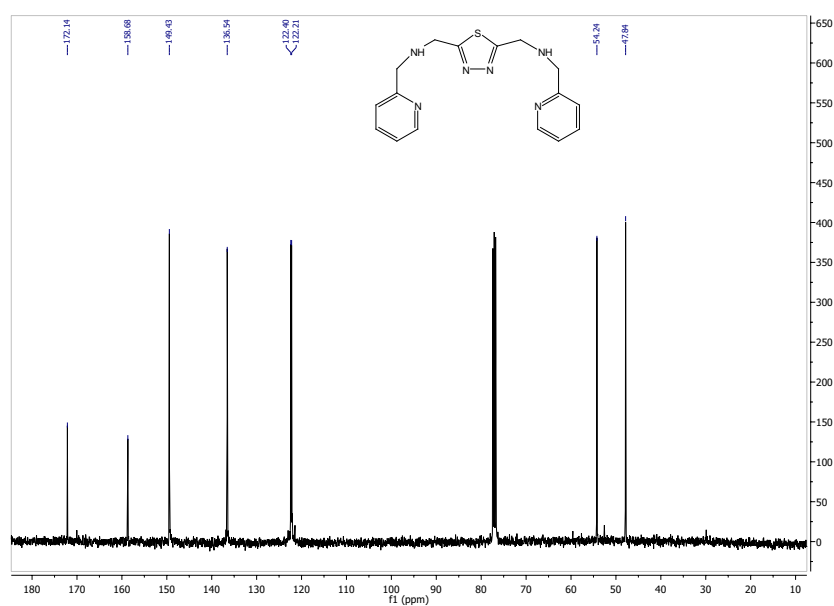Figure 3.7.: ^{1}H NMR spectrum of 2,5-Bis[(2-pyridylmethyl)amino]methyl-1,3,4-thiadiazole (**L1**).

Figure 3.8.: ^{13}C NMR spectrum of 2,5-Bis[(2-pyridylmethyl)amino]methyl-1,3,4-thiadiazole (**L1**).

3.8.2. X-ray Diffraction

Table 3.2.: Crystallographic parameters for compounds **1-3**.

	1·0.75MeOH · 0.5H_2O	**2**·0.75MeOH · 0.5H_2O	**3**·1.5MeOH ·0.5CH_2Cl_2
formula	$C_{32.75}H_{40}B_4F_{16}$ $Fe_2N_{12}O_{1.25}S_2$	$C_{32.75}H_{40}Cl_4Fe_2$ $N_{12}O_{17.25}S_2$	$C_{38}H_{43}F_{12}Fe_2$ $N_{12}O_{13.50}S_6Cl$
formula weight	1144.83	1195.39	1451.35
crystal system	monoclinic	monoclinic	orthorhombic
space group	$P2_1/n$	$P2_1/n$	$Pbca$
a /Å	16.5804(7)	16.7340(5)	19.0517(19)
b /Å	15.0043(6)	15.1646(5)	23.131(2)
c /Å	18.1666(7)	18.3762(6)	24.852(2)
α /°	90	90	90
β /°	96.875(1)	97.078(2)	90
γ /°	90	90	90
V /Å^3	4486.9(3)	4627.7(3)	10951.8(18)
Z	4	4	8
T /K	173	173	173
$\rho_{calcd.}$ [g/cm^3]	1.695	1.716	1.760
μ [mm^{-1}]	0.853	1.033	0.921
R(int)	0.0453	0.0848	0.1003
S	1.068	0.888	0.934
R1 (I > 2σ(I))	0.0498	0.0495	0.0463
wR2 (all data)	0.1456	0.1313	0.1284
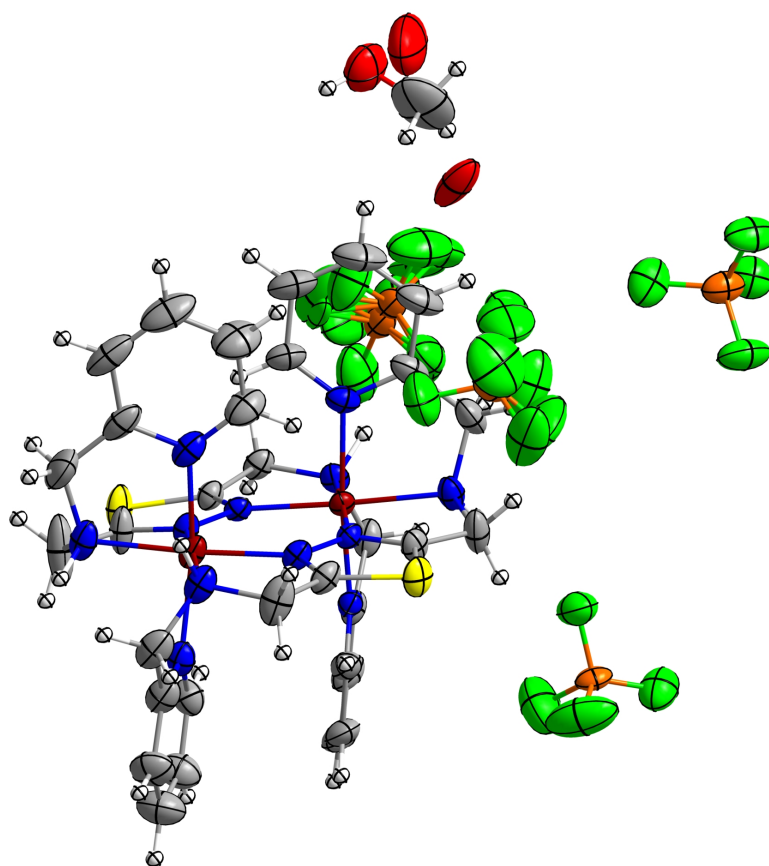
Figure 3.9.: Molecular structure of **1·0.75MeOH·0.5H$_2$O** ([Fe$_2$(μ-L1)$_2$](BF$_4$)$_4$ + 0.75
MeOH + 2*0.25H$_2$O) with thermal ellipsoids at 50 % probability level. Colour scheme:
dark red - Fe(II), yellow - S, blue - N, light red - O, orange - B, green - F, grey - C, white
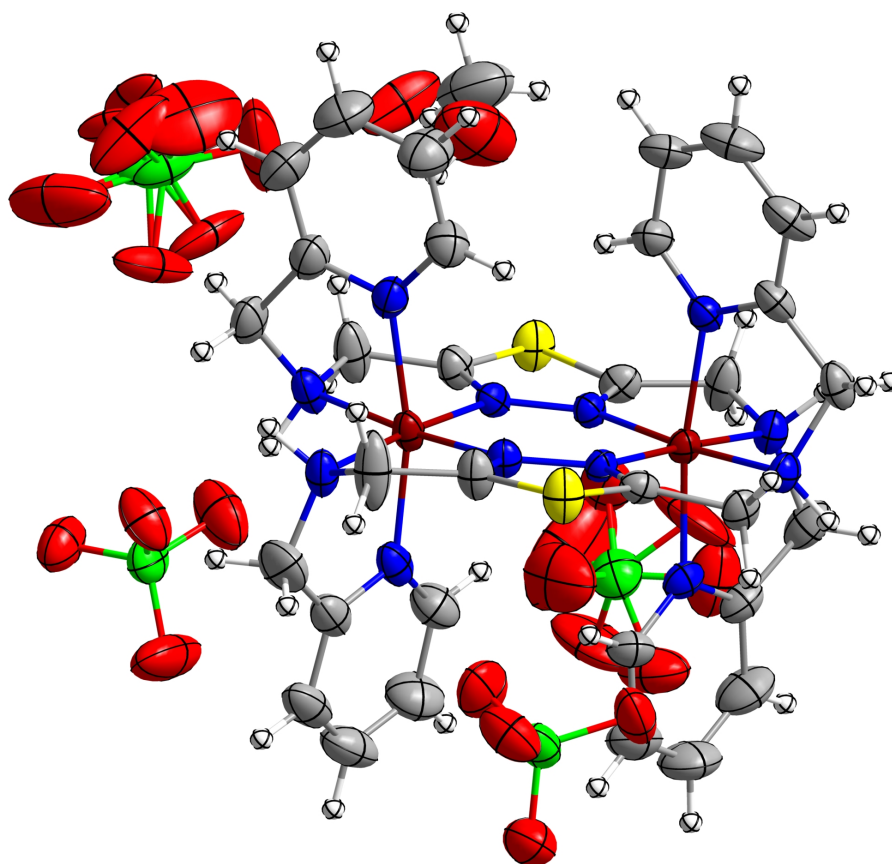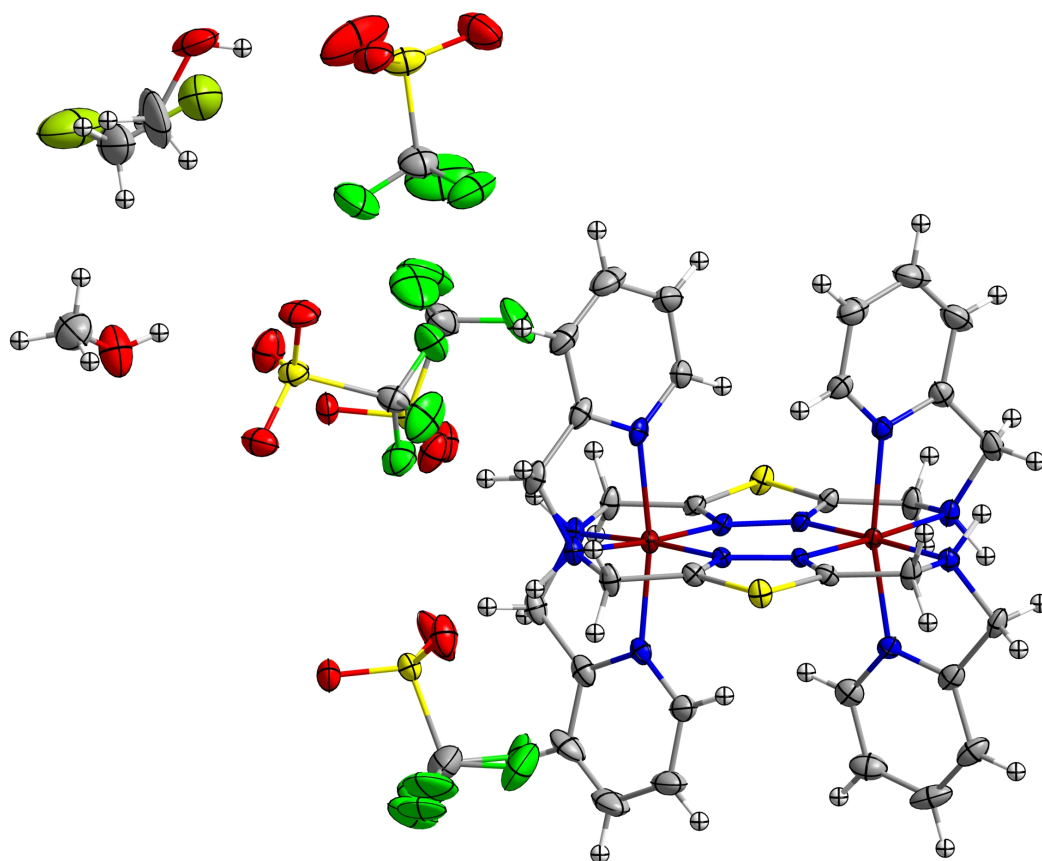- H.

Figure 3.10.: Molecular structure of **2·0.75MeOH·0.5H$_2$O** ([Fe$_2$(μ-L1)$_2$](ClO$_4$)$_4$ + 0.75 MeOH + 0.5H$_2$O) with thermal ellipsoids at 50 % probability level. Colour scheme: dark red - Fe(II), yellow - S, blue - N, light red - O, orange - B, green - F, grey - C, white - H.

Figure 3.11.: Molecular structure of **3·1.5MeOH·0.5CH$_2$Cl$_2$** ([Fe$_2$(μ-L1)$_2$](F$_3$CSO$_3$)$_4$ +
1.5 MeOH + 0.5CH$_2$Cl$_2$) with thermal ellipsoids at 50 % probability level. Colour
scheme: dark red - Fe(II), yellow - S, blue - N, light red - O, orange - B, green - F,
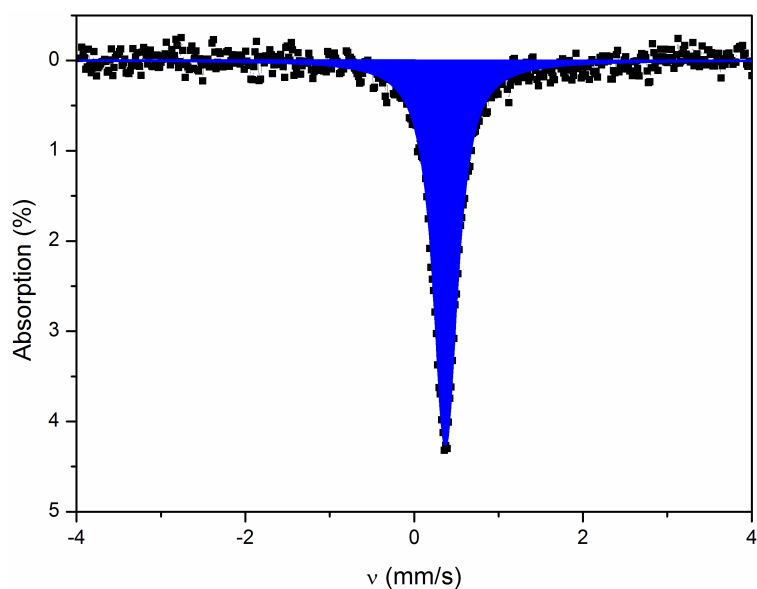grey - C, white - H.

3.8.3. Mössbauer Spectroscopy
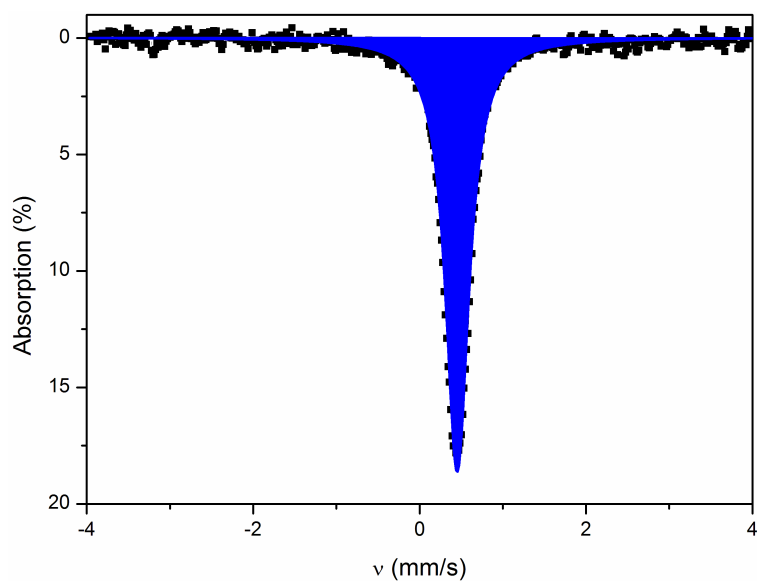
Figure 3.12.: Mössbauer spectrum of **1b** recorded at 80 K. The blue line represents the fit for the iron(II) LS singlet. Isomer shift δ = 0.4515 mm s^{-1} Lorentzian line width Γ = 0.1698 mm s^{-1} and Site population: 100 %.

Figure 3.13.: Mössbauer spectrum of **1b** recorded at 307 K. The blue line represents the fit for the iron(II) LS singlet. Isomer shift δ 0.3698 mm s^{-1}, Lorentzian line width Γ = 0.1659 mm s^{-1} and Site population: 100 %.

3.9. Cover Picture

EurJIC

European Journal of
Inorganic Chemistry

Fully Electronic
& Printed on Demand

22/2015
1st August Issue
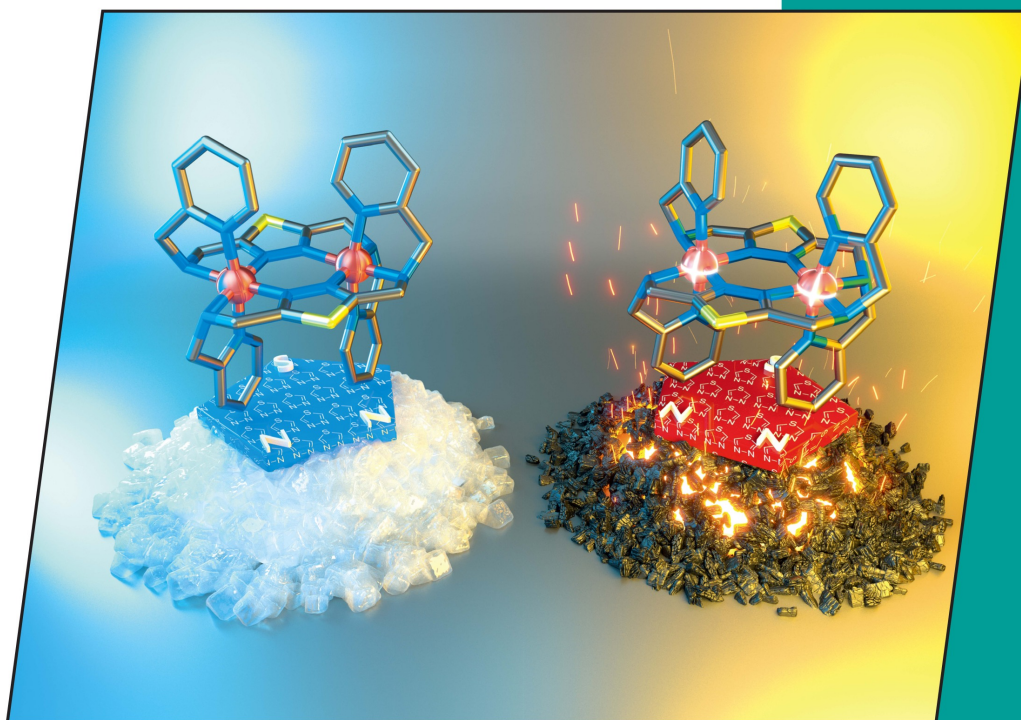
Cover Picture

Eva Rentschler et al.
Dinuclear Iron(II) SCO Compounds

Microreview

Elena G. Zhizhina, Yulia A. Rodikova et al.
Mo-V-Phosphoric Heteropoly Acids and Their Salts

A Journal of

ChemPubSoc
Europe

WILEY-VCH

www.eurjic.org

3.10. Summary

As described in section 3.4, the synthesis of a new 1,3,4-thiadiazole bridging ligand **L1**
(2,5-bis[(2-pyridylmethyl)amino]methyl-1,3,4-thiadiazole) was successful and dinuclear
iron(II) complexes with this ligand could be obtained. The dinuclear iron(II) complexes
consist of two ligand molecules, which are providing 12 nitrogen donor atoms for the N6
coordination sphere of the two iron(II) ions (figure 3.3). The three complexes with the
general formula $[Fe_2(\mu\text{-}L1)_2]X_4$, with three different counteranions [X = BF_4^- (**1**), ClO_4^-
(**2**) and $F_3CSO_3^-$ (**3**)], were obtained as single crystals and characterized with single-
crystal X-ray diffraction, variable-temperature magnetic susceptibility, Mössbauer mea-
surements and elemental analysis. All three complexes stabilize the diamagnetic [LS-
LS] state below room temperature and the magnetic measurements show a gradual
SCO towards high spin states starting at temperatures around room temperature. The
starting temperature and the steepness of the spin transition is the main difference in
the properties of these three complexes (figure 3.4). A similar magnetic behavior could
have been expected as a result of the strong structural similarities of the complexes,
considering the nearly identical Fe-N bond lengths, N-Fe-N bond angles and octahe-
dral distortion parameters Σ (table 3.1). The small differences seen in the magnetic
properties, however, arise from the interactions in the solid state. The counterions are
located near the complex cations in all three cases, forming classical and non-classical
hydrogen bonding interactions between the counterions and aliphatic $-CH_2-NH-CH_2-$
segments of the ligand. These interactions lead to a shift of electron density from the
counterions onto the complex cation and thus vary the ligand field splitting and the spin
transition behavior in this series of complexes.

Overall, the preparation of dinuclear iron(II) complexes with a 1,3,4-thiadiazole bridg-
ing ligand, the realization of the diamagnetic [LS-LS] ground state and preservation of
SCO properties was successful. It is important to mentioned that the reported isostruc-
tural ligand systems with a 1,2,4-triazole, pyrazolate or 1,3,4-oxadiazole heterocycle as
a central motif are unable to stabilize the diamagnetic [LS-LS] state in their dinuclear
iron(II) complexes.

4. Solvent-depending SCO behavior of dinuclear iron(II) complexes with a 1,3,4-thiadiazole bridging ligand

4.1. Introduction

As mentioned in section 1.2.5, non-coordinating solvent molecules can have large effects on the magnetic properties due to interactions in the solid state. Incorporated solvent molecules can cause a shift of the transition temperature, a variation of the shape of the spin transition curve, the spin ground state or even a complete loss of SCO properties. The solvent molecules are arranged near the complexes and mediate intermolecular interactions via classical and non-classical hydrogen bonding interactions.[64,79,110–117,144–149]

While a number of compounds with solvent-depending properties can be found, there is only a handful of examples in literature where solvent effects the spin-crossover behavior reversibly. A SCO-compound that is desolvated reveals a different magnetic property. In some cases, however, it is possible that exposure to the initially incorporated solvent recovers the properties of the solvated compound. Such molecular switches are highly selective chemo sensors for specific solvents. Especially of interest are SCO compounds with such features as they are capable of indicating these sensor properties in different ways. Beside a change of the magnetic moment, the ST often is accompanied by a color change of the complex, that allows to visualize the response on the solvent incorporation.[115–117]

The following chapter deals with a variation of the complex by incorporation of a different solvent. The 1,3,4-thiadiazole based bridging ligand **L1** has already been used in the publication in chapter 3. Switching to a dimethylformamide/diethyl ether mixture during the crystallization of the dinuclear iron(II) complexes resulted in the incorporation of DMF in the single crystals. This drastically influenced the electronic structure of the complexes and changed the SCO properties.

'Solvent-depending SCO behavior of dinuclear iron(II) complexes with a 1,3,4-thiadiazole bridging ligand'
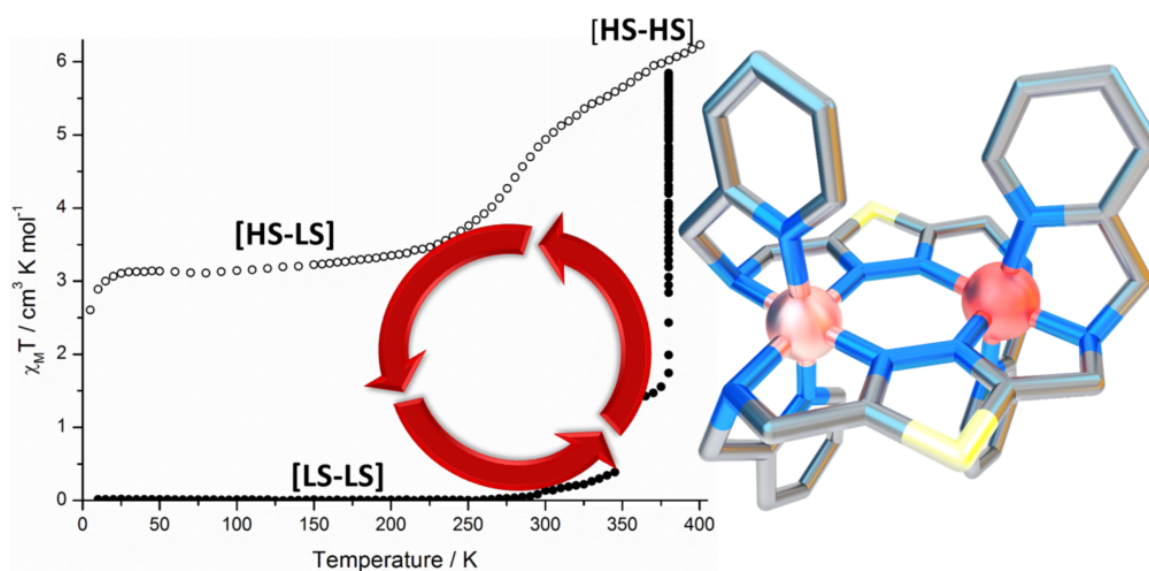
Christian F. Herold, Sergii I. Shylin, and Eva Rentschler

Abstract: Two new dinuclear iron(II) complexes $[Fe_2(\mu\text{-}L1)_2]X_4 \cdot$ 4DMF (X = BF_4^- (**1·4DMF**) and ClO_4^- (**2·4DMF**)) with a 1,3,4-thiadiazole bridging ligand have been synthesized and show a very distinct solvent-depending SCO behavior. The incorporated lattice DMF molecules affect the spin state. This behavior reveals a structural insight into the role of the solvent molecules on the spin transition.

The spin-crossover (SCO) phenomenon in transition metal complexes is still a very promising approach for the development of bistable magnetic materials.[1−3] One of the main advantages of spin-crossover complexes is the possibility to achieve a SCO with hysteresis around room temperature for future applications,[4−6] whereas single-molecule magnets, can only be used as molecular switches at liquid helium temperatures.[7,8] The disadvantage of SCO complexes however, is the strong dependency of the spin state and spin transition on cooperative interactions in the solid state.[1,9] The intermolecular interactions in SCO complexes are most commonly mediated through hydrogen bonding and π-π interactions, with the ligand system and the anions playing an important role.[9−12] A very important factor is the crystal solvent in the SCO compound that can affect the transition temperature, the kind of SCO or even the spin state of the system.[13] These changes can arise from divergent space groups and crystal packing or different hydrogen bonding interactions in the solid state, which influence the ligand field strength.[14] There are different examples in the literature describing solvent effects on the spin transition temperature[15−22], hysteresis width[15,19,22] or the spin state.[23−27] The effect can, in very few cases, even be reversibly triggered by desolvation and resolvation of the solvent molecules.[24−26]

In this paper, we present two dinuclear iron(II) SCO complexes $[Fe_2(\mu\text{-}L1)_2]X_4 \cdot$ 4DMF (X = BF_4^- (**1·4DMF**) and ClO_4^- (**2·4DMF**)) with magnetic properties highly depending on the solvent content in the solid state. The main structure of these complexes is analog to previously reported complexes from our group,[28] with the bis(tridentate) 1,3,4-thiadiazole bridging ligand **L1** (2,5-bis[(2-pyridylmethyl)amino]methyl-1,3,4-thiadiazole). A variation in the complex synthesis resulted in a completely different magnetic behav-

ior due to a different solvent content and molecular arrangement in the solid state.
At first, the complexes were isolated as a precipitate from a methanolic solution, then
the air-stable precipitates were dissolved in dry DMF and layered with dry Et_2O (see
the Supporting Information for details). Single crystals of the desired dinuclear iron(II)
complexes **1·4DMF** and **2·4DMF**, suitable for X-ray diffraction experiments, were iso-
lated and further studied by variable-temperature magnetic susceptibility and Möss-
bauer measurements, IR spectroscopy and elemental analysis.
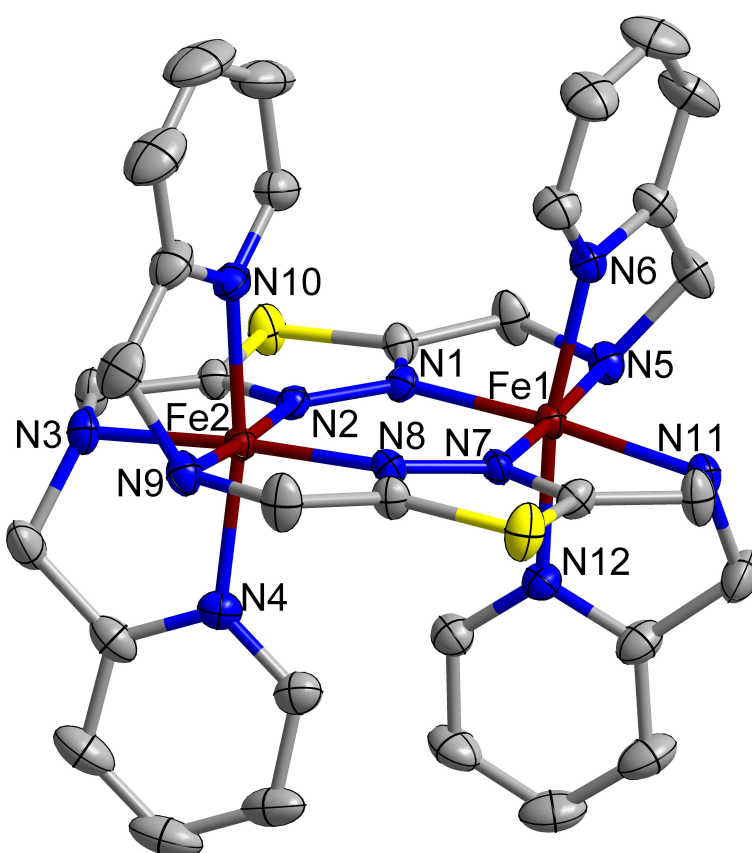
Figure 4.1.: Complex cation $[Fe_2(\mu\text{-L1})_2]^{4+}$ of **1·4DMF** with thermal ellipsoids drawn at
50% probability level. Hydrogen atoms, solvent molecules and counterions are omitted
for clarity.

Both complexes **1·4DMF** and **2·4DMF** crystallize in the *P2*$_1$ space group. Two iron(II)
ions are coordinated by two 1,3,4-thiadiazole bridging ligands **L1** (Figure 4.1) that pro-
vide 12 nitrogen donor atoms for the two FeN6 coordination environments. Each ligand

coordinates with one sidearm up and one down, similar to the previously reported complexes of this ligand.[28]

The average Fe-N bond lengths in **1·4DMF** and **2·4DMF** are in the range between 1.987 Å and 1.992 Å, and the octahedral distortion parameters Σ are between 58.71° and 59.81° (details: supporting information tables 4.1 to 4.3). These are typical values for iron(II) in the LS state.[1,28−30] Complexes **1·4DMF** and **2·4DMF** crystallize with four counterions, to compensate the charge of the complex cation, and four DMF molecules. Interestingly, the interactions between the complex cation and the solvent molecules and counterions are nearly identical for **1·4DMF** and **2·4DMF**. In both cases the four secondary amines of the complex cations form hydrogen bonds to the oxygen of three DMF molecules and to one counterion (Figure 4.2).
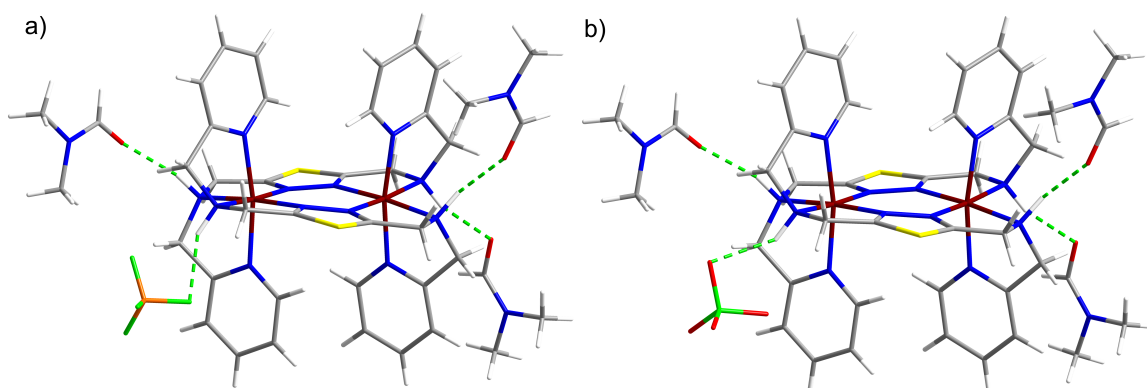
Figure 4.2.: Hydrogen bonding (green broken lines) from N-H groups of the ligand to DMF molecules and counterions (**1**: BF_4^-, **2**: ClO_4^-) in the crystal structures of **1·4DMF** (a) and **2·4DMF** (b), other DMF molecules and counterions are omitted for clarity.

The $\chi_M T$ temperature dependence of crystalline samples of **1·4DMF** and **2·4DMF** was investigated and showed a very unusual behavior.

At low temperatures a completely diamagnetic [LS-LS] ground state was observed, as expected in light of the Fe-N bond lengths from the crystal structures (tables 4.1 to 4.3). At temperatures around 350 K the magnetic susceptibility starts to show a paramagnetic behavior and upon cooling the diamagnetic [LS-LS] state cannot be regained.

A time dependent measurement of the magnetic susceptibility at 380 K showed an
increasing χ_MT value until a saturation was achieved (Figure 4.3, dots). Elemental
analysis and IR spectroscopy (see the Supporting Information for details) proved that
this magnetic behavior is caused by a loss of four DMF molecules from the single crys-
tals upon heating and results in the solvent free complex **1** ([Fe$_2(\mu$-L1)$_2$](BF$_4$)$_4$). This
led to a series of investigations and although the magnetic behavior was observed for
1·4DMF and **2·4DMF** (see Supporting Information Figure 4.9) we here only focus on
compound **1·4DMF** with BF$_4$ as counterion from now on, because the perchlorate com-
plex **2** is potentially explosive and has to be handled with care.
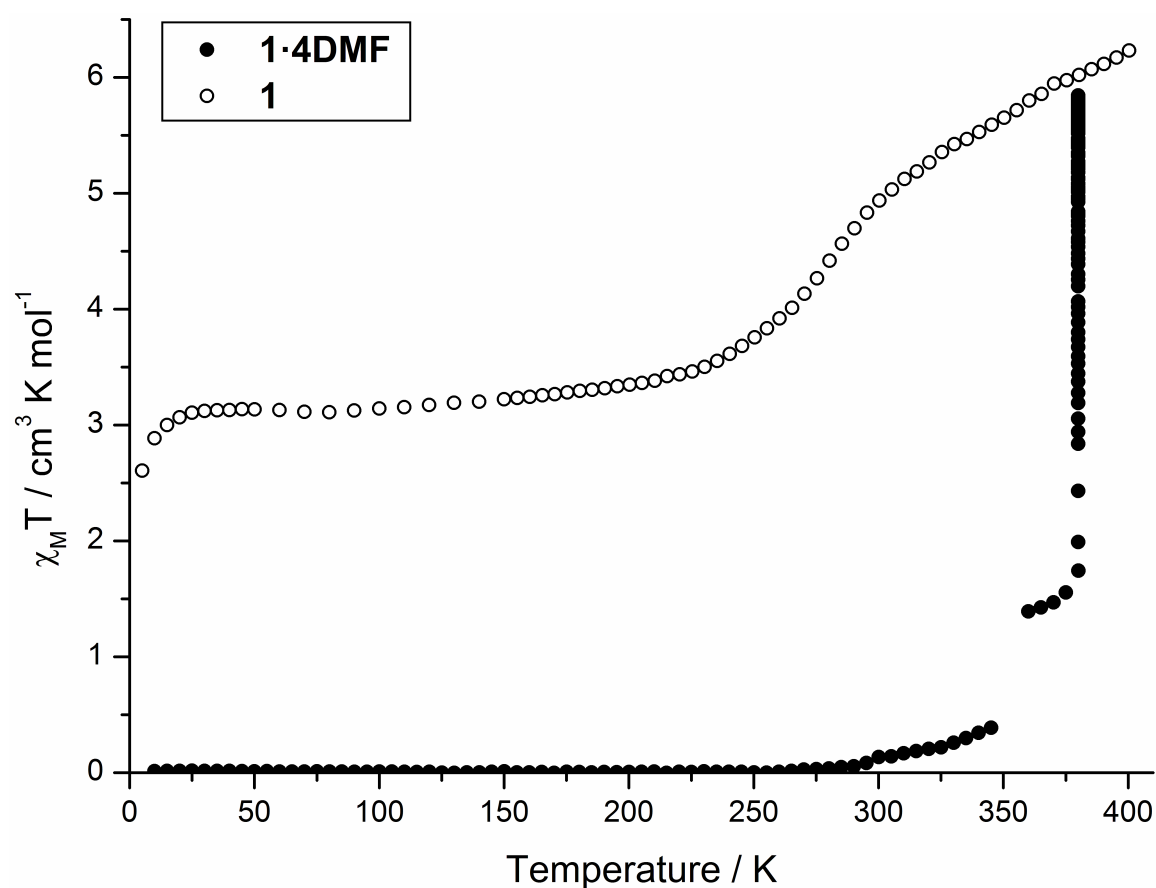
Figure 4.3.: Temperature dependence of χ_MT for compound **1·4DMF** (dots) and **1** (cir-
cles).

After complete desolvation of **1·4DMF**, under high vacuum at 150 °C, the magnetic
moment of the solvent free complex **1** reaches a χ_MT value of 6.23 cm^3 K mol^{-1} at

400 K and corresponds to the expected spin-only value of two HS iron(II) centers.[31]
Upon cooling a gradual spin transition at 280 K can be observed, that results in a large
plateau with a $\chi_M T$ value of 3.22 cm^3 K mol^{-1} at 150 K, which is characteristic for a
SCO of only one iron(II) in a dinuclear complex. Further cooling does not lead to a spin-
crossover to the initial diamagnetic [LS-LS] state. The temperature independence of
the plateau is a sign for a spin transition into the [HS-LS] state at low temperatures and
this has been confirmed with Mössbauer measurements of **1** (Figure 4.4).[32] The Möss-
bauer spectrum at 80 K shows a HS (δ = 1.086(3) mm s^{-1}, ΔE_Q = 2.616(5) mm s^{-1})
and LS (δ = 0.501(2) mm s^{-1}, ΔE_Q = 0.293(2) mm s^{-1}) doublet with an intensity ratio
close to the expected 1:1. At 293 K the relative area of the HS (δ = 0.98(1) mm s^{-1},
ΔE_Q = 2.24(2) mm s^{-1}) doublet increases to 72 % and the LS (δ = 0.40(1) mm s^{-1},
ΔE_Q = 0.17(2) mm s^{-1}) doublet decreases to 28 % which is also in agreement with
the magnetic data. The increased linewidth of the HS doublet at 293 K is a result
of a superposition of two types of HS iron(II), a [HS-LS] and [HS-HS] form. In addi-
tion, the Mössbauer spectrum of **1·4DMF** has been measured and shows a LS doublet
(δ = 0.470(1) mm s^{-1}, ΔE_Q = 0.086(5) mm s^{-1}) with a very small quadrupole splitting
at 80 K (see the Supporting Information for details). This LS doublet differs significantly
from the LS doublet of **1** at low temperatures. Thus, HS iron(II) contributes to the elec-
tric field gradient of neighboring LS iron(II), which leads to increasing of ΔE_Q. This
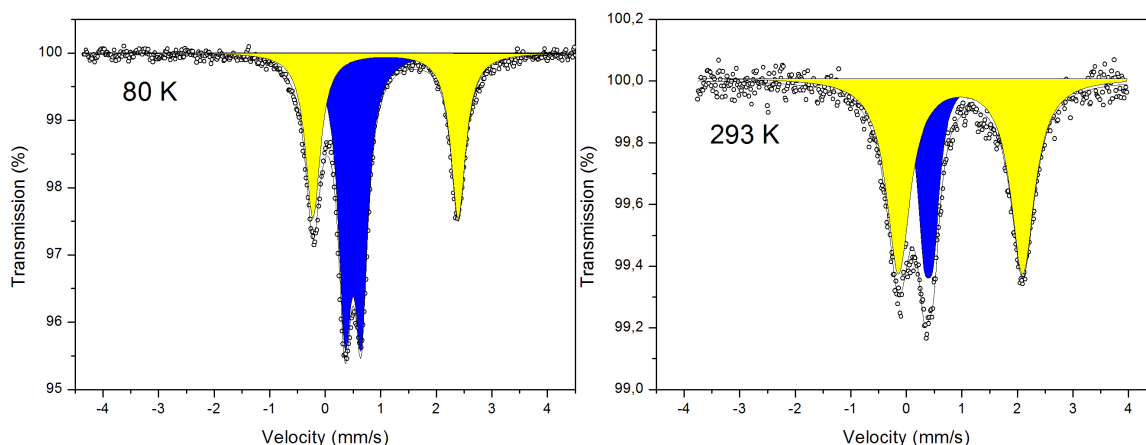feature allows to distinguish LS iron(II) centers in [LS-HS] and [LS-LS] pairs.

Figure 4.4.: Mössbauer spectra of compound **1** at 80 K (left) and 293 K (right).

The fact that **1** does not reach the [LS-LS] state at low temperatures indicates that the

DMF and their hydrogen bonds to the secondary amines of the complex cations play a very important role. Similar to previous studies,[13,27] there seems to be an increase of electron density on the nitrogen donor atom due to the hydrogen bond to the oxygen atom of the DMF molecule (Figure 4.2). That can also be seen in the IR spectrum of **1·4DMF** (see the Supporting Information for details) where the ν(C=O) stretching vibration of the DMF is at lower energies, showing a shift of electron density to-wards the secondary amine of the complex cation. This leads to a stabilization of the diamagnetic [LS-LS] state, while removal of the solvent results in a change of the spin state.
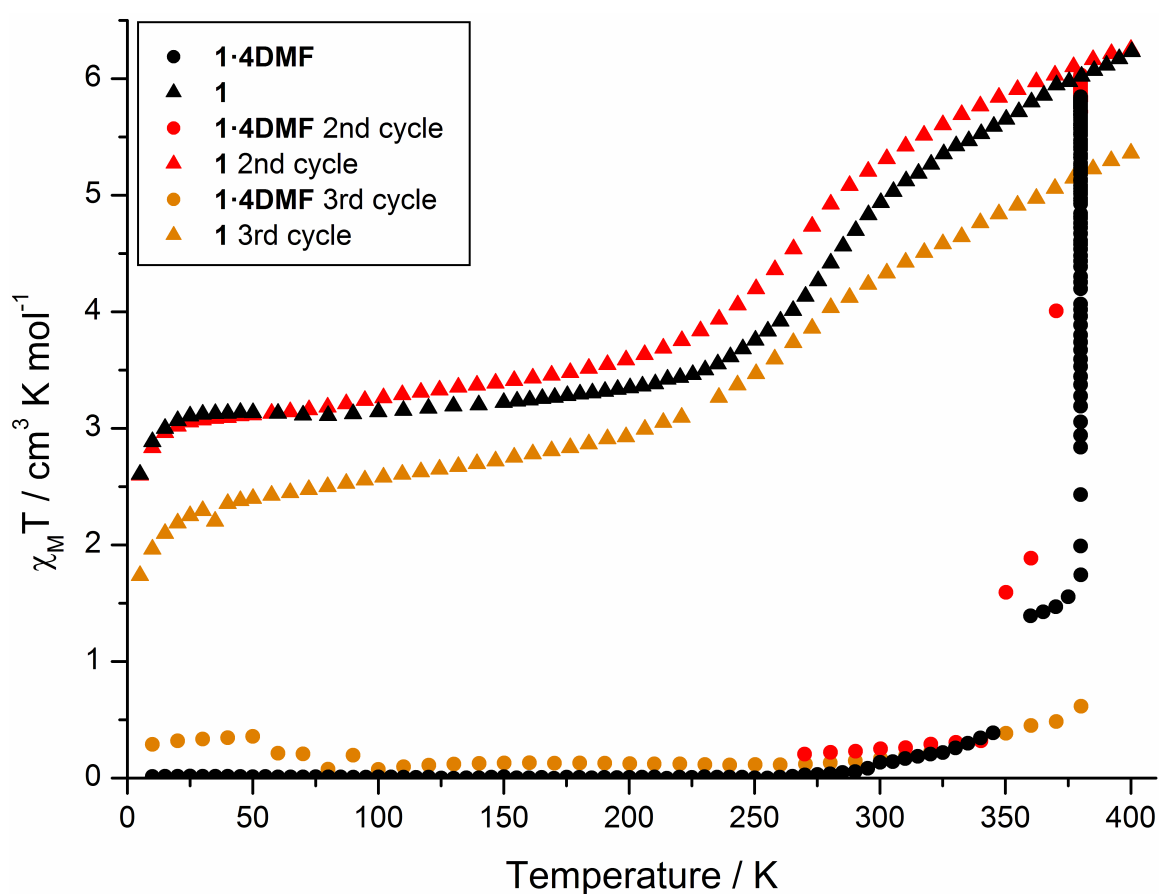
Figure 4.5.: Temperature dependence of χ_MT for for multiple desolvation/resolvation cycles of the com-pounds **1·4DMF** (dots) and **1** (triangles).

Further studies showed that **1** can be resolvated with DMF via vapor diffusion to regain the [LS-LS] state and it is possible to carry out multiple desolvation and resolvation cycles (Figure 5). The compound always returns to the [LS-LS] state via resolvation or the

[HS-HS] form, which can switch into the [HS-LS] state, by desolvation under reduced pressure.

The reason for the decreasing $\chi_M T$ value in further cycles is the hygroscopic nature of **1** and the partial formation of an aqua complex **1·H$_2$O**. This complex shows a [LS-LS] ground state and a gradual and incomplete SCO above 250 K, but cannot be desolvated again (Figure 4.11). These magnetic properties are nearly identical to those of the previously reported and analogue [Fe$_2$(μ-L1)$_2$](BF$_4$)$_4$*2H$_2$O,[28] which was synthesized in a different way and also stabilizes the [LS-LS] state at low temperatures and shows a gradual and incomplete SCO around 250 K. So the important connection between the two complexes, that has to be looked at, is the water in the compounds and the importance of the solvent content in the field of SCO. The presence of water inhibits the realization of the [HS-HS] state and result in the previously reported SCO properties.[28] Since we are unsuccessful to crystallize compound **1·H$_2$O** in its exact composition it is not possible to discuss the direct effect of the water on the iron(II) centers. As a reason why we can resolvate and desolvate the complex with the higher boiling DMF but not with water we assume that there are stronger interactions between the complex cation and the water, compared to the interactions with the DMF.

In conclusion, we were able to synthesize and characterize two forms of a dinuclear iron(II) SCO complex [Fe$_2$(μ-L1)$_2$]X$_4$, which show a completely different magnetic behavior in comparison to our previously complexes, that show a gradual and incomplete ST. These complexes exist in the [LS-LS] state, display a solvent-depending spin state switching into the [HS-HS] state upon heating and show a SCO into the [HS-LS] state upon cooling. A return into the [LS-LS] state is not possible at lower temperatures, however a resolution with the lost DMF via diffusion results in the formation of the initial [LS-LS] complex. Therefore, the complex **1·4DMF/1** can be considered as a perfect example for a chemo sensor for DMF, based on a SCO complex. Exposure to water results in an irreversible formation of **1·H$_2$O** and quenching of the reversible solvent-depending properties.

References

1. Gütlich, P.; Goodwin, H. A., In *Top. Curr. Chem.*, Springer Berlin Heidelberg: **2004**; pp 1-47.

2. Cambi, L.; Szegö, L., *Ber. Dtsch. Chem. Ges.* **1931**, *64*, 2591-2598.

3. Halcrow, M. A., *Chem. Commun.* **2013**, *49*, 10890-10892.

4. Dîrtu, M. M.; Neuhausen, C.; Naik, A. D.; Rotaru, A.; Spinu, L.; Garcia, Y., *Inorg. Chem.* **2010**, *49*, 5723-5736.

5. Virginie Niel; José María Martinez-Agudo; M. Carmen Muñoz; Ana Belén Gaspar; José Antonio Real, *Inorg. Chem.* **2001**, *40*, 3838-3839

6. Krober, J.; Codjovi, E.; Kahn, O.; Groliere, F.; Jay, C., *J. Am. Chem. Soc.* **1993**, *115*, 9810-9811

7. Rosado Piquer, L.; Sanudo, E. C., *Dalton Trans.* **2015**, *44*, 8771-8780.

8. Woodruff, D. N.; Winpenny, R. E.; Layfield, R. A., *Chem. Rev.* **2013**, *113*, 5110-5148.

9. Murray, K. S.; Kepert, C. J., *Top. Curr. Chem.*, Springer Berlin Heidelberg: **2004**; Vol. *233*, pp 195-228.

10. Zheng, S.; Siegler, M. A.; Roubeau, O.; Bonnet, S., *Inorg. Chem.* **2014**, *53*, 13162-13173.

11. Nassirinia, N.; Amani, S.; Teat, S. J.; Roubeau, O.; Gamez, P., *Chem. Commun.* **2014**, *50*, 1003-1005.

12. Arcis-Castillo, Z.; Zheng, S.; Siegler, M. A.; Roubeau, O.; Bedoui, S.; Bonnet, S., *Chem. Eur. J.* **2011**, *17*, 14826-14836.

13. Greenaway, A. M.; Sinn, E., *J. Am. Chem. Soc.* **1978**, *100*, 8080-8084.

14. Gütlich, P.; Hauser, A.; Spiering, H., *Angew. Chem., Int. Ed.* **1994**, *33*, 2024-2054

15. Harding, D. J.; Phonsri, W.; Harding, P.; Gass, I. A.; Murray, K. S.; Moubaraki, B.; Cashion, J. D.; Liu, L.; Telfer, S. G., *Chem. Commun.* **2013**, *49*, 6340-6342.

16. Amoore, J. J.; Kepert, C. J.; Cashion, J. D.; Moubaraki, B.; Neville, S. M.; Murray, K. S., *Chem. Eur. J.* **2006**, *12*, 8220-8227.

17. Rajadurai, C.; Qu, Z.; Fuhr, O.; Gopalan, B.; Kruk, R.; Ghafari, M.; Ruben, M., *Dalton Trans.* **2007**, *32*, 3531-3537.

18.   Bartel, M.; Absmeier, A.; Jameson, G. N. L.; Werner, F.; Kato, K.; Takata, M.;
Boca, R.; Hasegawa, M.; Mereiter, K.; Caneschi, A.; Linert, W., *Inorg. Chem.*
2007, *46*, 4220-4229.

19.   Chuang, Y. C.; Liu, C. T.; Sheu, C. F.; Ho, W. L.; Lee, G. H.; Wang, C. C.;
Wang, Y., *Inorg. Chem.* **2012**, *51*, 4663-4671.

20.   Leita, B. A.; Neville, S. M.; Halder, G. J.; Moubaraki, B.; Kepert, C. J.;
Letard, J. F.; Murray, K. S., *Inorg. Chem.* **2007**, *46*, 8784-8795.

21.   Zhang, W.; Zhao, F.; Liu, T.; Yuan, M.; Wang, Z. M.; Gao, S., *Inorg. Chem.*
2007, *46*, 2541-2555.

22.   Vieira, B. J. C.; Dias, J. C.; Santos, I. C.; Pereira, L. C. J.; da Gama, V.;
Waerenborgh, J. C., *Inorg. Chem.* **2015**, *54*, 1354-1362.

23.   Kanegawa, S.; Kang, S.; Sato, O., *Eur. J. Inorg. Chem.* **2013**, 725-729.

24.   Wang, H.; Sinito, C.; Kaiba, A.; Costa, J. S.; Desplanches, C.; Dagault, P.;
Guionneau, P.; Létard, J.-F.; Negrier, P.; Mondieig, D., *Eur. J. Inorg. Chem.*
2014, 4927-4933.

25.   Lennartson, A.; Southon, P.; Sciortino, N. F.; Kepert, C. J.; Frandsen, C.; Mor-
up, S.; Piligkos, S.; McKenzie, C. J., *Chem. Eur. J.* **2015**, *21*, 16066-16072.

26.   Steinert, M.; Schneider, B.; Dechert, S.; Demeshko, S.; Meyer, F., *Angew.
Chem., Int. Ed.* **2014**, *53*, 6135-6139.

27.   Giménez-López, M. C.; Clemente-León, M.; Coronado, E.; Romero, F. M.;
Shova, S.; Tuchagues, J.-P., *Eur. J. Inorg. Chem.* **2005**, 2783-2787.

28.   Herold, C. F.; Carrella, L. M.; Rentschler, E., *Eur. J. Inorg. Chem.* **2015**,
3632-3636.

29.   Klingele, M. H.; Moubaraki, B.; Cashion, J. D.; Murray, K. S.; Brooker, S.,
Chem. Commun. **2005**, 987-989.

30.   Gütlich, P.; Gaspar, A. B.; Garcia, Y., *Beilstein J. Org. Chem.* **2013**, *9*, 342-391.

31.   Ksenofontov, V.; Gaspar, A. B.; Niel, V.; Reiman, S.; Real, J. A.; Gütlich, P.,
Chem. Eur. J. **2004**, *10*, 1291-1298.

32.   Real, J. A.; Gaspar, A. B.; Muñoz, M. C.; Gütlich, P.; Ksenofontov, V.; Spiering,
H., In *Top. Curr. Chem.*, Springer Berlin Heidelberg: **2004**; pp 167-193.

4.2. Supporting Information

4.2.1. Experimental Section

General Methods and Materials:

All chemicals were purchased from Alfa Aesar, Deutero, Fisher Chemicals, Sigma-Aldrich and Acros Organics and used without further purification. The solvents for the complex synthesis were degassed with Argon. Magnetic susceptibility data was collected with a Quantum Design SQUID magnetometer MPMSXL in a temperature range of 2-400 K with an applied field of 1 kOe. ^{57}Fe Mössbauer spectra were recorded and analyzed by fitting to Lorentzian lines at the Johannes Gutenberg-University Mainz by Sergii I. Shylin and Dr. Vadim Ksenofontov. Elemental analysis (C, H, N and S) was measured at the micro-analytical laboratories of the Johannes Gutenberg-University Mainz. Infrared spectra (FT-IR) were recorded as potassium bromide pellets in the range from 4000 cm^{-1} to 400 cm^{-1} with a JASCO FT/IR-4200 at the Johannes Gutenberg-University Mainz. X-ray diffraction data were collected with a Bruker SMART at the Johannes Gutenberg-University Mainz at 173 K (**1·4DMF**) and 193 K respectively (**2·4DMF**). The structures were solved with superflip[1] and olex2.solve, and refined with SHELXL[2] with the program Olex2.[3] CCDC-1448812 (for **1·4DMF**) and -1448813 (for **2·4DMF**) contain the supplementary crystallographic data for this paper. These data can be obtained free of charge from The Cambridge Crystallographic Data Centre via www.ccdc.cam.ac.uk/data_request/cif.

Synthesis:

The 1,3,4-thiadiazole bridging ligand L1 (2,5-bis[(2-pyridylmethyl)amino]methyl-1,3,4-thiadiazole) was prepared according to the previously described procedure.[4]

Caution! *The prepared perchlorate complexes are potentially explosive. Even though ne explosions occurred, only small amounts should be prepared and handled with care!*

Synthesis of [Fe$_2$(μ-L1)$_2$](BF$_4$)$_4$*4DMF (1·4DMF):

An orange solution of 2,5-bis[(2-pyridylmethyl)amino]methyl-1,3,4-thiadiazole (L1) (261 mg, 0.8 mmol) in methanol (10 mL) was added to a solution of Fe(BF$_4$)*6H$_2$O (270 mg, 0.8 mmol) in methanol (15 mL) and immediately a light brown precipitate was formed. The reaction mixture was stirred for one hour, the precipitate filtered and washed with methanol.

Yield: 264 mg (0.24 mmol, 59 %).

Single crystals of **1·4DMF** were obtained by dissolving the light brown precipitate in dry dimethylformamide and layering the dark red solution with dry diethyl ether. The dark red single crystals were isolated after 3-4 weeks and complete diffusion of the solvents.

Elemental Analysis: C$_{44}$H$_{64}$B$_4$F$_{16}$Fe$_2$N$_{16}$S$_2$O$_4$ ([Fe$_2$(μ-L1)$_2$](BF$_4$)$_4$*4DMF): calc. C 37.64, H 4.59, N 15.96, S 4.57; found C 37.83, H 4.26, N 16.34, S 4.69.
IR(KBr, cm^{-1}): 3425(w), 3099(w), 2903(w), 1656(m), 1610(s), 1488(s), 1439(s), 1388(s), 1295(s), 1253(m), 1084(w), 1058(w), 1038(w), 896(m), 767(s), 661(s), 533(s), 522(s).

Preparation of **1** after dehydration of **1·4DMF** under HV at 150°C:
Elemental Analysis: C$_{32}$H$_{36}$B$_4$F$_{16}$Fe$_2$N$_{12}$S$_2$ ([Fe$_2$(μ-L1)$_2$](BF$_4$)$_4$): calc. C 34.57, H 3.26, N 15.12, S 5.77; found C 34.46, H 3.21, N 15.11, S 5.90.
IR(KBr, cm^{-1}): 3431(w), 3103(w), 2905(w), 1631(w), 1610(s), 1572(s), 1487(s), 1442(m), 1385(m), 1350(m), 1296(m), 1083(w), 1057(w), 898(m), 771(s), 533(s), 522(s).

Preparation of **1·H$_2$O**:
A sample of **1·H$_2$O** was obtained by vapor diffusion of water into a powder sample of **1**.

Elemental Analysis: C$_{32}$H$_{38}$B$_4$F$_{16}$Fe$_2$N$_{12}$S$_2$O ([Fe$_2$(μ-L1)$_2$](BF$_4$)$_4$*1H$_2$O): calc. C 34.02, H 3.39, N 14.88; found C 34.15, H 3.05, N 14.73.

Synthesis of [Fe$_2$(μ-L1)$_2$](ClO$_4$)$_4$*4DMF (2·4DMF):

An orange solution of 2,5-bis[(2-pyridylmethyl)amino]methyl-1,3,4-thiadiazole (L1) (261 mg, 0.8 mmol) in methanol (10 mL) was added to a solution of Fe(BF$_4$)*6H$_2$O (270 mg, 0.8 mmol) in methanol (15 mL) and immediately a light brown precipitate was formed. The reaction mixture was stirred for one hour, the precipitate filtered and washed with methanol.

Yield: 242 mg (0.21 mmol, 52 %).

Single crystals of **2·4DMF** were obtained by dissolving the light brown precipitate in dry dimethylformamide and layering the dark red solution with dry diethyl ether. The dark red single crystals were isolated after 3-4 weeks and complete diffusion of the solvents.

Elemental Analysis: C$_{44}$H$_{64}$Cl$_4$Fe$_2$N$_{16}$S$_2$O$_{20}$ ([Fe$_2$(μ-L1)$_2$](BF$_4$)$_4$*4DMF): calc. C 36.33, H 4.43, N 15.41, S 4.41; found C 36.53, H 4.05, N 15.84, S 4.68.

IR(KBr, cm^{-1}): 3428(w), 3097(w), 2904(w), 1714(s), 1658(w), 1488(s), 1440(m), 1385(s), 1292(s), 1145(m), 1118(m), 1081(m), 766(s), 668(m), 635(s), 626(s).

4.2.2. Crystallographic Data

Table 4.1.: Crystallographic parameters for compounds **1·4DMF** and **2·4DMF**

	1·4DMF	**2·4DMF**
formula	$C_{44}H_{64}B_4F_{16}Fe_2N_{16}O_4S_2$	$C_{44}H_{64}Cl_4Fe_2N_{16}O_{20}S_2$
formula weight	1404.17	1456.73
crystal system	monoclinic	monoclinic
space group	$P2_1$	$P2_1$
a / Å	11.2504(7)	11.2852(13)
b / Å	23.3121(17)	23.6660(3)
c / Å	11.3825(6)	11.4497(13)
α / °	90	90
β / °	93.733(2)	93.887(2)
γ / °	90	90
V / Å^3	2979.0(3)	3050.9(6)
Z	2	2
T / K	173	193
$\rho_{calcd.}$ [g/cm^3]	1.565	1.584
μ [mm-1]	0.664	0.804
R(int)	0.0546	0.0303
S	0.956	1.037
R1 (I > 2σ(I))	0.0369	0.0390
wR2 (all data)	0.0844	0.0933
av. Fe-N / Å$^{[a]}$	1.987/1.990	1.989/1.992
Σ / ° [a],[b]	59.13/59.66	58.71/59.81

[a] Fe1/Fe2. [b] Octahedral distortion parameter Σ (sum of the deviation from 90° of the 12 cis-N-Fe-N angles in the FeN6 coordination sphere).

Table 4.2.: Selected bond lengths (Å) and angles (°) for compound of **1· 4DMF**.

| Fe-N bond lengths		N-Fe-N angles	
Fe1-N1	1.935(2)	N1-Fe1-N5	83.00(10)
Fe1-N5	2.024(2)	N1-Fe1-N6	95.27(14)
Fe1-N6	1.991(3)	N1-Fe1-N7	96.84(10)
Fe1-N7	1.942(2)	N1-Fe1-N11	175.21(14)
Fe1-N11	2.034(3)	N1-Fe1-N12	92.18(14)
Fe1-N12	1.994(3)	N5-Fe1-N11	97.38(11)
		N6-Fe1-N5	81.96(14)
Fe2-N2	1.945(2)	N6-Fe1-N11	89.51(12)
Fe2-N3	2.036(3)	N7-Fe1-N5	176.14(16)
Fe2-N4	2.003(3)	N7-Fe1-N6	94.23(14)
Fe2-N8	1.932(2)	N7-Fe1-N11	83.11(11)
Fe2-N9	2.038(3)	N7-Fe1-N12	92.28(14)
Fe2-N10	1.987(3)	N12-Fe1-N5	91.57(14)
		N12-Fe1-N6	169.46(13)
		N12-Fe1-N11	83.04(12)
		N2-Fe2-N3	82.64(10)
		N2-Fe2-N4	94.99(14)
		N2-Fe2-N9	175.50(15)
		N2-Fe2-N10	93.29(14)
		N4-Fe2-N3	82.59(14)
		N4-Fe2-N9	89.48(13)
		N4-Fe2-N10	169.02(12)
		N8-Fe2-N2	96.81(10)
		N8-Fe2-N3	175.61(15)
		N8-Fe2-N4	93.12(14)
		N8-Fe2-N9	83.45(11)
		N8-Fe2-N10	93.04(14)
		N9-Fe2-N3	97.44(11)
		N10-Fe2-N3	91.34(14)
		N10-Fe2-N9	82.21(13)

Table 4.3.: Selected bond lengths (Å) and angles (°) for compound of **2· 4DMF**.

Fe-N bond lengths		N-Fe-N angles	
Fe1-N1	1.934(3)	N1-Fe1-N5	82.98(11)
Fe1-N5	2.033(3)	N1-Fe1-N6	94.77(14)
Fe1-N6	1.995(3)	N1-Fe1-N7	96.84(11)
Fe1-N7	1.940(3)	N1-Fe1-N11	175.54(14)
Fe1-N11	2.041(3)	N1-Fe1-N12	92.68(14)
Fe1-N12	1.990(3)	N5-Fe1-N11	97.34(12)
		N6-Fe1-N5	82.14(15)
Fe2-N2	1.942(3)	N6-Fe1-N11	89.68(13)
Fe2-N3	2.041(3)	N7-Fe1-N5	176.04(16)
Fe2-N4	1.994(3)	N7-Fe1-N6	93.94(14)
Fe2-N8	1.935(3)	N7-Fe1-N11	83.15(11)
Fe2-N9	2.040(3)	N7-Fe1-N12	92.60(14)
Fe2-N10	1.997(4)	N12-Fe1-N5	91.36(14)
		N12-Fe1-N6	169.43(13)
		N12-Fe1-N11	82.87(13)
		N2-Fe2-N3	82.74(11)
		N2-Fe2-N4	95.04(15)
		N2-Fe2-N9	175.64(16)
		N2-Fe2-N10	93.06(15)
		N4-Fe2-N3	82.65(15)
		N4-Fe2-N9	89.30(14)
		N4-Fe2-N10	169.13(12)
		N8-Fe2-N2	97.04(11)
		N8-Fe2-N3	175.63(16)
		N8-Fe2-N4	93.03(14)
		N8-Fe2-N9	83.01(12)
		N8-Fe2-N10	93.15(14)
		N9-Fe2-N3	97.54(12)
		N10-Fe2-N3	91.23(14)
		N10-Fe2-N9	82.58(14)
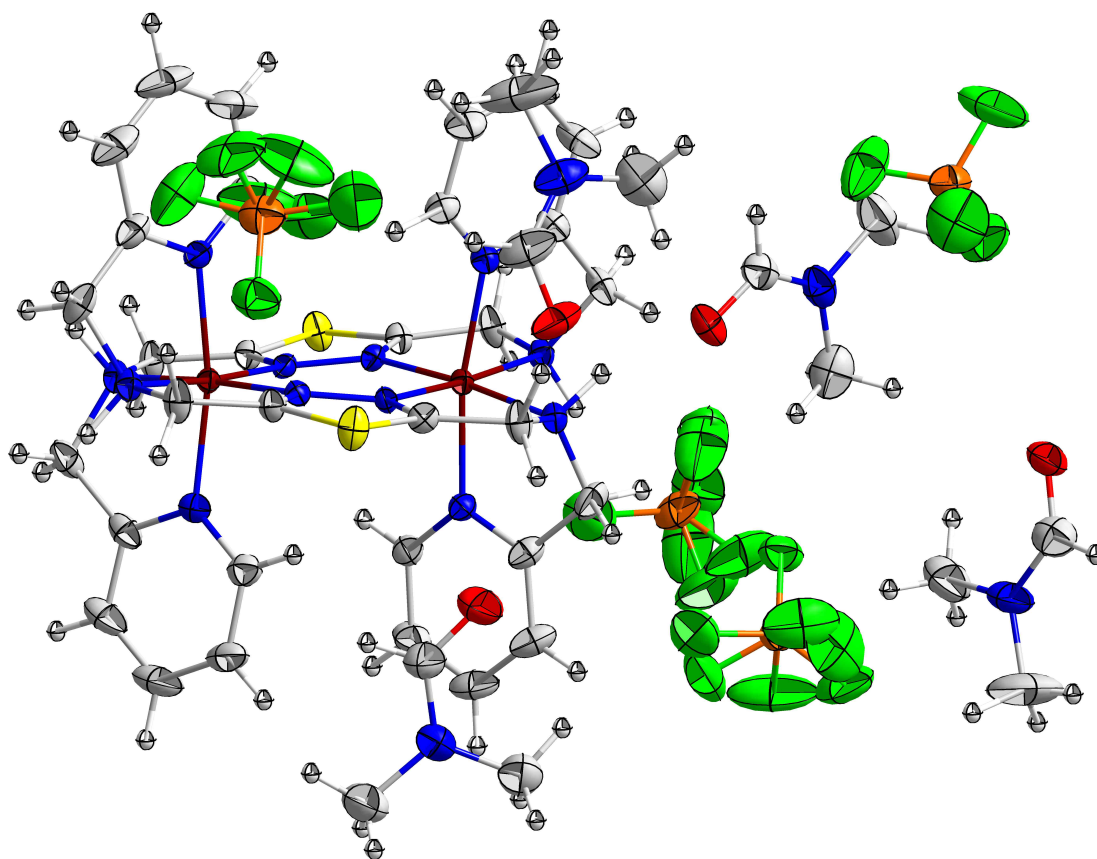
Figure 4.6.: Crystal structure of **1· 4DMF** ([Fe$_2$(μ-L1)$_2$](BF$_4$)$_4$*4DMF).

With thermal ellipsoids drawn at 50% probability level. Colour scheme: dark red - Fe, yellow - S, blue - N, red - O, orange - B, green - F, grey - C, white - H.
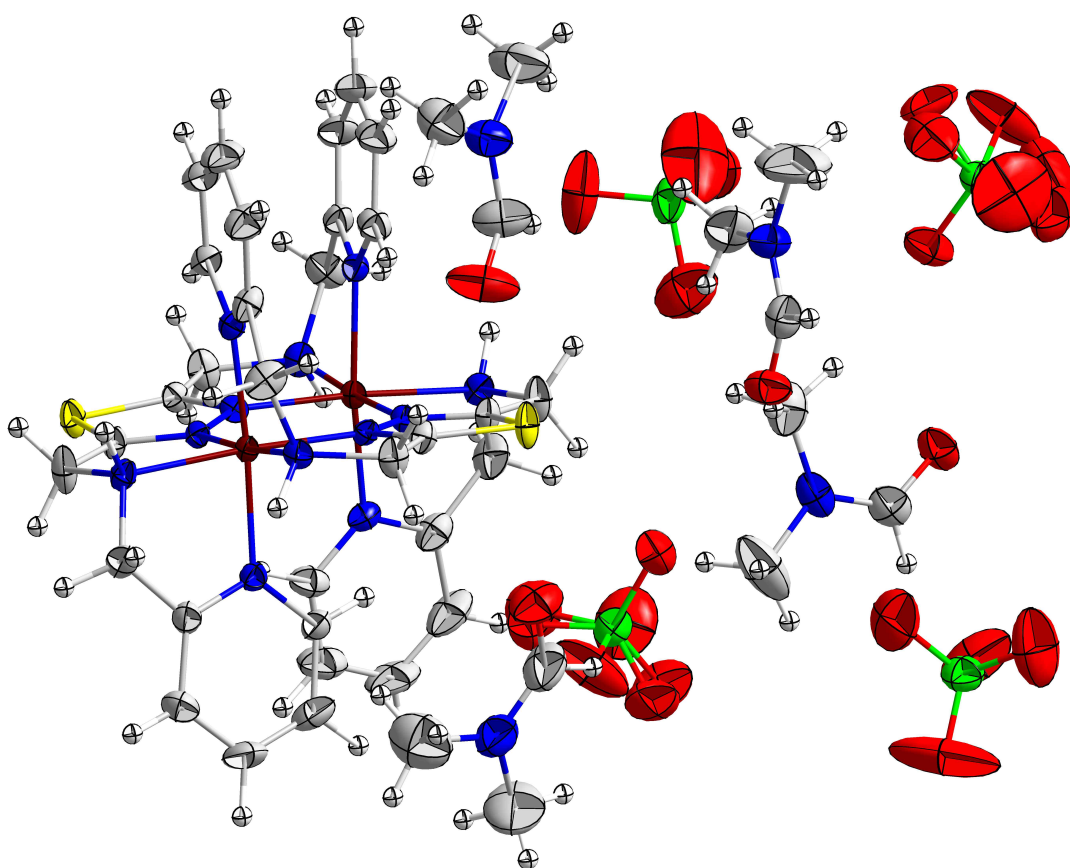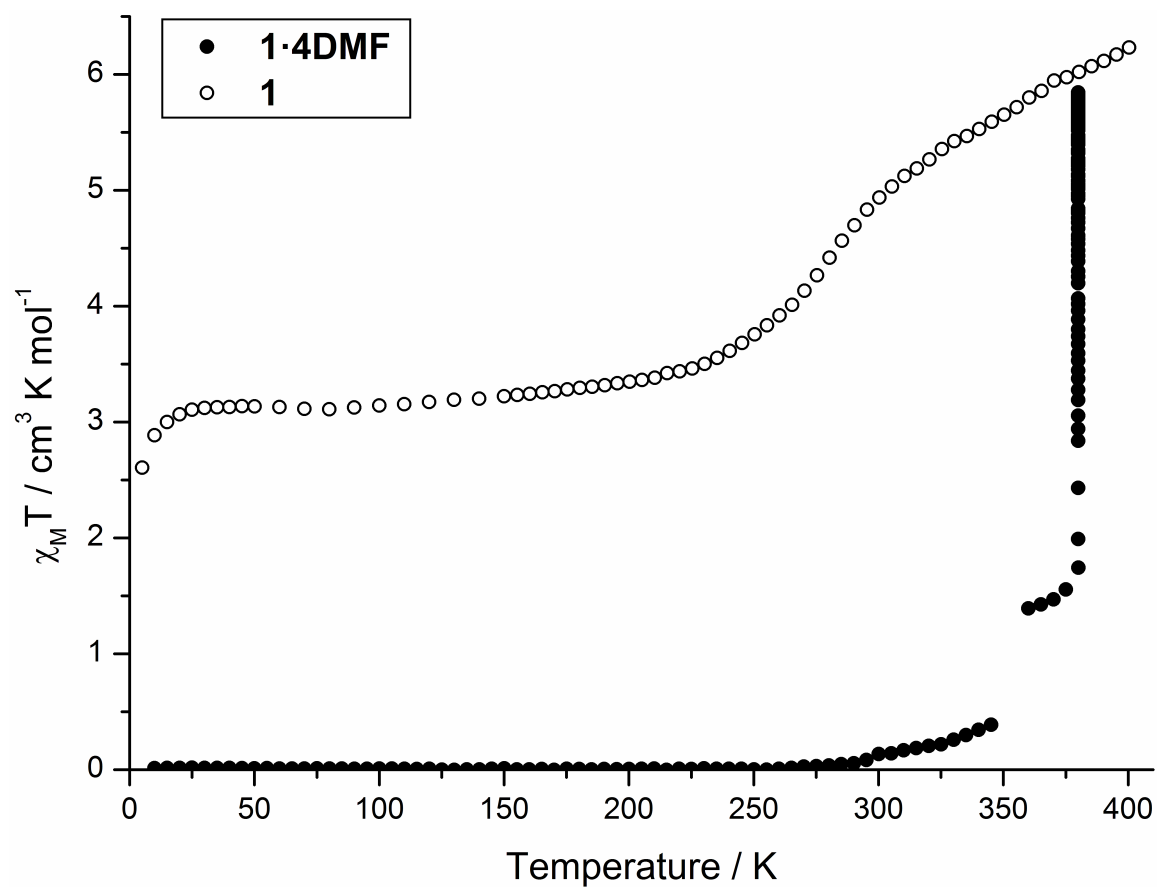
Figure 4.7.: Crystal structure of **2· 4DMF** ([Fe$_2$(μ-L1)$_2$](ClO$_4$)$_4$*4DMF).

With thermal ellipsoids drawn at 50% probability level. Colour scheme: dark red - Fe,
yellow - S, blue - N, red - O, green - Cl, grey - C, white - H.

4.2.3. Magnetic Measurements

Figure 4.8.: Temperature dependence of $\chi_M T$ for compound **1· 4DMF** ([Fe$_2$(μ-L1)$_2$](BF$_4$)$_4$*4DMF) and **1** ([Fe$_2$(μ-L1)$_2$](BF$_4$)$_4$).

Figure 4.9.: Temperature dependence of $\chi_M T$ for compound **2· 4DMF** ([Fe$_2$(μ-L1)$_2$](ClO$_4$)$_4$*4DMF) and **2** ([Fe$_2$(μ-L1)$_2$](ClO$_4$)$_4$).
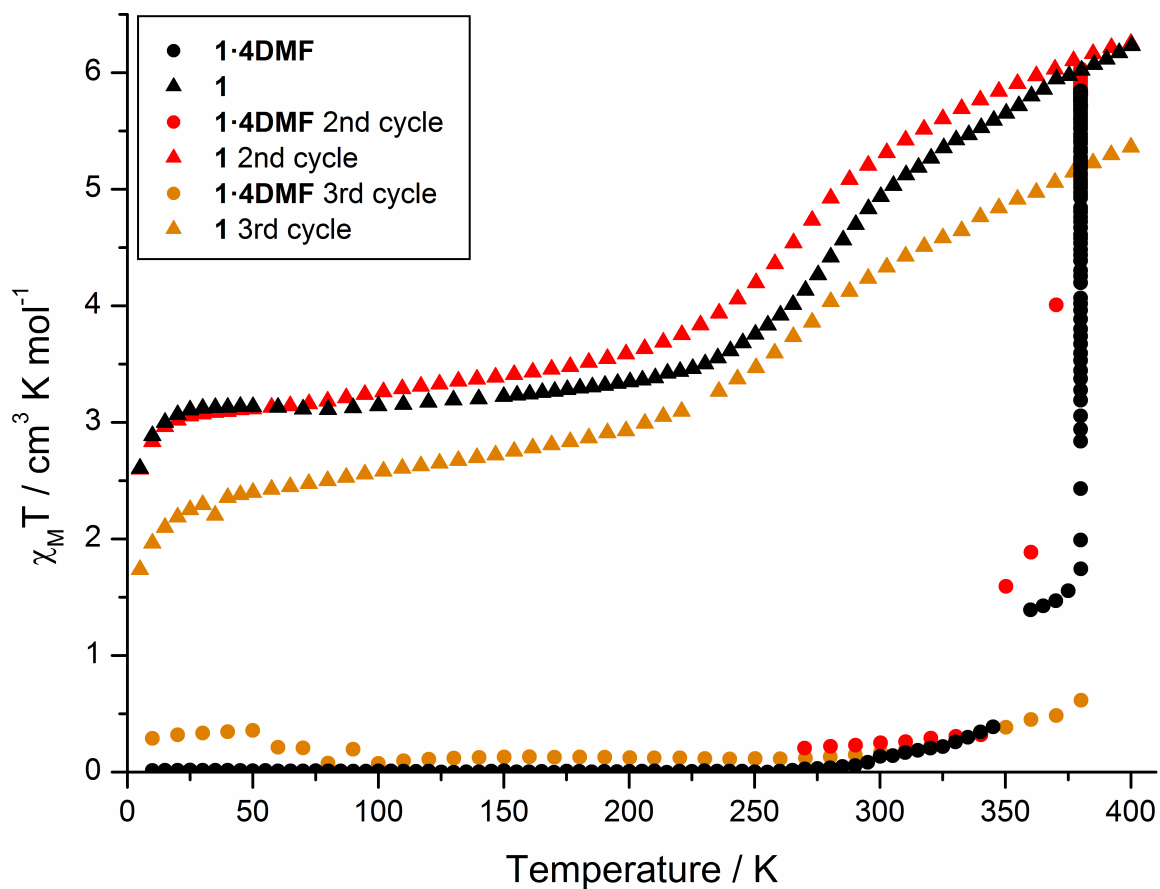
Figure 4.10.: Temperature dependence of $\chi_M T$ for multiple desolvation/resolvation cycles of the compounds **1·4DMF** ([Fe$_2$(μ-L1)$_2$](BF$_4$)$_4$*4DMF) (dots) and **1** ([Fe$_2$(μ-L1)$_2$](BF$_4$)$_4$) (triangles).
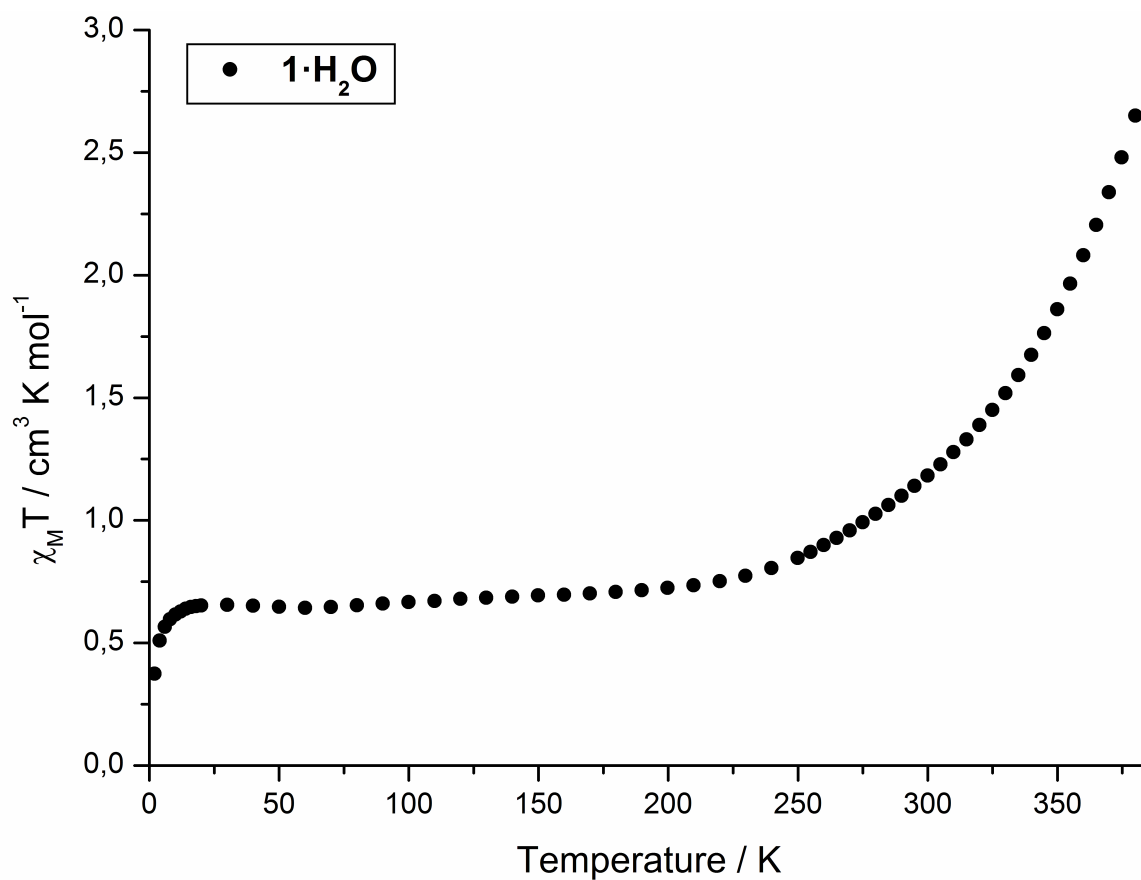
Figure 4.11.: Temperature dependence of $\chi_M T$ for compound **1**· **H$_2$O** ([Fe$_2$(μ-L1)$_2$] (BF$_4$)$_4$*1H$_2$O).

4.2.4. Mössbauer Spectroscopy
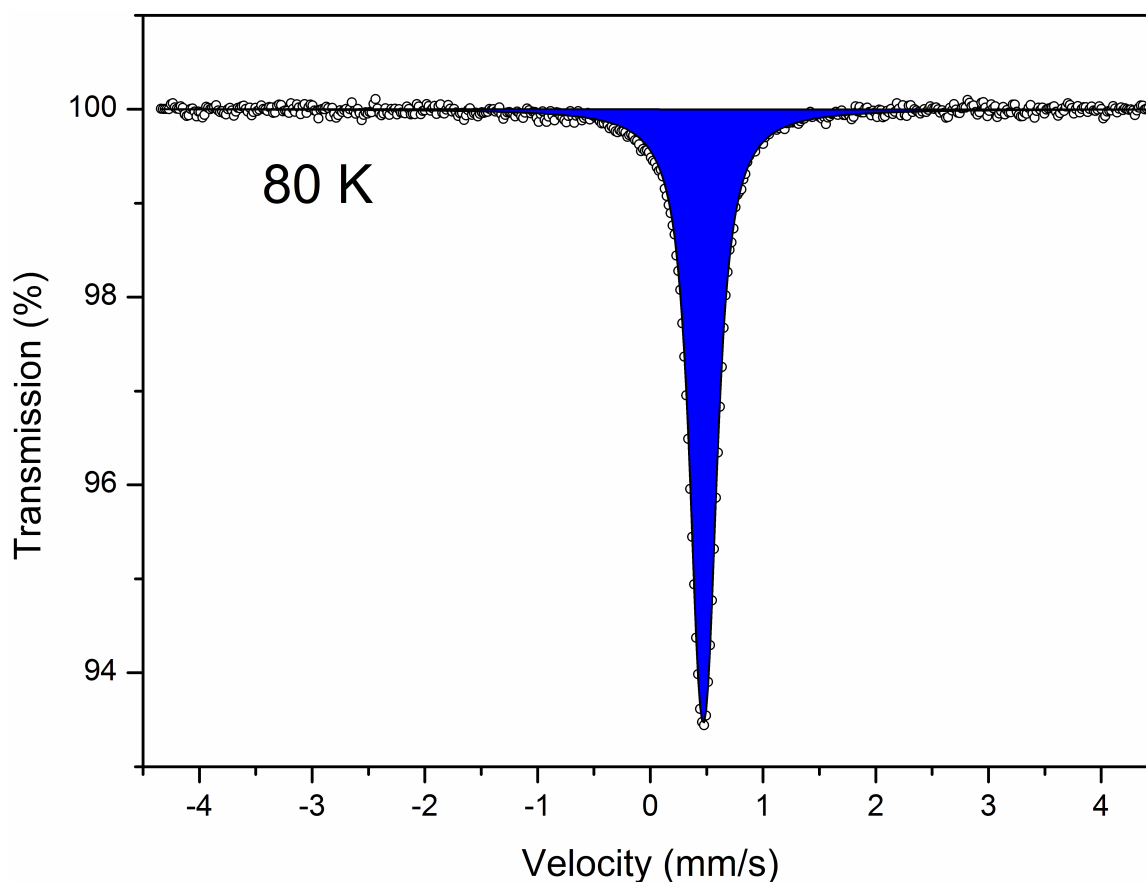
Figure 4.12.: Mössbauer spectrum of compound **1· 4DMF** ([Fe$_2$(μ-L1)$_2$](BF$_4$)$_4$*4DMF) at 80 K.

Table 4.4.: Mössbauer parameters for compound **1· 4DMF** at 80 K with the isomer shift δ, quadrupole splitting ΔE_Q, lorentzian line width Γ and site population.

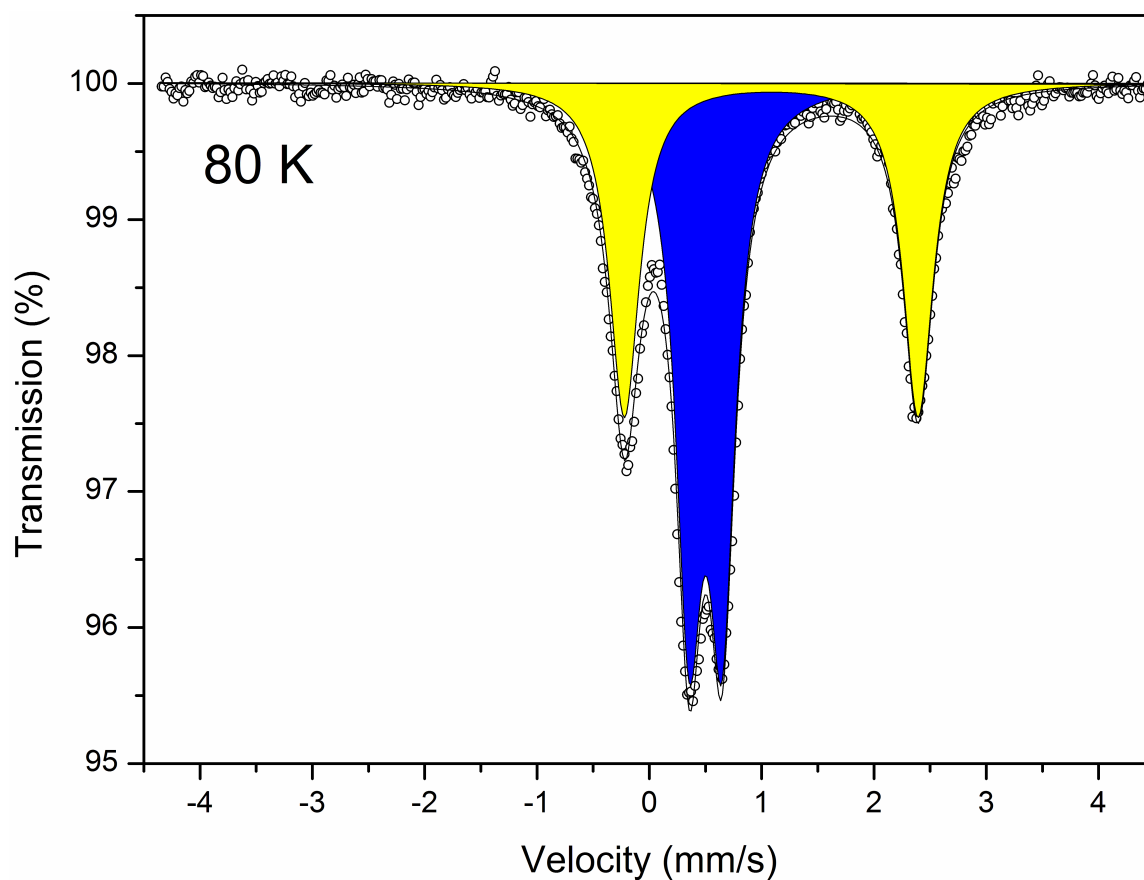| Site parameters	Isomer Shift	Quadrupole Splitting	Lorentzian line width	Site population
	δ (mm/s)	ΔE_Q (mm/s)	Γ (mm/s)	(%)
Doublet 1	0.47007	0.0857	0.1174	100
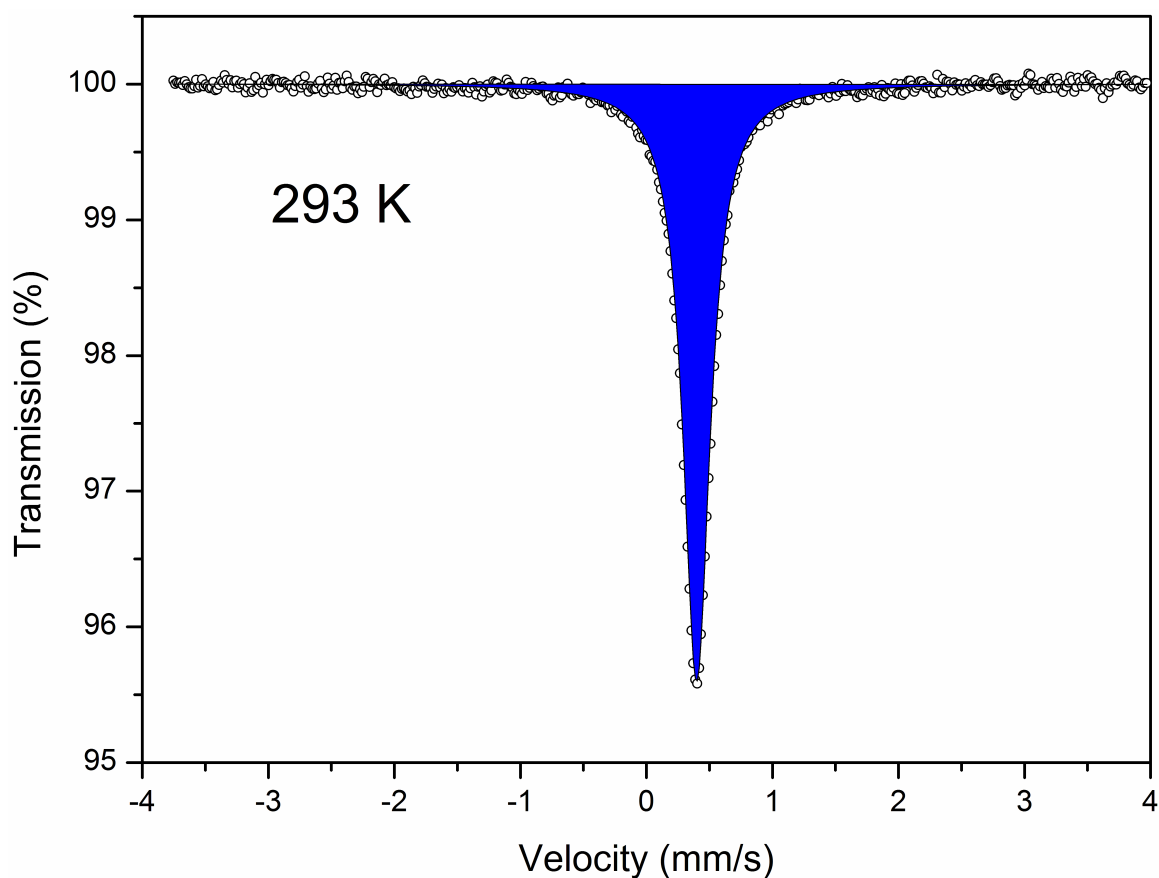
Figure 4.13.: Mössbauer spectrum of compound **1**· **4DMF** ($[Fe_2(\mu\text{-L1})_2](BF_4)_4$*4DMF)
at 293 K.

Table 4.5.: Mössbauer parameters for compound **1**· **4DMF** at 293 K with the isomer
shift δ, lorentzian line width Γ and site population.

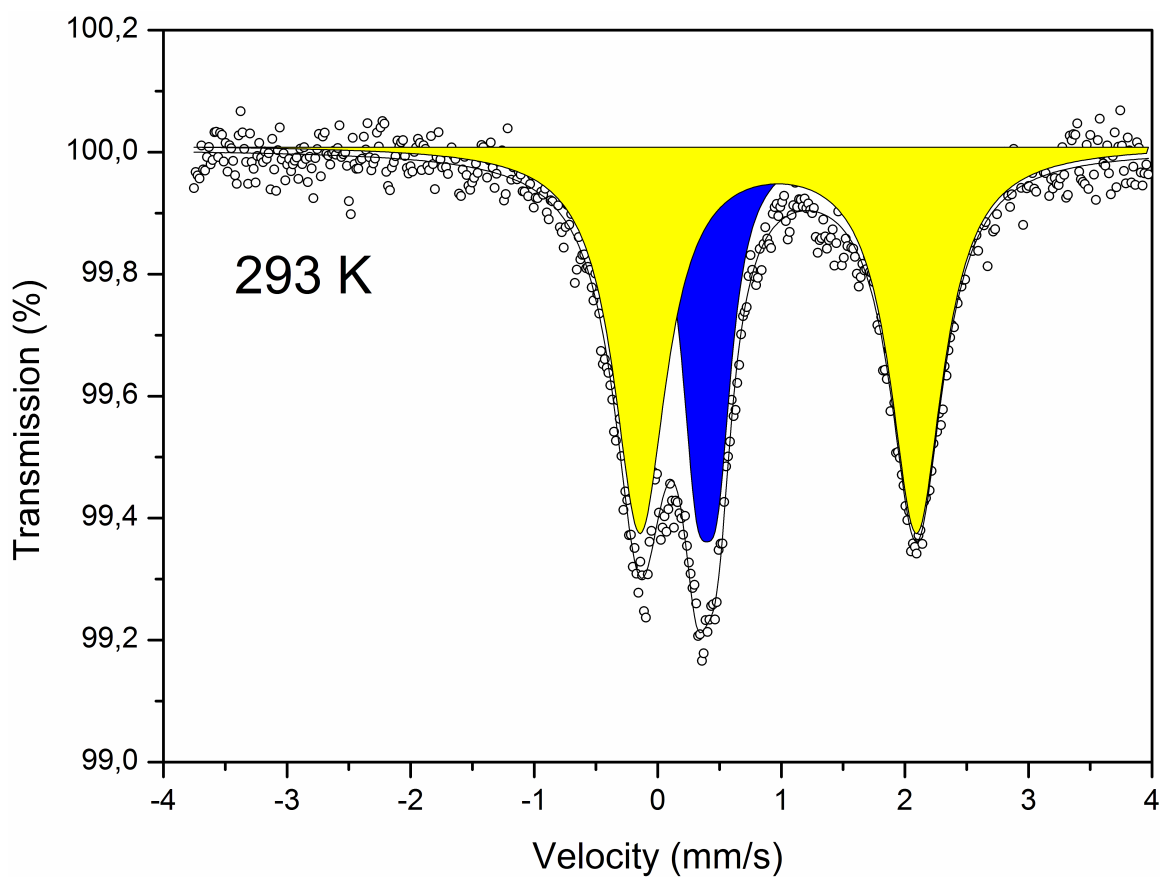| Site parameters			
	Isomer Shift	Lorentzian line width	Site population
	δ (mm/s)	Γ (mm/s)	(%)
Singlet 1	0.3983	0.1308	100

Figure 4.14.: Mössbauer spectrum of compound **1** ($[Fe_2(\mu\text{-L1})_2](BF_4)_4$) at 80 K.

Table 4.6.: Mössbauer parameters for compound **1** at 80 K with the isomer shift δ, quadrupole splitting ΔE_Q, lorentzian line width Γ and site population.

Site parameters				
	Isomer Shift δ (mm/s)	Quadrupole Splitting ΔE_Q (mm/s)	Lorentzian line width Γ (mm/s)	Site population (%)
Doublet 1	0.5005	0.2932	0.1438	53.92
Doublet 2	1.0856	2.6156	0.1638	46.08

Figure 4.15.: Mössbauer spectrum of compound **1** ($[Fe_2(\mu\text{-L1})_2](BF_4)_4$) at 293 K.

Table 4.7.: Mössbauer parameters for compound **1** at 293 K with the isomer shift δ, quadrupole splitting ΔE_Q, lorentzian line width Γ and site population.

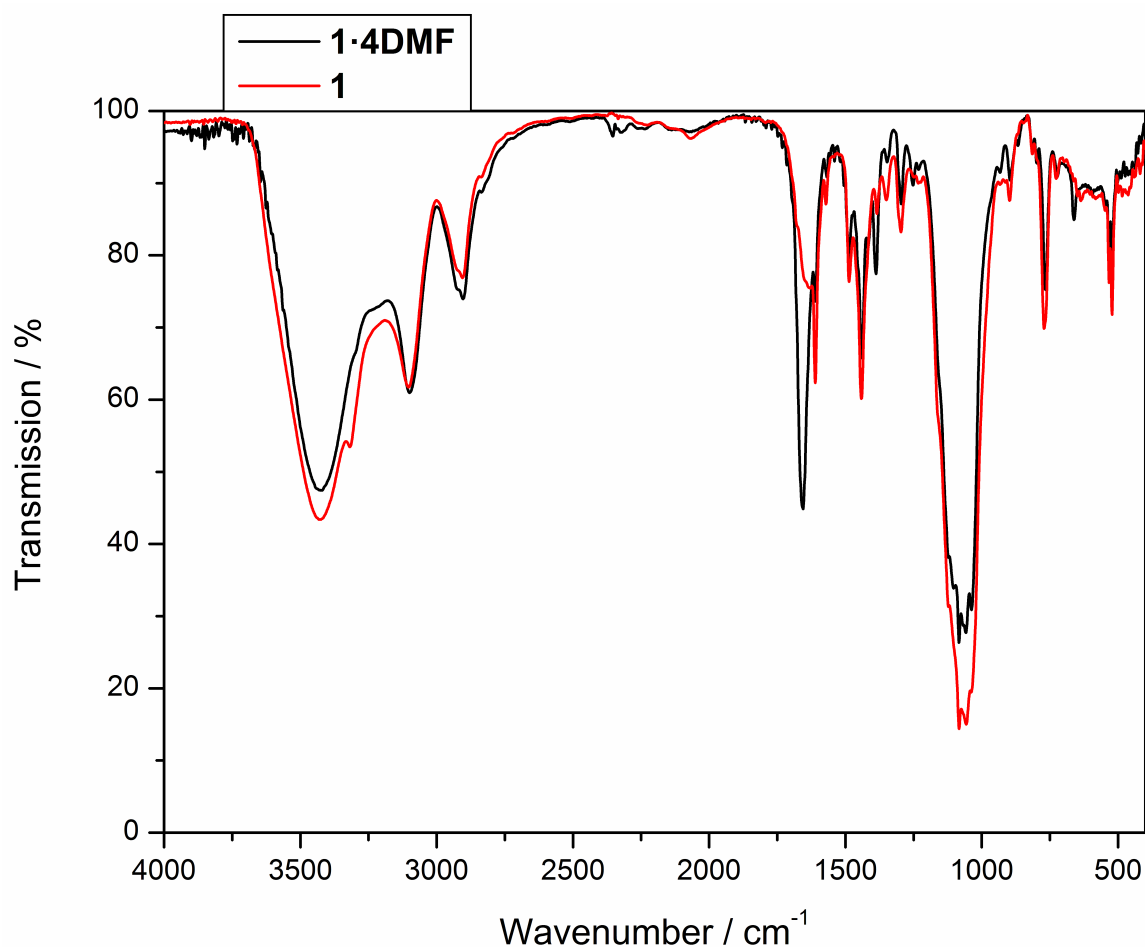| Site parameters	Isomer Shift	Quadrupole Splitting	Lorentzian line width	Site population
	δ (mm/s)	ΔE_Q (mm/s)	Γ (mm/s)	(%)
Doublet 1	0.397	0.168	0.147	28.1
Doublet 2	0.975	2.237	0.260	71.9

4.2.5. Infrared Spectroscopy

Figure 4.16.: Overlay of the infrared spectra of compound **1· 4DMF** ([Fe$_2$(μ-L1)$_2$](BF$_4$)$_4$*4DMF) and **1** ([Fe$_2$(μ-L1)$_2$](BF$_4$)$_4$).

The main difference in the infrared spectra of compound **1· 4DMF** ([Fe$_2$(μ-L1)$_2$](BF$_4$)$_4$ *4DMF) and **1** ([Fe$_2$(μ-L1)$_2$](BF$_4$)$_4$) are the absorption bands at 1656 cm^{-1}, 1388 cm^{-1} and 661 cm^{-1} which cannot be detected in the spectrum of the desolvated sample **1** or are at least extremely weak. The first absorption band (at 1656 cm^{-1}) in the spectrum of **1· 4DMF** can be assigned to the ν(C=O) stretching vibration, the second band (at 1388 cm^{-1}) to the δ(CH) bending vibration and the third band (at 661 cm-1) to the δ(C=O) bending vibration of the DMF in the single crystals and thus confirms the results of the elemental analysis and the loss of all four DMF molecules during the desolvation.[5,6]

Furthermore, the ν(C=O) stretching vibration of the DMF is shifted to a lower wavenumber compared to the ν(C=O) stretching vibration of pure DMF, which appears at 1689 cm^{-1}.[5] This shift to lower energies is a sign for an elongated and weaker C=O bond, which is caused by the hydrogen bonding interactions to the secondary amines of the complex cation and the shift of electron density from the DMF oxygen atom towards the N-H of the ligand in the complex cation of **1· 4DMF**.
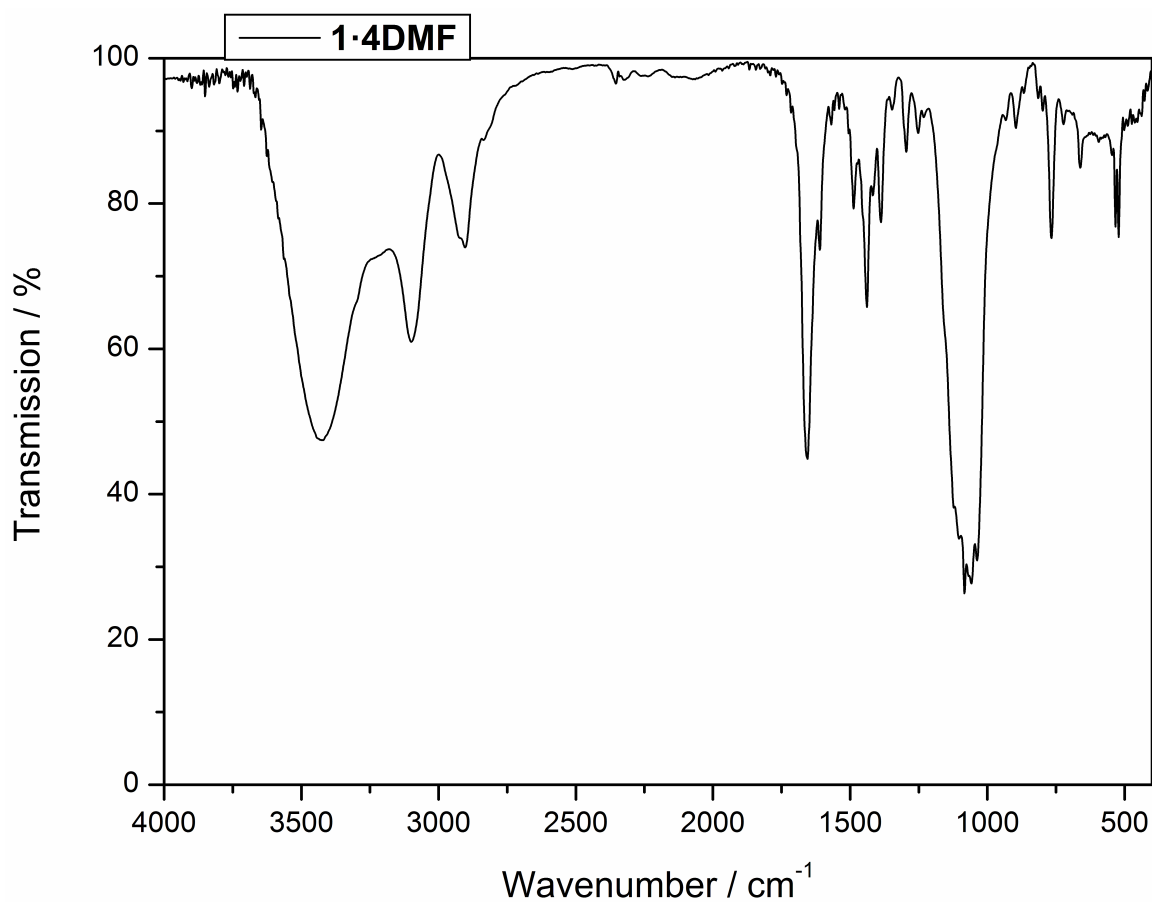

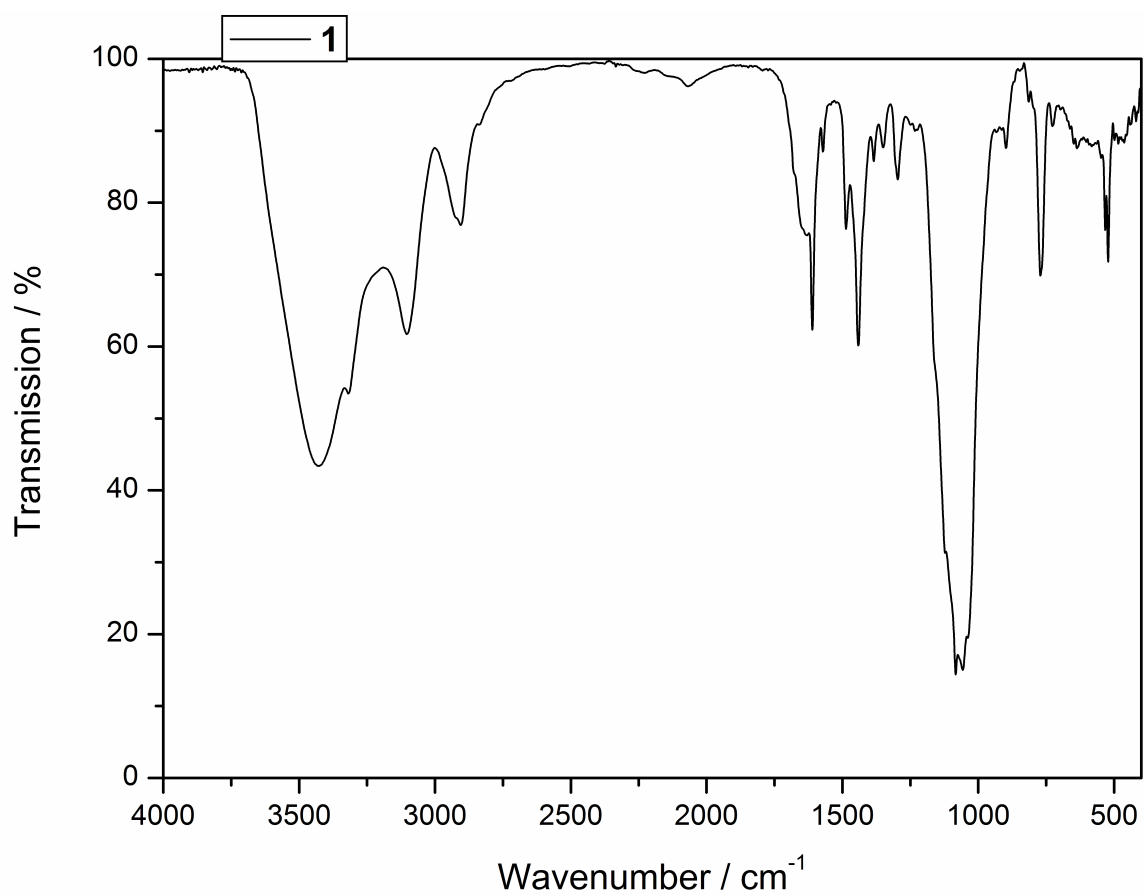Figure 4.17.: Infrared spectrum of compound **1· 4DMF** ([Fe$_2$(μ-L1)$_2$](BF$_4$)$_4$*4DMF).

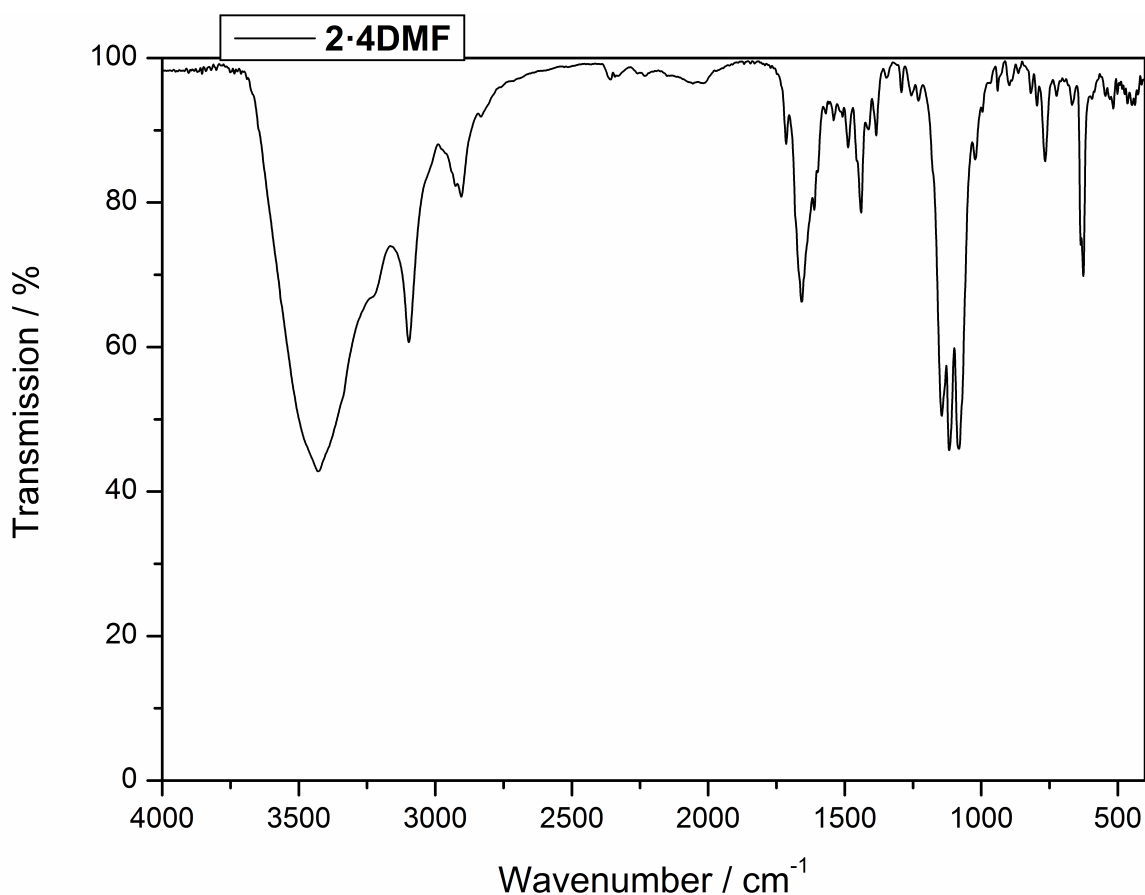Figure 4.18.: Infrared spectrum of compound **1** ($[Fe_2(\mu\text{-L1})_2](BF_4)_4$).

Figure 4.19.: Infrared spectrum of compound **2· 4DMF** ($[Fe_2(\mu\text{-}L1)_2](ClO_4)_4{}^*4DMF$).

4.2.6. References

1. Palatinus, L.; Chapuis, G., *J. Appl. Crystallogr.* **2007**, *40*, 786-790.

2. Sheldrick, G. M., *Acta Crystallogr., Sect. C: Struct. Chem.* **2015**, *71*, 3-8.

3. Dolomanov, O. V.; Bourhis, L. J.; Gildea, R. J.; Howard, J. A. K.; Puschmann, H., *J. Appl. Cryst.* **2009**, *42*, 339-341.

4. Herold, C. F.; Carrella, L. M.; Rentschler, E., *Eur J Inorg Chem* **2015**, 3632-3636.

5. M.B. Shundalau, P. S. C., A.I. Komyak, A.P. Zazhogin, M.A. Ksenofontov, D.S. Umreiko, *J. Appl. Spectrosc.* **2011**, 78.

6. Lumley Jones, R., *J. Mol. Spectrosc.* **1963**, *11*, 411-421.

4.3. Summary

Investigation of two new dinuclear iron(II) spin-crossover complexes with a 1,3,4-thia-diazole bridging ligand **L1** (2,5-bis[(2-pyridylmethyl)amino]methyl-1,3,4-thiadiazole) show the influence of the solvent molecules in the solid state and the effects of intermolecular interactions on the spin transition behavior. A variation of the solvents used for crystallization led to a completely new magnetic behavior, despite the fact that the complex itself consists of the same constitution.

The intermolecular interactions discussed in chapter 3 are realized by classical and non-classical hydrogen bonds between the aliphatic amines of the complex cation and the counterions. In this publication, they are formed between the aliphatic amines and one counterion and three dimethylformamide molecules. In all complexes, a shift of electron density towards the bridging amines, leads to a larger ligand field splitting and stabilization of the diamagnetic [LS-LS] state. The main difference in chapter 4 is the possibility to remove the dimethylformamide from the single crystals, which is not possible in the case of the previously reported complexes.

Removal of the dimethylformamide at elevated temperatures and under reduced pressure leads to the formation of the solvent free complexes **1** ([Fe$_2$(μ-**L1**)$_2$](BF$_4$)$_4$) and **2** ([Fe$_2$(μ-**L1**)$_2$](ClO$_4$)$_4$) and a stabilization of the [HS-HS] state around 400 K. The smaller shift of electron density onto the complex cation results in a lower ligand field splitting and a different spin state at high temperatures.

The solvent free complexes **1** and **2** stabilize the [HS-HS] state around 400 K and show a half-SCO at 280 K. It is not possible to return to the [LS-LS] state at low temperatures. It has been pointed out in section 1.2.7, that these half-SCO's in dinuclear SCO complexes can have their origin in isolated [HS-LS] complexes or a 1:1 mixture of complexes being in the [HS-HS] and [LS-LS] state. The magnetic measurements and Mössbauer data revealed that the complexes in the plateau region consist of isolated [HS-LS] molecules. This can be seen in the temperature independence of the χ_MT value in the plateau region of the magnetic measurements. The magnetic susceptibility would show a stronger decrease at low temperatures due to an antiferromagnetic coupling of the iron(II) centers in the [HS-HS] complexes of a 1:1 mixture. Moreover, the Mössbauer measurements yield the final proof for the isolated [HS-LS] molecules

at low temperatures. A comparison of the LS doublets of **1·4DMF** and **1** at 80 K shows a significant deviation of the quadrupole splitting (**1·4DMF**: $\triangle E_Q$ = 0.0857 mm/s and **1**: $\triangle E_Q$ = 0.2932 mm/s). This is a clear sign for different electronic environments caused by the neighboring HS iron(II) ion in the isolated [HS-LS] state. Furthermore, the Mössbauer spectrum of **1** near $T_{1/2}$ confirms the formation of the [HS-LS] complexes in the plateau region. The increased linewidth of the HS doublet of **1** at room temperature is a result of the superposition of two distinguishable HS iron(II) doublets from the [HS-LS] and [HS-HS] form.

As already stated, the stabilization of the [HS-LS] form in dinuclear complexes is a sign of stronger intramolecular interactions compared to intermolecular interactions. Due to the loss of DMF, intermolecular interactions are suppressed and the intramolecular interaction dominate. The remaining intermolecular interaction between the complex cations and the counterion is much weaker. This results in the dominant intramolecular interaction and the stabilization of the [HS-LS] state. The gradual nature of the spin transition from the [HS-HS] to the [HS-LS] state is also a result of the weak intermolecular interactions. Strong cooperativity is necessary for an abrupt spin-crossover behavior.

With the change of the spin-state above room temperature being a solvent effect, further studies evidenced the reversibility of this behavior. Vapor diffusion of DMF into the desolvated compound **1** resulted in the recovery of the [LS-LS] state and the initial properties. The desolvation and resolvation processes can be performed multiple times. All three spin states can be accessed depending on the solvent content and the temperature (figure 4.5). This shows, that the complex **1** is a perfect example for a chemo sensor for DMF.

Exposure of **1** to vapor diffusion of water showed a significant change of the magnetic behavior. The incorporation of one water molecule per complex (**1·H₂O**) into a sample of **1** leads to the stabilization of the diamagnetic [LS-LS] state and a gradual and incomplete spin transition starting at 250 K. Unfortunately, even high vacuum and temperatures above 150 °C do not result in the removal of the water from the sample, thus the [HS-HS] state cannot be regained. Although water has a much lower boiling point compared to DMF, the incorporation of water is not reversible. This suggests that the interaction between the complex cation and the water is much stronger than the inter-

actions with DMF. Strong hydrogen bonding interactions with water have to be reason for the prevented desolvation of **1·H$_2$O** and recovery of the solvent free complex **1**. Interestingly, the magnetic properties of **1·H$_2$O** are very similar to the properties of the previously reported complex [Fe$_2$(μ-L1)$_2$](BF$_4$)$_4$·2H$_2$O (see figure 3.4, complex **1b**).

In conclusion, two new compounds have been reported, that show extremely interesting SCO properties and are a perfect example for the influences of solvents on the spin-crossover behavior. Such a reversibility of the solvent effect is very uncommon and there is only one reported dinuclear SCO system showing comparable properties. An addressability of all three spin states depending on the temperature and solvent content is very unusual. But more importantly, the reversible switching at room temperature between the diamagnetic solvated and paramagnetic desolvated complex shows the fascinating sensor capability of this compound.

5. Iron(II) complexes with 2nd generation bridging ligands

The results from chapters 3 and 4 led to the design of a series of further new 1,3,4-thiadiazole bridging ligands. The modifications of the ligands follow different strategies in order to influence the ligand field splitting of the dinuclear iron(II) complexes. Every adjustment aims towards the stabilization of the paramagnetic [HS-HS] state at room temperature. The strategies include a blocking of intermolecular interactions, the use of steric effects and the tunability of the ligand field strength with coordinating anions. The dinuclear iron(II) complexes with these ligands have been synthesized to investigate the resulting effects on the magnetic properties.

5.1. Iron(II) complexes with L2

The ligand field splitting in iron(II) complexes with **L1** (2,5-bis[(2-pyridylmethyl)amino]-methyl-1,3,4-thiadiazole) should be in a suitable range for dinuclear iron(II) complexes in the [HS-HS] state. However, a stabilization of the [LS-LS] state at room temperature was observed due to hydrogen bonding interactions with electron donating solvents or counterions. Inspired by these findings I designed a ligand where the mentioned hydrogen bonds would be blocked, realized by a replacement of the *N-H* protons by a methyl group. These substitutions effectively suppress classical hydrogen bonding interactions between the complex cation and counterions or solvent molecules. This should lead to a stabilization of the desired and previously elusive [HS-HS] state at room temperature.

The replacement of the primary 2-picolylamine with the secondary N-(2-picolyl)methyl-amine led to the synthesis of **L2** (2,5-bis[N-methyl-N-(2-pyridylmethyl)aminomethyl]-1,3,4-thiadiazole, figure 5.1). N-(2-picolyl)methylamine was prepared from a reaction of 2-(chloromethyl)pyridine hydrochloride with methylamine, according to a modified literature procedure.[150] A nucleophilic substitution reaction of 2,5-bis(chloromethyl)-1,3,4-

thiadiazole (**TDA**) with N-(2-picolyl)methylamine yielded **L2**. Both aliphatic amines in **L2** are substituted with methyl groups to prevent intermolecular interactions via hydrogen bonding interactions. The positive inductive effect of the methyl groups on the nitrogen donors is very small and should have only a minor effect on the ligand field splitting.
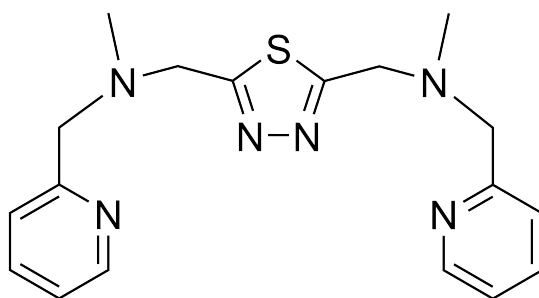

Figure 5.1.: The 1,3,4-thiadiazole based ligand **L2** (2,5-bis[N-methyl-N-(2-pyridylmethyl)aminomethyl]-1,3,4-thiadiazole).

Three dinuclear iron(II) complexes with the general formula $[Fe_2(\mu\text{-}\mathbf{L2})_2]X_4$ have been synthesized using three different counterions X (**C1**: BF_4^-, **C2**: ClO_4^- and **C3**: $F_3CSO_3^-$).

Polycrystalline samples of the tetrafluoroborate and perchlorate complexes were obtained from vapor diffusion of diethyl ether into methanolic solutions of **L2** and the corresponding iron(II) salt. Recrystallization from acetonitrile/diethyl ether yielded colorless single crystals of **C1** and **C2** suitable for X-ray diffraction measurements. The triflate complex **C3** was obtained in form of colorless single crystals by incremental addition of tetrahydrofuran to a solution of **L2** and iron(II) triflate in acetonitrile.

All three complexes **C1** ($[Fe_2(\mu\text{-}\mathbf{L2})_2](BF_4)_4 \cdot 2MeCN$), **C2** ($[Fe_2(\mu\text{-}\mathbf{L2})_2](ClO_4)_4 \cdot 1MeCN$ +0.75MeOH) and **C3** ($[Fe_2(\mu\text{-}\mathbf{L2})_2](F_3CSO_3)_4 \cdot 2THF$) crystallize in the triclinic spacegroup $P\bar{1}$. The asymmetric unit of **C1** and **C3** contains one complete ligand molecule, one iron(II) center, two anions and one solvent molecule. The second half of the complex is generated by an inversion centre between the two iron(II) centers (figure C.1, figure C.3).

The crystal structure of **C2** differs from the structures of **C1** and **C3**. The cell volume is twice as large and the asymmetric unit contains two ligand molecules, two iron(II)

ions, four perchlorate ions, one acetonitrile molecule and a split methanol. The ligand molecules and iron(II) centers do not build up one complex cation, but two distinguishable half complex cations. The two different solvent molecules are located near the ligands and short contacts lead to the two distinguishable complex cations. Thus, the two iron(II) centers in **C2** have been treated and discussed individually, although the bond lengths and angles are very similar. Inversion centers in the middle of the complexes lead to a generation of the complete dinuclear complexes by symmetry (figure C.2).

The dinuclear complex cations in **C1**, **C2** and **C3** consist of two ligand molecules providing the 12 nitrogen donor atoms for a FeN6 coordination environment. Figure 5.2 shows the $[Fe_2(\mu\text{-}\mathbf{L2})_2]_4^+$ complex cation of **C1**. The complex cations in **C2** and **C3** have nearly the same structure with negligible deviations in the Fe-N bond lengths and N-Fe-N angles.
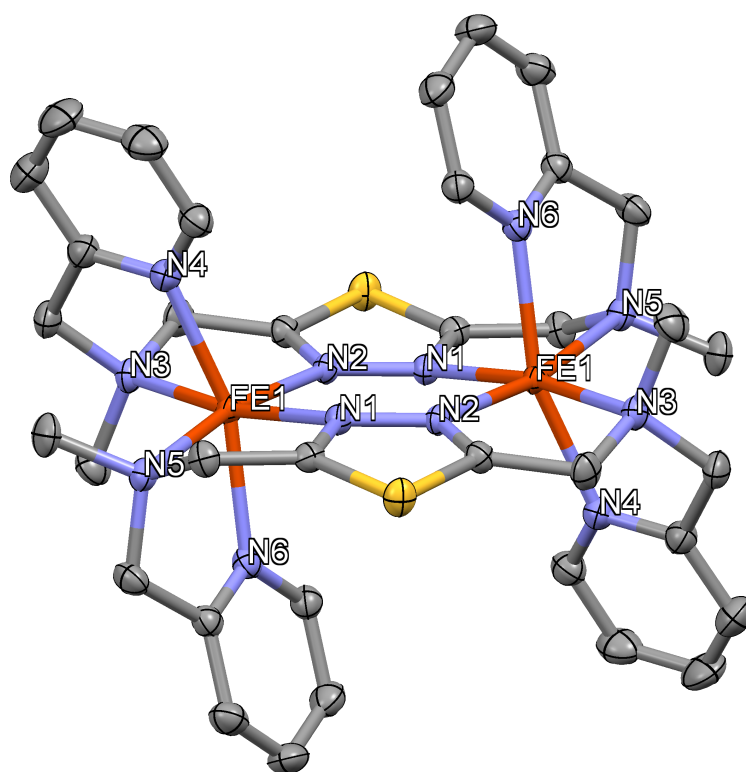

Figure 5.2.: Representative view of the complex cation $[Fe_2(\mu\text{-}\mathbf{L2})_2]_4^+$ from **C1**. Nitrogen atoms are blue, sulfur atoms are yellow, iron atoms are red and carbon atoms are grey. Hydrogen atoms have been omitted for clarity.

Interestingly, this new ligand **L2** binds with both sidearms up or down in a *cis*-axial mode. This has also been the case in the complexes with the **L1**-analog 1,2,4-triazole (PMAT)[78] and 1,3,4-oxadiazole[106] ligands, which stabilized the [HS-HS] state at room temperature. Previously reported [LS-LS] complexes with the 1,3,4-thiadiazole ligand **L1** and the [HS-LS] complex with the analog pyrazolate ligand[141] coordinated in a *trans*-axial mode with one sidearm up and one sidearm down.

The average Fe-N bond lengths of 2.211 Å (**C1**), 2.207/2.208 Å (**C2**, Fe1/Fe2) and 2.210 Å (**C3**) are in good agreement with literature values of iron(II) centers in the HS state. Besides the distortion of the octahedral coordination environment, the 1,3,4-thiadiazole heterocycles of the two ligand molecules are shifted parallel relative to each other. It can be seen in figure 5.3 that the 1,3,4-thiadiazoles do not form a plane with the two iron(II) centers. Furthermore, the N_{Py}-Fe-N_{Py}-axes are highly tilted to one side. A very important parameter that expresses this distortion around the metal center is the octahedral distortion parameter Σ, which is the sum of the deviations from 90° of the 12 *cis*-N-Fe-N angles. Given the large differences in the geometry of iron(II) HS and LS complexes, this parameter can be used to determine the spin-state in iron(II) complexes. Stronger distorted iron(II) HS complexes display a higher Σ compared to LS complexes. The calculated Σ values are 124.73° (**C1**), 125.10°/126.54° (**C2**, Fe1/Fe2) and 123.84° (**C3**) and are a clear sign for iron(II) in the HS state. The Σ values show a significant octahedral distortion compared to the LS iron(II) complexes with **L1** (Σ values between 57.59° and 66.09°).

The changes in the octahedral geometry of the iron(II) centers are a result of the additional methyl group on the aliphatic amines of the ligand. Thus, the displacement of the pyridine rings and shift of the N_{Py}-Fe-N_{Py}-axes are a result of steric hindrance. The intramolecular distance between the methyl group and pyridine ring is small, thus repulsion leads to the shifted arrangement. In addition, switching from a secondary to tertiary amine leads to different CH_2-N-CH_2 angles and a lower flexibility around the nitrogen donor atom. This results in the nitrogen donors being pushed out of the thiadiazole plane and leads to an additional distortion in the complex cation.

The complexes show a close packing in the solid state, but there is no evidence of π-π interactions between aromatic rings of neighboring cations. The pyridine rings are
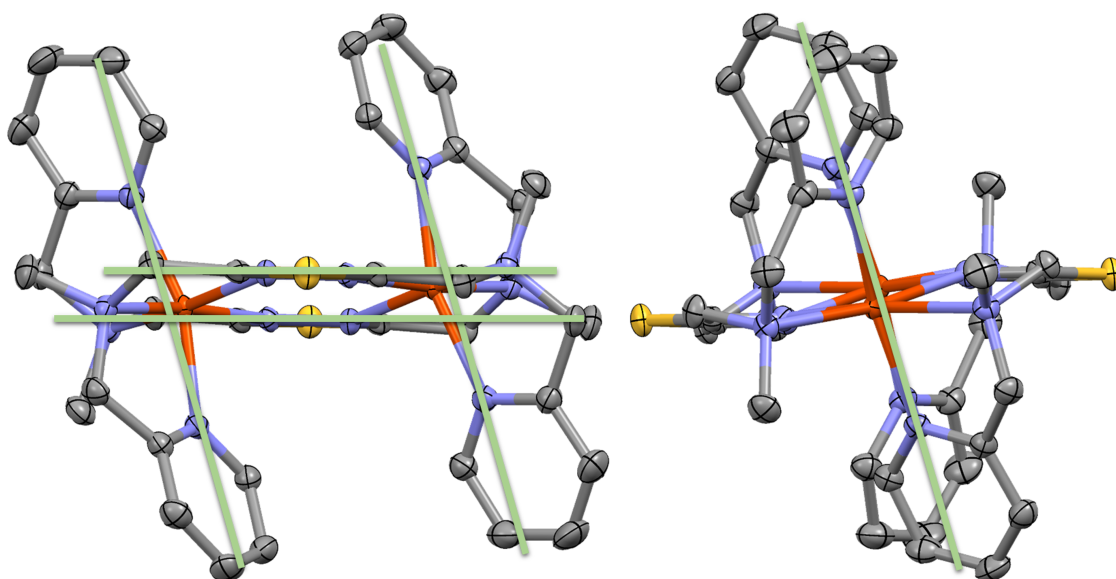
Figure 5.3.: Frontal (left) and side (right) view on the complex cation $[Fe_2(\mu\text{-}\mathbf{L2})_2]_4^+$ from **C1**. Nitrogen atoms are blue, sulfur atoms are yellow, iron atoms are red and carbon atoms are grey. Hydrogen atoms have been omitted for clarity. The green bars have been added for clarification of the distortion.

arranged near methyl groups of the next cation, which only results in weak short contacts. The interactions between cations mediated by counterions or solvent molecules are also of a weak nature in consequence of the intentional blocking of classical hydrogen bonding interactions. The remaining intermolecular interactions between the complex cation and the counterions are non-classical hydrogen bonds and short contact, and thus very weak.

The magnetic measurements of the three dinuclear iron(II) complexes confirm the assumptions from the Fe-N bond lengths and octahedral distortion parameters from the crystal structures. The complexes stabilize the [HS-HS] state at room temperature with $\chi_M T$ values of 6.91 cm^3 K mol^{-1} (**C1**), 6.79 cm^3 K mol^{-1} (**C2**) and 6.88 cm^3 K mol^{-1} (**C3**) at 300 K. These $\chi_M T$ values are in agreement with the expected spin-only value of a dinuclear iron(II) complex in the HS state. Thus, the undertaken ligand modification resulted in the expected change of the spin state of the iron(II) complexes at room temperature from low-spin to high-spin. There is no sign for a spin-crossover with lowering the temperature to 5 K (figure 5.4). The decreasing $\chi_M T$ values below 50 K to 1.84 cm^3 K mol^{-1} (**C1**), 2.09 cm^3 K mol^{-1} (**C2**) and 1.60 cm^3 K mol^{-1} (**C3**) at 5 K have

their origin in a combination of antiferromagnetic coupling and zero-field splitting of the single ion ground-state quintet.

The g-value, the antiferromagnetic coupling J and the zero-field splitting parameter D have been simulated. The results are summarized in table 5.1 and are in good agreement with data from the literature for iron(II) complexes.[151–153]
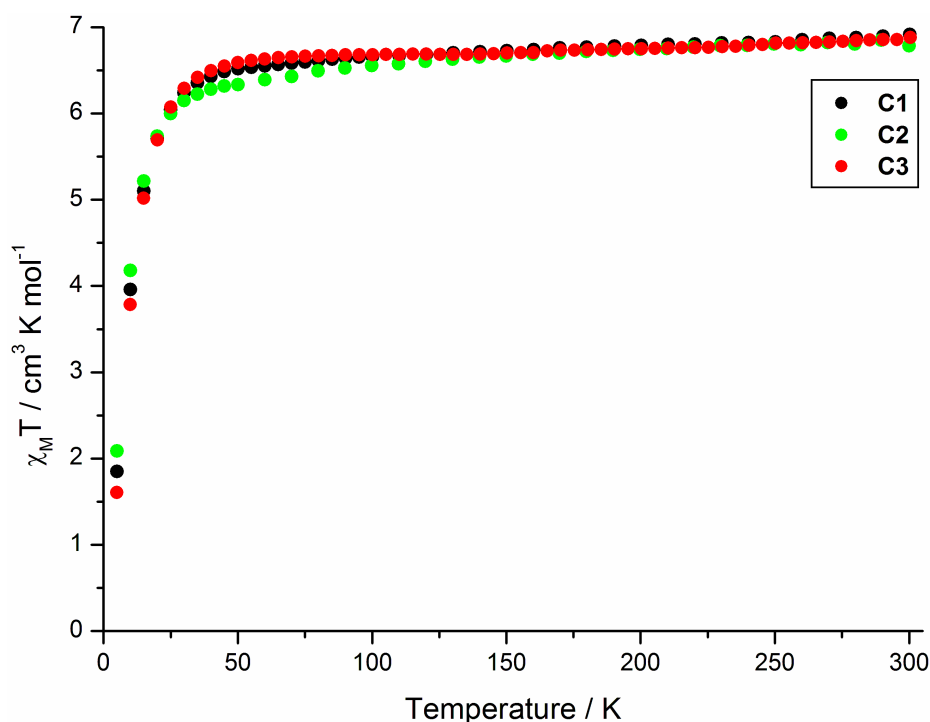

Figure 5.4.: $\chi_M T$ vs. T data for the compounds **C1** (black), **C2** (green) and **C3** (red). Data per dinuclear complex.

The magnetic exchange between the iron(II) centers is mediated through the 1,3,4-thiadiazole. In regard to the strong distortion in the complex cations with the two iron(II) centers being out of plane of the 1,3,4-thiadiazoles, a very weak antiferromagnetic coupling between the metal centers can be expected. The distortion of the complex cation is also the reason for the loss of the spin-crossover properties. A spin transition into the [HS-LS] or [LS-LS] state is accompanied by a pronounced geometry change. These shorter Fe-N bond lengths and lower octahedral distortions can not be realized due to the steric hindrance between the methyl groups and pyridine rings.

Table 5.1.: Results for the simulation of the magnetic data of **C1**, **C2** and **C3**.

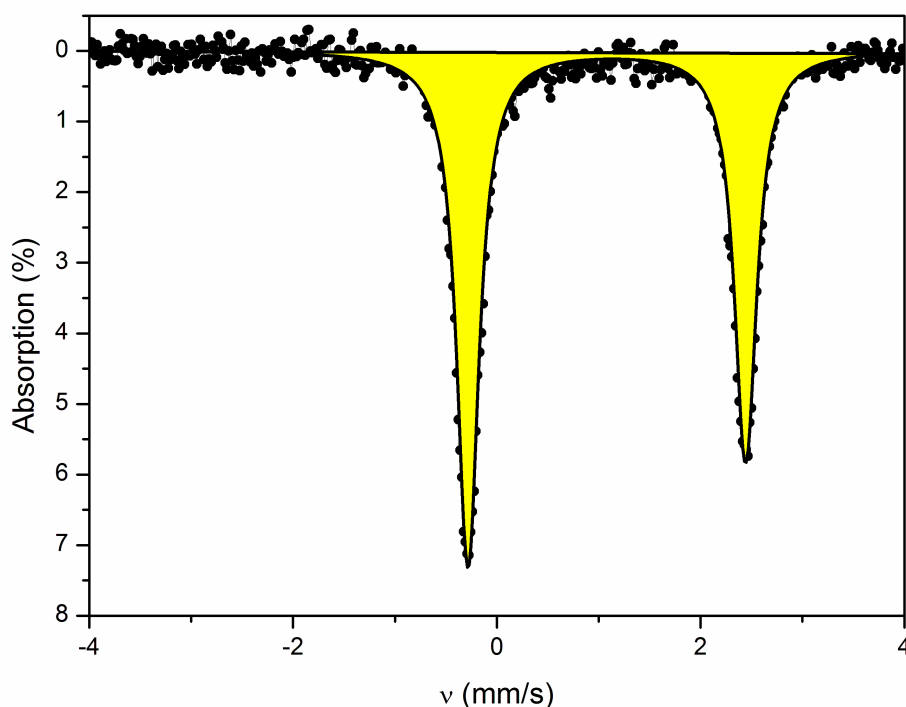|	Landé factor g	Exchange parameter J	Zero-field splitting parameter $|D|$
C1	2.137	-0.430 cm^{-1}	5.90 cm^{-1}
C2	2.125	-0.468 cm^{-1}	4.03 cm^{-1}
C3	2.137	-0.452 cm^{-1}	5.96 cm^{-1}

Figure 5.5.: Mössbauer spectrum of **C1** recorded at 70 K. Isomer shift δ = 1.0787 mm s^{-1}, quadrupole splitting ΔE_Q = 2.7258 mm s^{-1}, Lorentzian line width Γ = 0.1332 mm s^{-1} and site population: 100 %.

The Mössbauer measurement of **C1** at 70 K (figure 5.5) is consistent with the magnetic measurement and shows only one doublet for the [HS-HS] state in the dinuclear iron(II) complex. The isomer shift and the quadrupole splitting are in the expected range for iron(II) in the HS state. The reason for the doublet asymmetry is a preferential orientation of the single crystals in the sample holder.

In conclusion, the synthesis of dinuclear complexes with the new 1,3,4-thiadiazole bridging ligand **L2** was successful. The key feature of these new complexes are the tertiary amines, which can no longer form hydrogen bonds to molecules in the periphery of the complex cation. The deliberate blocking of the secondary amines led to a stabilization of the desired [HS-HS] state at room temperature. The counterions and solvent molecules now have a smaller influence on the ligand field splitting of these complexes. Unfortunately, these complexes show no spin transition at lower temperatures and are locked in the [HS-HS] state. The pronounced distortion of the cations is the reason for the loss of spin-crossover properties.

5.2. Iron(II) complexes with L3

The successful change of the spin state at room temperature in complexes with **L2** inspired the investigation of improved ways to accomplish this change to the [HS-HS] state. The pronounced distortion in the previously reported complexes **C1-C3** with **L2** resulted in a loss of the spin-crossover properties. Thus, the here presented new ligand **L3** aims towards a forced elongation of the metal-donor atom bond lengths to reduce the ligand field splitting but has a higher flexibility than **L2**. This should lead to a stabilization of the desired [HS-HS] state at room temperature and allow a geometry change that usually accompanies the spin transition.

The modification of the ligand is the replacement of the aminomethylpyridine sidearms by aminoethylpyridine sidearms. The additional methylene group leads to a six-membered coordination ring instead of a five-membered ring upon complexation with iron(II). A consequence of this change is an elongation of the iron(II)-N(Py) donor atom distance and thus a decrease of the ligand field splitting.

The synthesis of **L3** (2,5-bis[(2-pyridylethyl)aminomethyl]-1,3,4-thiadiazole, figure 5.6) was carried out analog to the synthesis of **L1**, except for the use of 2-(2-pyridyl)ethyl-amine as a primary amine in the nucleophilic substitution reaction with 2,5-bis(chloro-methyl)-1,3,4-thiadiazole (**TDA**).

Vapor diffusion of diethyl ether into a solution of **L3** and iron(II) tetrafluoroborate in acetonitrile yielded **C4** in form of colorless single crystals suitable for X-ray diffraction
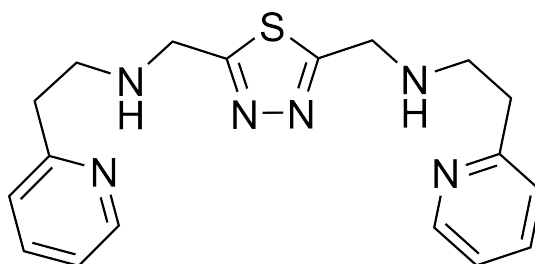
Figure 5.6.: The 1,3,4-thiadiazole based ligand **L3** (2,5-bis[(2-pyridyl-ethyl)aminomethyl]-1,3,4-thiadiazole)

experiments. The dinuclear complex **C4** ([Fe$_2$(μ-**L3**)$_2$](BF$_4$)$_4$·1.25MeCN) has been synthesized and characterized by mass spectrometry, elemental analysis and variable-temperature magnetic susceptibility measurements. Although the complex **C4** has been isolated as single crystals a characterization by X-ray diffraction experiments was not possible due to the slow oxidation of the crystals under ambient conditions. The complex has been synthesized in inert atmosphere and a decomposition before the measurement prevented the crystal structure determination. Thus, the characterization of the complex **C4** is based on elemental analysis and mass spectrometry. The ESI-MS spectra of **C4** shows mainly signals for combinations of two ligand molecules with one or two iron(II) centers and counterions. Given the conditions during the measurement, this can be seen as a clear evidence for the synthesis of these dinuclear iron(II) complexes. The elemental analysis of the single crystals confirmed the proposed composition of the complex and has been calculated for a residual solvent content of 1.25 acetonitrile molecules per complex cation.

The oxidation sensitivity of the iron(II) complex, which made the complex synthesis under inert atmosphere necessary, is a clear sign for a lower ligand field splitting. The oxidation from iron(II) to iron(III) is a first indication of the complexes being in the HS state.

The magnetic measurements of a crystalline sample of **C4** (figure 5.7) shows the stabilization of a [HS-HS] state at room temperature. A χ_MT value of 6.18 cm^3 K mol^{-1} at 300 K is in agreement with the expected spin-only value. The magnetic moment shows no evidence for a spin transition at lower temperatures and is very constant
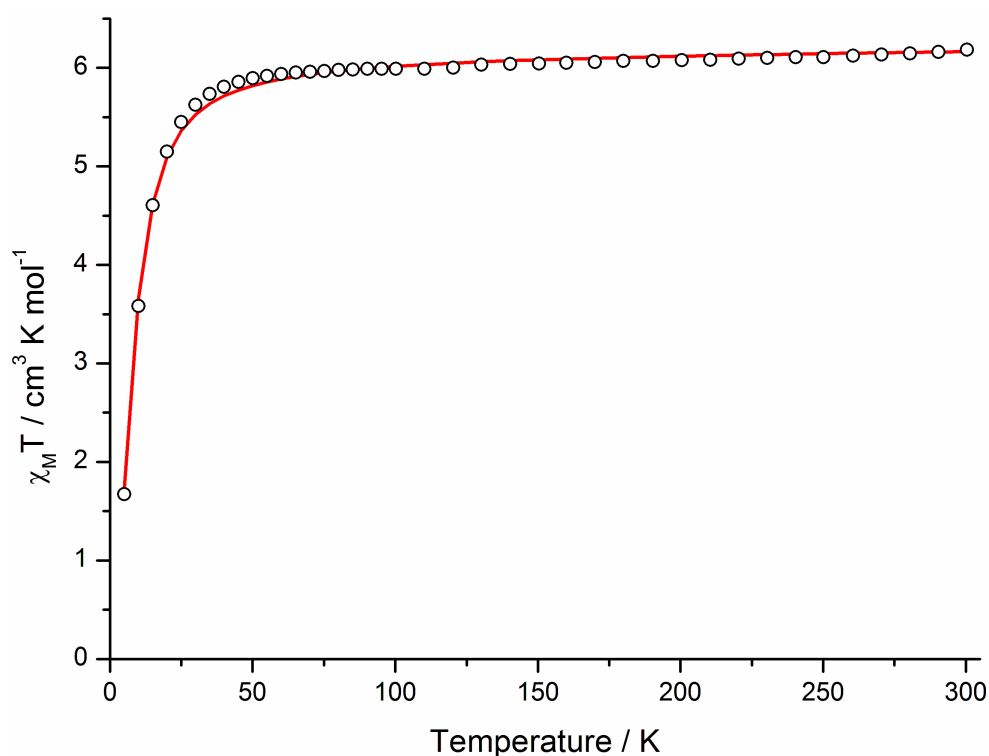
Figure 5.7.: χ_MT vs. T data for **C4**. The experimental data is presented in circles and the fit of the magnetic data as a red line. Data per dinuclear iron(II) complex.

up to a temperature of 50 K. The decrease of the molar magnetic susceptibility below 50 K results in a χ_MT value of 1.67 cm^3 K mol^{-1} at 5 K. This decrease is a result of an antiferromagnetic coupling between the two iron(II) centers and zero-field splitting of the single ion ground-state quintet. The magnetic data has been simulated and a good agreement with the experimental data was found for the parameters g = 2.025, J = -0.419 cm^{-1}, $|D|$ = 5.94 cm^{-1} and a temperature independent paramagnetism (TIP = $2 \cdot 10^{-4}$ cm^{3}mol^{-1}). The simulated data are in agreement for literature values of iron(II) systems.[151–153]

The observed antiferromagnetic coupling is very weak and this explains the constant moment above 50 K. The magnitude of the J value is nearly identical to the simulated exchange parameter of the complexes **C1-C3**. Only the g-value differs from the simulated values of **C1-C3** and results in a lower molar magnetic susceptibility of compound **C4**.

In conclusion, the modification of the ligand system and the use of ethylpyridine arms led to the intended stabilization of the [HS-HS] state at room temperature. Unfortunately, the loss of the SCO properties and the sensitivity of the complexes to oxidation are a result of a too big change of the complex geometry. The elongation of the Fe-N bond lengths leads to a smaller ligand field splitting and the change of the spin state at room temperature. This change of the Fe-N bond lengths was probably too pronounced. Therefore, the ligand field splitting for iron(II) complexes is no longer in the critical range for a thermally induced spin transition. This presents the complexes to switch into the [HS-LS] or [LS-LS] state.

5.3. Iron(II) complexes with L4 and L5

The initial findings described in section 5.2, with the distinct air-sensitivity of the iron(II) complexes, inspired the synthesis of the ligands **L4** and **L5**. Although the modification in section 5.2 resulted in the desired [HS-HS] state, an oxidation of iron(II) to iron(III) was favored under ambient conditions due to a too pronounced geometry change in the complex. This was also the reason for the loss of the spin-crossover properties.

The new bridging ligands **L4** and **L5** were designed for a smaller change of the geometry of the complexes. The ligand modifications to introduce further functional groups in *meta*-position to the nitrogen donor followed the idea presented in section 1.2.4.1, with the substitution of 1,10-phenanthrolin. Several studies showed, that an incorporation of methyl or methoxy groups at this *meta*-position can change the spin state from a low-spin to high-spin state at elevated temperatures. As a result, diamagnetic LS iron(II) complexes can gain SCO properties. These substituents add steric hindrance into the complex and thus influence the Fe-N bond length. Thereby the HS state is favored at room temperature and a SCO to the LS state upon cooling can be accomplished.[83–85,154–156]

The new bridging ligand **L4** (2,5-bis[[2-(6-methyl-pyridyl)methyl)aminomethyl]-1,3,4-thiadiazole, figure 5.8) has been synthesized in a nucleophilic substitution reaction between 2,5-bis(chloromethyl)-1,3,4-thiadiazole (**TDA**) and 2-aminomethyl-6-methyl-pyridine. The 2-aminomethyl-6-methyl-pyridine has been prepared according to liter-
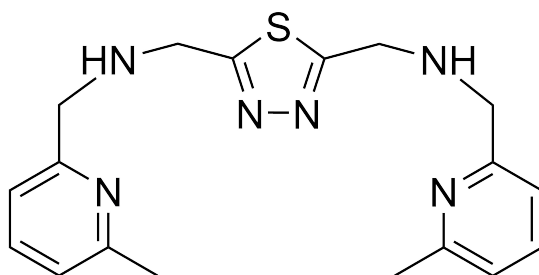
Figure 5.8.: The 1,3,4-thiadiazole based ligand **L4** (2,5-bis[(2-(6-methyl-pyridyl)methyl) aminomethyl]-1,3,4-thiadiazole)

ature procedures starting from 6-methyl-pyridine-2-carboxaldehyde.[157,158]

This new ligand was used for the synthesis of iron(II) complexes. The isolation of these complexes as single crystals suitable for X-ray diffraction experiments was not successful. Thus it is not possible to have a closer look at the structure of the complex and the intermolecular interactions in the solid state. An isolation was solely successful for powder samples. One of these samples has been characterized with mass spectrometry, elemental analysis and variable-temperature magnetic susceptibility measurements. The complex has, according to elemental analysis and mass spectrometry, the general formula [Fe$_2$(μ-**L4**)$_2$](BF$_4$)$_4$·0.5H$_2$O (**C5**) and was synthesized by precipitation from an ethanolic solution of **L4** and iron(II) tetrafluoroborate.

The temperature dependence of the molar magnetic susceptibility has been measured (figure 5.9), but the data quality does not allow a satisfying simulation. The reason is presumably the inhomogeneity of the powder sample. Therefore, the data will only be discussed qualitatively. The χ_MT value of 5.92 cm^3 K mol^{-1} at 300 K clearly shows a [HS-HS] state at room temperature. The absolute value is below the expected spin-only value for a dinuclear iron(II) complex in the HS state, but it clearly shows the effect of the incorporated methyl groups. The steric hindrance of the substituent led to a realization of a paramagnetic ground state at room temperature. There is no sign of a spin-crossover upon cooling. The missing cooperativity in the amorphous sample can be a reason for the loss of SCO behavior, since these solid state interactions have a large influence on the magnetic properties.
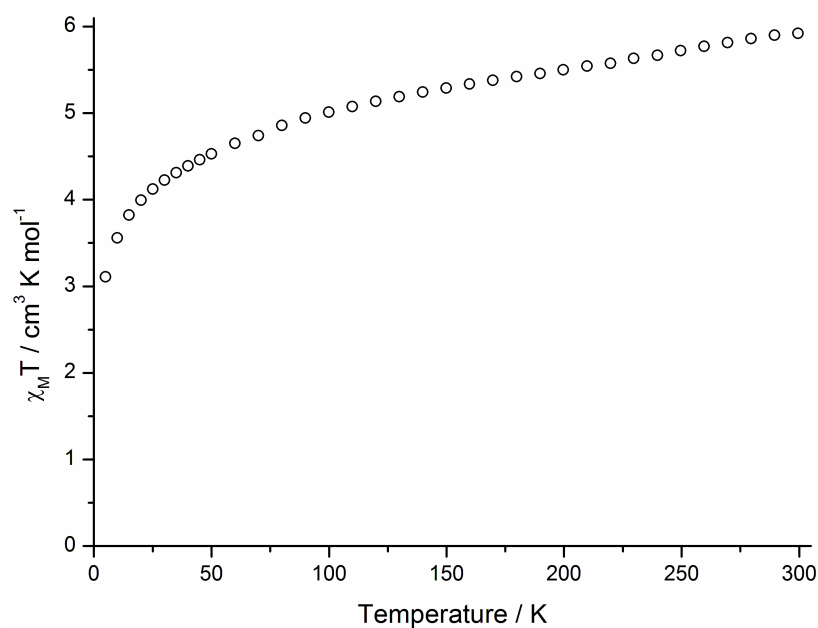
Figure 5.9.: $\chi_M T$ vs. T data for **C5**. The experimental data is presented in circles. Data per dinuclear iron(II) complex.

The ligand design for the analog methoxy-substituted ligand **L5** (2,5-bis[(2-(6-methoxy-pyridyl)methyl)aminomethyl]-1,3,4-thiadiazole, figure 5.10) followed the same idea with the incorporation of the methoxy substituent for steric effects instead of a methyl group.
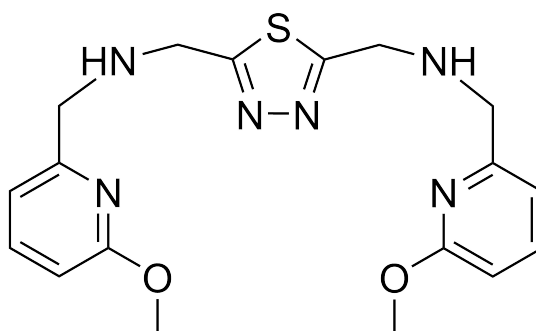

Figure 5.10.: The 1,3,4-thiadiazole based ligand **L5** (2,5-bis[(2-(6-methoxy-pyridyl)methyl)aminomethyl]-1,3,4-thiadiazole)

L5 (2,5-bis[(2-(6-methoxy-pyridyl)methyl)aminomethyl]-1,3,4-thiadiazole, figure 5.10) has been synthesized with an improved approach and a schematic representation can be found in figure 5.11. First 2,5-bis(azidomethyl)-1,3,4-thiadiazole has been syn-

thesized in a nucleophilic substitution reaction between **TDA** and sodium azide.[159] The reduction to the 2,5-bis(aminomethyl)-1,3,4-thiadiazole has been accomplished in a Staudinger reaction.[160] Here, the 2,5-bis(azidomethyl)-1,3,4-thiadiazole reacts with triphenylphosphine, which leads to the elimination of nitrogen. The resulting phosphazene can be hydrolyzed to give the desired 2,5-bis(aminomethyl)-1,3,4-thiadiazole. The final step of the ligand synthesis is a condensation reaction of the 2,5-bis(aminomethyl)-1,3,4-thiadiazole with 6-methoxy-2-pyridine-carboxaldehyde, followed by a reduction of the *in-situ* formed imine with sodium borohydride.

This synthetic pathway has been used to obtain more alternatives for the two sidearms of the ligand. Most aromatic heterocycles suitable for ligands aiming towards iron(II) SCO complexes are only commercially available as carboxaldehydes. Hence, the synthesized 2,5-bis(aminomethyl)-1,3,4-thiadiazole can be used as a precursor for various further new bridging ligands.
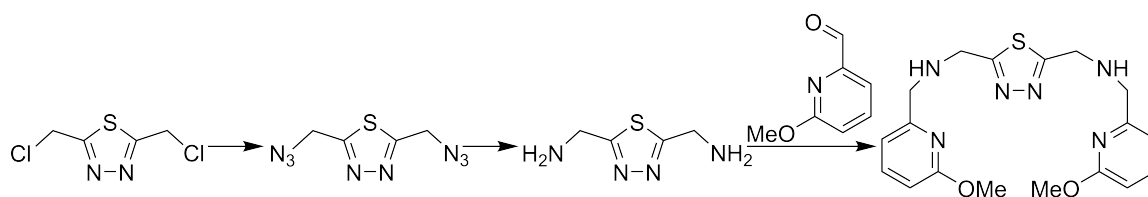

Figure 5.11.: Schematic representation for the synthesis of the ligand **L5** (2,5-bis[(2-(6-methoxy-pyridyl)methyl)aminomethyl]-1,3,4-thiadiazole)

The ligand **L5** was used for the synthesis of dinuclear iron(II) complexes, but all isolated compounds were of polycrystalline nature. Recrystallization methods and variations of the solvents or the counterions yielded no sample suitable for X-ray diffraction experiments. Thus, the characterization of the complex was limited to elemental analysis and mass spectrometry. These techniques confirmed the formation of a dinuclear iron(II) complex with **L5** from a liquid-liquid diffusion experiment with iron(II) tetrafluoroborate. The mass spectra shows mainly signals for two ligand molecules with one or two iron(II) ions and counterions. The solvent content in the general formula of the polycrystalline complex **C6** ([Fe$_2(\mu$-L5)$_2$](BF$_4$)$_4\cdot$1.5MeCN) has been calculated from elemental analysis data.

The temperature dependence of the molar magnetic susceptibility has been measured

in the temperature range from 5 to 300 K (figure 5.12). A χ_MT value of 6.57 cm^3 K mol^{-1} at 300 K shows a stabilization of the [HS-HS] state and room temperature. The molar magnetic susceptibility is very constant with decreasing temperature and shows no spin transition. The magnetic moment decreases below 50 K, resulting in a value of 1.64 cm^3 K mol^{-1} at 5 K. The decrease below 50 K is the result of an antiferromagnetic coupling of the iron(II) centers and a zero-field splitting contribution. A simulation of the magnetic data yielded the *g*-value (*g* = 2.124), exchange parameter (*J* = -1.29 cm^{-1}) and zero-field splitting parameter (|D| = 0.738 cm^{-1}). These values are in agreement with iron(II) complexes from the literature. In comparison to the complexes **C1-C4**, the simulated parameters for **C6** show a stronger antiferromagnetic coupling and a smaller zero-field splitting contribution. The stabilization of the [HS-HS] state at room temperature with this methoxy-substituted ligand **L5** was successful, but the spin-crossover properties are lost in **C6** as well.
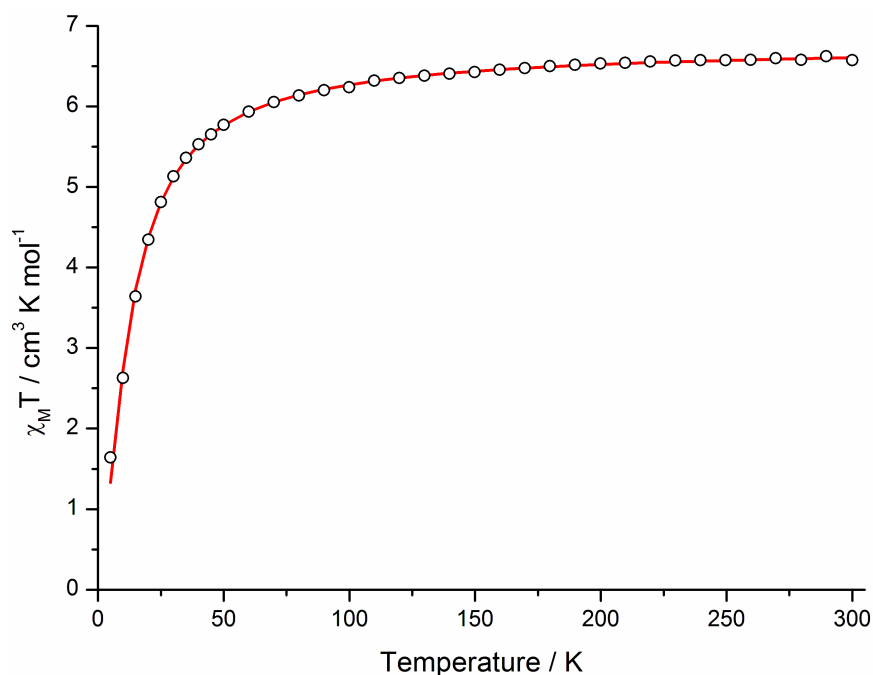

Figure 5.12.: χ_MT vs. T data for **C6**. The experimental data is presented in circles and the fit of the magnetic data as a red line. Data per dinuclear iron(II) complex.

In conclusion, the substitution in the *meta*-position of the nitrogen donor atom of the pyridine ring with a methyl or methoxy group led to the desired stabilization of the [HS-HS] state at room temperature. In addition, the air-sensitivity of the complexes com-

pared to **C4** was reduced as well. Unfortunately, a structure determination *via* X-ray diffraction experiments was not possible due to the amorphous or polycrystalline nature of the isolated complexes. Thus, a discussion of the complex structure and geometry is not possible. To get more information about the nature of the molecular structure and packing in the crystal, further experiments to synthesize crystalline samples with the two ligands should be made.

5.4. Iron(II) complexes with L6

The bis-tetradentate 1,3,4-thiadiazole bridging ligand **L6** has been synthesized to have a direct influence on the ligand field splitting of the iron(II) centers. This ligand contains eight nitrogen donor atoms to chelate two metal centers. The residual four coordination sites on the two metal centers can be occupied by coordinating anions or co-ligands (figure 5.13). This gives rise to the ability to directly fine-tune the ligand field splitting and influence the magnetic properties of the complexes.
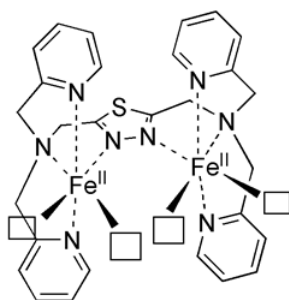

Figure 5.13.: The expected structure of a dinuclear iron(II) complex with **L6**. The free coordination sites have been visualized with squares.

L6 (2,5-bis[N,N-bis(2-pyridylmethyl)aminomethyl]-1,3,4-thiadiazole, figure 5.14) has been synthesized in a nucleophilic substitution reaction between 2,5-bis(chloromethyl)-1,3,4-thiadiazole (**TDA**) and bis(picolyl)amine.

The synthesis of dinuclear iron(II) complexes with different coordinating anions yielded three dinuclear compounds with the general formula [Fe$_2$(μ-**L6**)$_2$(NCE)$_4$] (E = S in **C7**,
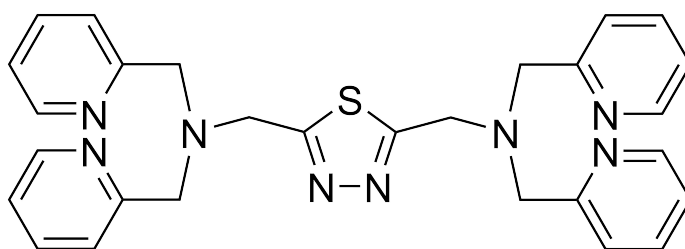
Figure 5.14.: The 1,3,4-thiadiazole based ligand **L6** (2,5-bis[N,N-bis(2-pyridylmethyl) aminomethyl]-1,3,4-thiadiazole)

Se in **C8** and BH_3 in **C9**). The complexes have been isolated as powders from precipitation reactions with **L6** and mononuclear iron(II) precursor complexes [Fepy$_4$(NCE)$_2$] (py = pyridine). The recrystallization of these powders and other reaction conditions did not yield any single crystals suitable for X-ray diffraction experiments. Thus, the characterization of these compounds is based on elemental analysis, IR spectroscopy and variable-temperature magnetic susceptibility measurements. Elemental analysis confirmed the isolation of the complexes as powders (**C7**, **C8** and **C9**) in the expected composition.

The IR spectroscopy can been used to gain informations with regard to the spin state of the iron(II) centers and the binding mode of the anions. The $\nu(C\equiv N)$ stretching vibration is a useful sensor and appeared for the complexes at 2061 cm^{-1} (NCS in **C7**), 2066 cm^{-1} (NCSe in **C8**) and 2186 cm^{-1} (NCBH$_3$ in **C9**). These values are in good agreement with literature data for NCE anions bound to iron(II) in the HS state. The $\nu(C\equiv N)$ stretching vibrations of NCS and NCSe are usually in the range of 2020-2080 cm^{-1} for the HS state, compared to $\approx$2100 cm^{-1} for the LS state.[142,161,162] Furthermore, it can be seen, that the NCS and NCSe anions are bound with the nitrogen atoms. Vibration bands higher than $\approx$2100 cm^{-1} would also be a sign for S-bound NCS and Se-bound NCSe. The $\nu(C\equiv N)$ stretching vibration of NCBH$_3$ is usually detected at higher wavenumbers above 2100 cm^{-1}, which is also the case in **C9**.[142,163,164] This is a confirmation of the proposed complex structure [Fe$_2$(μ-**L6**)$_2$(NCE)$_4$] with a coordination of the anions to the iron(II) centers.[161]

The temperature dependence of the molar magnetic susceptibility has been measured for all three compounds and is shown in figure 5.15. The data at 300 K is in agreement with the findings from the IR spectroscopy and shows a stabilization of a paramagnetic

ground state. The χ_MT value of 6.27 cm^3 K mol^{-1} at 300 K for the thiocyanate complex **C7** is in the range of the spin-only value for a dinuclear iron(II) complex in the HS state. The χ_MT values of 5.48 cm^3 K mol^{-1} (**C8**) and 5.13 cm^3 K mol^{-1} (**C9**) at 300 K are significantly smaller and are an indication for a smaller *g*-value. There is no sign for a spin transition at lower temperatures. The decrease of the magnetic moment has its origin in antiferromagnetic coupling between the iron(II) centers and a zero-field splitting contribution. This results in χ_MT values of 2.91 cm^3 K mol^{-1} (**C7**), 2.49 cm^3 K mol^{-1} (**C8**) and 3.01 cm^3 K mol^{-1} (**C9**) at 5 K.
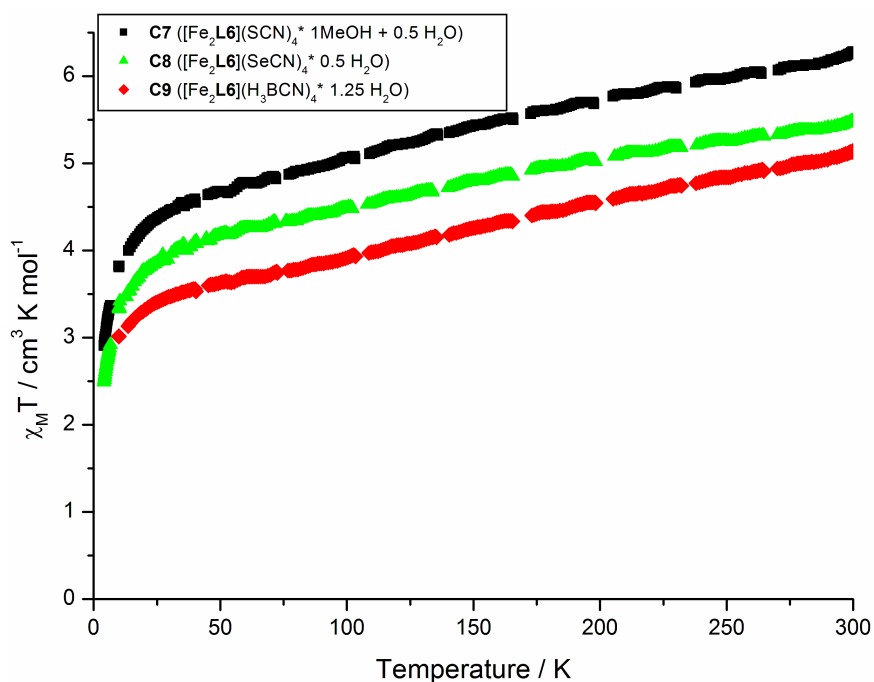
Figure 5.15.: χ_MT vs. T data for **C7** (black), **C8** (green) and **C9** (red). Data per dinuclear iron(II) complex.

The temperature dependence of the magnetic moment for **C7**, **C8** and **C9** is conspicuously similar and deviates mainly in the absolute values of the magnetic moment. Unfortunately, it is not possible to adequately simulate the magnetic data to gain informations about the *g*-value, exchange parameter and zero-field splitting parameter. Thus, the *g*-value has been calculated with the χ_MT values at 300 K and the following relation:

$$\chi = \frac{Ng^2\beta^2}{3kT}S(S+1)$$

with the Avogadro constant N, the Bohr magneton β, the Boltzman constant k and the spin quantum number S.[165]

This gave g-values of 2.045 for **C7**, 1.911 for **C8** and 1.849 for **C9**. The g-values for **C7**, **C8** and **C9** reveal a decrease from the thiocyanate **C7** to the cyanborohydrite **C9** complex. A smaller g-value for metal ions in octahedral complexes has its origin in spin-orbit coupling due to a distortion of the octahedral geometry and a mixing of ground states with excited states. Smaller g-values can be found for d^6-complexes with an compressed octahedral geometry. This changes the ligand field splitting and leads to an energetic convergence of the d_{xy} and $d_{x^2-y^2}$ orbitals (figure 5.16). An increasing compression of the octahedron leads to stronger spin-orbit coupling and a decreasing g-value. An elongation of the octahedron on the other side results in a larger g-value.
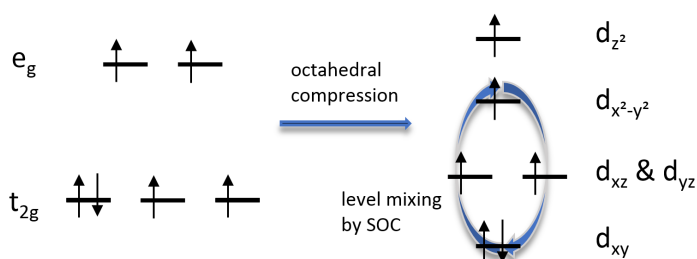

Figure 5.16.: Schematic representation of the mixing of different orbitals due to a compression of the octahedral geometry.

The structural differences in this series of complexes, which lead to these different g-values, can be explained with the π-donor abilities of the coordinating anions. The thiocyanate is the strongest π-donor ligand and thus binds stronger to the iron(II) centers. This can be seen in the IR spectra of the complexes. The $\nu(C{\equiv}N)$ stretching vibration of the thiocyanate has been detected at the lowest energy, which indicates the strongest shift of electron density towards the metal center. The selenocyanate and cyanborohydride anions are weaker π-donor ligands and the anions with lower π-donor ability have a weaker bond to the iron(II) centers. This results in longer iron-NCE bond lengths and the stronger distortion of the octahedral geometry. A stronger distortion leads to a stronger energetic convergence of the d_{xy} and $d_{x^2-y^2}$ orbitals (figure 5.16), an increased mixing of the ground states with exited states and finally a lower g-value.

In conclusion, the synthesis of dinuclear iron(II) complexes with the bis-tetradentate 1,3,4-thiadiazole bridging ligand **L6** was successful. Although, it was not possible to isolate the complexes in form of single crystals for a closer structural investigation, the magnetic measurements revealed the HS state at room temperature. The differences in the *g*-values for the three compounds correlate to the geometry of the complexes and arise from a compression of the octahedral coordination environment.

6. Summary and Outlook

This research aimed at the synthesis of the first dinuclear iron(II) spin-crossover complexes with 1,3,4-thiadiazole bridging ligands. The first synthesized compounds are based on a well-known ligand system, which has been varied by the incorporation of the 1,3,4-thiadiazole heterocycle. These compounds were investigated and further modifications of the ligand system have been made to get a better understanding about the various influences on the spin-crossover properties. The presented six new ligand systems and their iron(II) complexes show very different magnetic properties. Furthermore, they demonstrate the various strategies that can be used to influence the spin ground states or the spin-crossover behavior.

The incorporation of the 1,3,4-thiadiazole heterocycle into the previously reported bridging ligand PMAT led to the synthesis of **L1** (2,5-bis[(2-pyridylmethyl)amino]methyl-1,3,4-thiadiazole) and dinuclear iron(II) complexes showing a spin transition at higher temperatures. The previously elusive [LS-LS] state can be stabilized by the dinuclear complexes at low temperatures. The **L1**-analog triazole, pyrazolate and oxadiazole were unable to reach this diamagnetic ground state due to the highly constrained nature of the complexes. Thus, the use of the 1,3,4-thiadiazole was the key idea and succeeded in the synthesis of these spin-crossover complexes with a diamagnetic ground state at low temperatures. The spin-crossover in these complexes is gradual, incomplete towards the [HS-HS] state and starts around room temperature.

Inclusion of a different solvent into iron(II) complexes with **L1** resulted in a drastic change of the magnetic properties. A strong solvent-dependency of the spin-crossover behavior has been found for these compounds. Such a reversible change of the properties is very unusual and the present complexes are prime examples for a chemo sensor for specific solvents. The solvated and desolvated complexes in chapter 4 now stabilize all three possible spin states ([HS-HS], [HS-LS] and [LS-LS]) of dinuclear spin-crossover complexes, because of the strong solvent effect on the spin ground state of the complexes. These states can be addressed selectively, depending on the temper-

ature and amount of solvent in the complex. The solvated complex is diamagnetic and the desolvated complex shows a spin transition from the [HS-LS] into the [HS-HS] state around room temperature. The desolvation and resolvation is completely reversible and can be performed multiple times.

The bridging ligand **L2** (2,5-bis[N-methyl-N-(2-pyridylmethyl)aminomethyl]-1,3,4-thia-diazole) has been synthesized on the basis of the probed properties of the first ligand system and was designed to stabilize the [HS-HS] state at room temperature. This deliberate change of the magnetic properties has been accomplished with a substitution of the secondary amines. The added methyl groups suppressed classical hydrogen bonding interactions and led to highly distorted dinuclear iron(II) complexes. The variation of the geometry resulted in the loss of spin-crossover properties, because of the inability to accomplish the accompanied change in the iron-nitrogen bond lengths and angles. The strong distortion in the complexes are a consequence of the pronounced shifted and tilted arrangement of the ligand molecules. These complex show a too distorted geometry and this rigidity in the complex cation inhibits the geometry change during the spin transition.

The ligands **L3** (2,5-bis[(2-pyridylethyl)aminomethyl]-1,3,4-thiadiazole), **L4** (2,5-bis[(2-(6-methyl-pyridyl)methyl)aminomethyl]-1,3,4-thiadiazole) and **L5** (2,5-bis[(2-(6-methoxy-pyridyl)methyl)aminomethyl]-1,3,4-thiadiazole) were designed to stabilize the [HS-HS] state at room temperatures. The idea for the ligand modification was a forced elongation of the iron-nitrogen bond lengths. This was realized with ethylpyridine side-arms in **L3** and with substituents in the *meta*-position of the pyridine nitrogen donor atoms in **L4** and **L5**. The modifications changed the spin state of the iron(II), but it led to a loss of the spin-crossover properties as well. The complexes with **L4** and **L5** have not been obtained as single crystals. Thus, it was not possible to study the molecular structure and the intermolecular interactions between the complexes.

Finally, the bis-tetradentate ligand **L6** (2,5-bis[N,N-bis(2-pyridylmethyl)aminomethyl]-1,3,4-thiadiazole) was used for the synthesis of dinuclear iron(II) complexes with only one ligand molecule and free coordination sites at the iron(II) centers. This allows a

direct influence on the magnetic properties with co-ligands and/or coordinating anions. All obtained iron(II) complexes show a paramagnetic ground state, but no spin transition. The IR and magnetic data allowed to correlate between the π-donor ability of the coordinating anions with the complex geometry.

In conclusion, the presented results show the great potential of 1,3,4-thiadiazole bridging ligands for the synthesis of dinuclear iron(II) spin-crossover complexes. Future efforts should focus on the crystallization of complexes with the new ligands **L3-L6**. Insights into the structure of these iron(II) complexes would be very helpful to determine which changes could improve the spin-crossover properties.

The synthesized 2,5-bis(aminomethyl)-1,3,4-thiadiazole is a perfect starting point for new ligand systems. These ligands could be synthesized analog to **L5** in a condensation reaction and reduction of the *in-situ* formed imine. Various aldehydes with aromatic nitrogen donor heterocycles can be used for a series of new ligands (figure 6.1) that should be suitable for iron(II) SCO complexes. Moreover, the five membered heterocycles (imidazole and thiazole) should also lead to a stabilization of the [HS-HS] state at room temperature. The deviating angles in the ligand structure ought to result in a longer distance between the iron(II) centers and the nitrogen donor atoms.
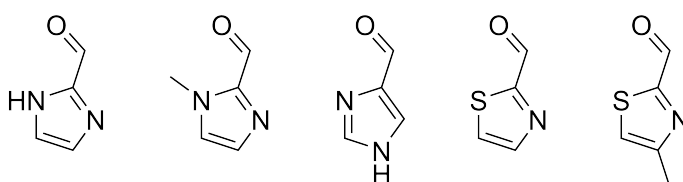
Figure 6.1.: Aldehydes for the synthesis of new 1,3,4-thiadiazole bridging ligands.

Finally, the synthesized 2,5-bis(azidomethyl)-1,3,4-thiadiazole can be used to synthesize new ligands in copper(I)-catalyzed azide-alkyne cycloadditions (CuAAC). These reactions have the advantage of mild reaction conditions and a modest purification. The resulting thiadiazole and triazole containing ligands provide four nitrogen donor atoms. Dinuclear complexes with a general formula of $[Fe_2(\mu\text{-L})_2]X_4$ would have four

free coordination sites for the use of coordinating anions or co-ligands to fine-tune the magnetic properties.[166,167]

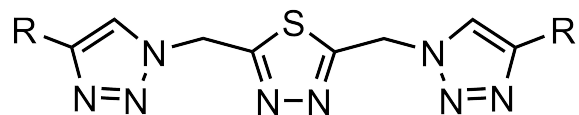Figure 6.2.: General structure for new ligands synthesized *via* click reactions.

7. Experimental Section

7.1. Methods and Materials

7.1.1. Materials

All chemicals were purchased from Alfa Aesar, Acros Organics, Deutero, Fisher Chemicals, Sigma-Aldrich and TCI Chemicals and used without further purification. The solvents for the complex syntheses were degassed with argon. All complex syntheses were performed in an argon or nitrogen atmosphere to prevent the oxidation of iron(II) to iron(III).

7.1.2. X-ray Crystallography

Single-crystal X-ray diffraction data were collected with a Bruker SMART APEX II CCD diffractometer at the Johannes Gutenberg-University Mainz at 173 K. The structures were solved with superflip[168] and olex2.solve, and refined with SHELXL[169] with the program Olex2.[170]

7.1.3. SQUID Measurements

Magnetic susceptibility data were collected with a Quantum Design SQUID magnetometer MPMSXL (at the Johannes Gutenberg-University Mainz) and with a Quantum Design PPMS magnetometer (at Industrial Research Limited, Lower Hutt, New Zealand) in a temperature range of 2-400 K with an applied field of 1 kOe. The molar susceptibility was calculated with the program julX 1.4.1 of Eckhard Bill (MPI Mülheim/Ruhr).

The simulation of the magnetic data has been performed with PHI.[171] The used Hamiltonian in the program PHI

$$\hat{H} = \hat{H}_{SO} + \hat{H}_{EX} + \hat{H}_{CF} + \hat{H}_{ZEE}$$

contains the spin-orbit coupling Hamiltonian ($\hat{H}_{SO}$), exchange interaction Hamiltonian ($\hat{H}_{EX}$), Crystal Field Hamiltonian ($\hat{H}_{CF}$) and Zeeman Hamiltonian ($\hat{H}_{ZEE}$). It was possible to solely consider the exchange interaction Hamiltonian ($\hat{H}_{EX}$) and Crystal Field Hamiltonian ($\hat{H}_{CF}$) for the treated systems.

$$\hat{H}_{EX} = -2 \sum_{i<1}^{i,j\in N} J_{ij} \vec{S}_i \cdot \vec{S}_j$$

$$\hat{H}_{CF} = \sum_{i=1}^{N} \sum_{k=2,4,6} \sum_{q=-k}^{k} B_{k_i}^q \theta_k \hat{O}_{k_i}^q$$

In some cases a temperature independent paramagnetism (*TIP*) had to be included in the simulation.

7.1.4. NMR-Spectroscopy

The NMR spectra were recorded at room temperature using a Bruker DRX 400 spectrometer ($\nu(^1\text{H})$ = 400.13 MHz, $\nu(^{13}\text{C})$ = 100.61 MHz). The data was processed and analyzed with the programs Bruker TopSpin 1.3 and MestReNova.[172]

7.1.5. Mössbauer Measurements

^{57}Fe Mössbauer spectra were recorded at 70 K, 80 K, 293 K or 307 K on a self-made Mössbauer spectrometer with a CryoVac He-Bath-Cryostat. The data was recorded and analyzed by fitting to Lorentzian lines by Sergii I. Shylin and Dr. Vadim Ksenofontov at the Johannes Gutenberg-University Mainz.

7.1.6. Mass Spectrometry

ESI-MS (ElectroSpray Ionization mass spectrometry) and FD-MS (Field Desorption mass spectrometry) data were recorded at the Institute of Organic Chemistry of the Johannes Gutenberg-University Mainz. The ESI mass spectra were recorded on a Waters/MicroMass Q-Tof Ultima 3 spectrometer and the FD mass spectra with a Finnigan MAT95XP.

7.1.7. Elemental Analysis

Elemental analyses (C, H, N and S) were measured at the micro-analytical laboratory of the Johannes Gutenberg-University Mainz with a Foss Heraeus Vario EL elemental analyzer. and at the Campbell micro-analytical laboratory of the University of Otago in Dunedin, New Zealand.

7.1.8. Infrared Spectroscopy

Infrared spectra (FT-IR) were recorded as potassium bromide pellets in the range from $4000\,cm^{-1}$ to $400\,cm^{-1}$ with a JASCO FT/IR-4200. The data processing was performed with JASCO Spectra Manager.

7.2. Syntheses

7.2.1. Ligand Syntheses

N-(2-picolyl)methylamine, 2-formaldoxime-6-methylpyridine, 2-aminomethyl-6-methyl-pyridine, 2,5-bis(azidomethyl)-1,3,4-thiadiazole and bis(picolyl)amine were synthesized according to a modified literature procedure.[150,157–159,173]

7.2.1.1. L2

[183.05]   [122.17]   [354.48]
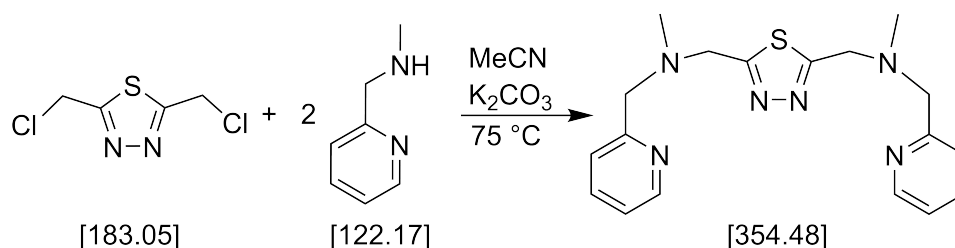
A suspension of N-(2-picolyl)methylamine (1,22 g, 10.0 mmol) and potassium carbonate (3,46 g , 25.0 mmol) in acetonitrile (200 mL) was heated to 75 °C. A solution of 2,5-bis(chloromethyl)-1,3,4-thiadiazole (0,92 g, 5.0 mmol) in acetonitrile (50 mL) was added and the reaction mixture was heated overnight. The potassium carbonate was filtered and the filtrate evaporated to dryness under reduced pressure, resulting in a brown oil. The oil was purified by column chromatography (silica, chloroform/methanol 9:1) to give the pure ligand as an orange oil.

Yield: 1,52 g (4.29 mmol, 86 %).

^{1}**H NMR** (400 MHz, CDCl$_3$, 25 °C): (figure B.1)

δ = 8.55 (d, $^3J_{H,H}$ = 4.9 Hz, 1.8 Hz, 0.9 Hz, 4H, H5-Py), 7.68 (td, $^3J_{H,H}$ = 7.7 Hz, 1.9 Hz, 4H, H4-Py), 7.47 (d, $^3J_{H,H}$ = 7.8 Hz, 1.1 Hz, 4H, H2-Py), 7.18 (dd, $^3J_{H,H}$ = 7.6 Hz, 4.9 Hz, 1.2 Hz, 4H, H3-Py), 4.02 (s, 4H, CH$_2$-TDA), 3.80 (s, 4H, CH$_2$-Py), 2.37 (s, 6H, CH$_3$).

^{13}**C NMR** (100 MHz, CDCl3, 25 °C): (figure B.2)

δ = 171.35 (C-TDA), 158.37 (C1-Py), 149.26 (C5-Py), 136.57 (C4-Py), 122.91 (C2-Py),

122.27 (C3-Py), 63.25 (CH_2-Py), 55.96 (CH_2-TDA), 42.76 (CH_3) ppm.

Elemental Analysis: (**L2** + 1.1 H_2O): calc. C 57.76, H 6.52, N 22.45, S 8.57; found C 57.91, H 6.93, N 22.00, S 9.08.

FD-MS (DMSO): m/z (%) = 354.1 (100) [L2$^+$], 355.1 (44) [L2$^+$], 356.1 (11) [L2$^+$]. (figure E.1)

7.2.1.2. L3

[183.05]   [122.17]   [354.48]
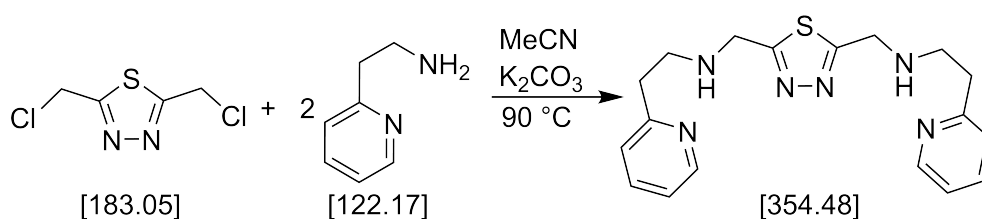
A suspension of 2-(2-pyridine)ethylamine (4,58 g, 37.5 mmol) and potassium carbonate (5,18 g, 37.5 mmol) in acetonitrile (500 mL) was heated to 90 °C. A solution of 2,5-bis(chloromethyl)-1,3,4-thiadiazole (1,37 g, 7.5 mmol) in acetonitrile (50 mL) was added dropwise over a period of 30 min. The suspension was heated for further 7 hours after complete addition. The mixture was cooled to room temperature, the potassium carbonate filtered and the filtrate evaporated to dryness under reduced pressure. The resulting brown oil was purified by column chromatography (aluminium oxide, chloroform/methanol 99:1 and slowly increasing methanol content to 3 %) to give the pure product as a brown oil.

Yield: 1,89 g (5.34 mmol, 71 %).

^{1}**H NMR** (400 MHz, CDCl$_3$, 25 °C): (figure B.3)

δ = 8.49 (ddd, $^3J_{H,H}$ = 4.9 Hz, 1.9 Hz, 0.9 Hz 2H, H5-Py), 7.57 (td, $^3J_{H,H}$ = 7.6 Hz, 1.9 Hz, 2H, H4-Py), 7.14 (d, $^3J_{H,H}$ = 7.8 Hz, 2H, H2-Py), 7.09 (ddd, $^3J_{H,H}$ = 7.6 Hz, 4.9 Hz, 1.2 Hz, 2H, H3-Py), 4.16 (s, 4H, CH_2-TDA), 3.07 (t, $^3J_{H,H}$ = 6.3 Hz, 4H, CH_2), 2.97 (t, $^3J_{H,H}$ = 6.6 Hz, 4H, CH_2-Py), 2.29 (s, 2H, NH) ppm.

^{13}**C NMR** (100 MHz, CDCl$_3$3, 25 °C): (figure B.4)

δ = 172.39 (C-TDA), 159.80 (C1-Py), 149.31 (C5-Py), 136.39 (C4-Py), 123.30 (C2-Py),

121.35 (C3-Py), 48.68 (CH$_2$-Py), 48.21 (CH$_2$), 38.07 (CH$_2$-TDA) ppm.

Elemental Analysis: (**L3** + 2/11 CHCl$_3$): calc. C 58.05, H 5.94, N 22.34, S 8.52; found C 58.31, H 6.16, N 22.09, S 8.63.

FD-MS (MeOH): m/z (%) = 355.4 (100) [L3+H$^+$], 356.3 (12) [L3+H$^+$], 709.5 (95) [2xL3 +H$^+$], 710.5 (15) [2xL3+H$^+$]. (figure E.2)

7.2.1.3. L4

[183.05]   [122.17]   [354.48]
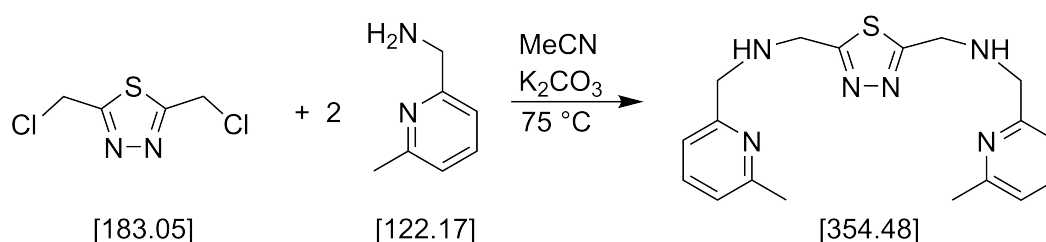
A suspension of 2-aminomethyl-6-methylpyridine (0,75 g, 6.1 mmol) and potassium carbonate (1,38 g, 10.0 mmol) in acetonitrile (300 mL) was heated to 75 °C. A solution of 2,5-bis(chloromethyl)-1,3,4-thiadiazole (0,366 g, 2.0 mmol) in acetonitrile (50 mL) was added dropwise and the reaction mixture heated overnight. The mixture was cooled to room temperature, the potassium carbonate filtered and the filtrate evaporated to dryness under reduced pressure. The resulting brown oil was purified by column chromatography (silica, chloroform/methanol 9:1) resulting in the pure product as a yellow oil.

Yield: 0,51 g (1.44 mmol, 72 %).

^{1}H NMR (400 MHz, CDCl$_3$, 25 °C): (figure B.5)

δ = 7.39 (t, 2H, $^3J_{H,H}$ = 7.7 Hz, H3-Py), 6.96 (d, 2H, $^3J_{H,H}$ = 7.7 Hz, H2-Py), 6.89 (d, 2H, $^3J_{H,H}$ = 7.7 Hz, H4-Py), 4.09 (s, 4H, CH$_2$-TDA), 3.80 (s, 4H, CH$_2$-Py), 2.71 (s, 2H, NH), 2.39 (s, 6H, CH$_3$) ppm.

^{13}C NMR (100 MHz, CDCl$_3$3, 25 °C): (figure B.6)

δ = 172.15 (C-TDA), 157.97(C5-Py), 157.83 (C1-Py), 136.66 (C3-Py), 121.62 (C4-Py), 119.16 (C2-Py), 54.29 (CH$_2$-Py), 47.80 (CH$_2$-TDA), 24.38 (CH$_3$) ppm.

ESI-MS (MeOH): m/z (%) = 355.2 (100) [L4+H$^+$], 356.2 (26) [L4+H$^+$], 357.2 (7) [L4+H$^+$], 377.2 (24) [L4+Na$^+$]. (figure E.3)

7.2.1.4. 2,5-Bis(aminomethyl)-1,3,4-thiadiazole
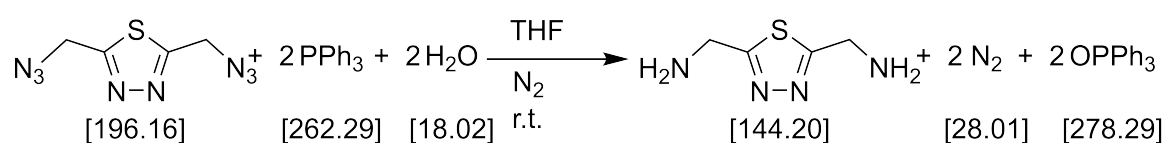
2,5-Bis(azidomethyl)-1,3,4-thiadiazole (2,70 g, 13.76 mmol) was dissolved in tetrahydrofuran (130 mL) and triphenylphosphine (8,66 g, 33.0 mmol) was added to the solution, resulting in an immediate gas evolution. Water (8 mL) was added after one hour of stirring at room temperature and the solution stirred in a nitrogen atmosphere for further 40 hours. The solvent was removed under reduced pressure and the resulting crude orange solid purified by column chromatography (silica). The residual triphenylphospine and formed triphenylphosphine oxide was eluted with chloroform/methanol (4:1). The product was isolated with chloroform/methanol (2:1 and 1% triethylamine) as a light yellow solid.

Yield: 1,96 g (13.6 mmol, 99 %).

^{1}**H NMR** (400 MHz, CDCl$_3$, 25 °C): (figure B.7)

δ = 4.29 (s, 4H, CH$_2$-TDA), 1.80 (s, 4H, NH) ppm.

^{13}**C NMR** (100 MHz, CDCl$_3$3, 25 °C): (figure B.8)

δ = 173.78 (C-TDA), 41.55 (CH$_2$-TDA) ppm.

FD-MS (MeOH): m/z (%) = 145.2 (91) [TDA-Amin+H$^+$], 289.1, (100) [2xTDA-Amin+H$^+$]. (figure E.4)

7.2.1.5. L5

[144.20] [121.14] [354.48]
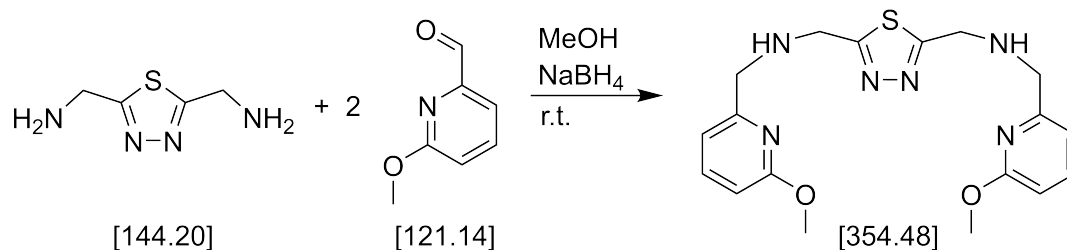
2,5-Bis(aminomethyl)-1,3,4-thiadiazole (0,84 g, 5.83 mmol) and 6-methoxy-2-pyridine-carboxaldehyde (1,60 g, 11.67 mmol) were dissolved in 180 mL dry methanol under an argon atomsphere. The solution was stirred at room temperature for 45 minutes and heated under reflux for 6 hours. The solution was cooled with an ice bath and sodium borohydride (1,17 g, 30.9 mmol) was added in small portions. After complete addition the solution was stirred at room temperature overnight. The solvent was removed under reduced pressure. The resulting crude product was dissolved in water, extracted with dichloromethane and the combined organic phases dried with sodium sulfate. Purification by column chromatography (silica, chloroform/methanol 9:1) resulted in the pure product as an orange oil.

Yield: 1,09 g (2.82 mmol, 48 %).

^{1}**H NMR** (400 MHz, CDCl$_3$, 25 °C): (figure B.9)

δ = 7.43 (t, 2H, $^3J_{H,H}$ = 7.7 Hz, H3-Py), 6.75 (d, 2H, $^3J_{H,H}$ = 7.2 Hz, H2-Py), 6.53 (d, 2H, $^3J_{H,H}$ = 8.2 Hz, H4-Py), 4.15 (s, 4H, CH$_2$-TDA), 3.83 (s, 6H, -OCH$_3$), 3.79 (s, 4H, CH$_2$-Py), 2.66 (s, 2H, NH) ppm.

^{13}**C NMR** (100 MHz, CDCl$_3$3, 25 °C): (figure B.10)

δ = 172.26 (C-TDA), 163.80(C5-Py), 156.28 (C1-Py), 138.89 (C3-Py), 114.63 (C4-Py), 108.93 (C2-Py), 53.71 (CH$_2$-Py), 53.17 (-OCH$_3$), 47.70 (CH$_2$-TDA) ppm.

FD-MS (MeOH): m/z (%) = 387.2 (100) [L5+H$^+$], 773.2 (36) [2xL5+H$^+$], 774.1 (21) [2xL5+H$^+$]. (figure E.5)

7.2.1.6. L6

[183.05] [199.26] [508.65]
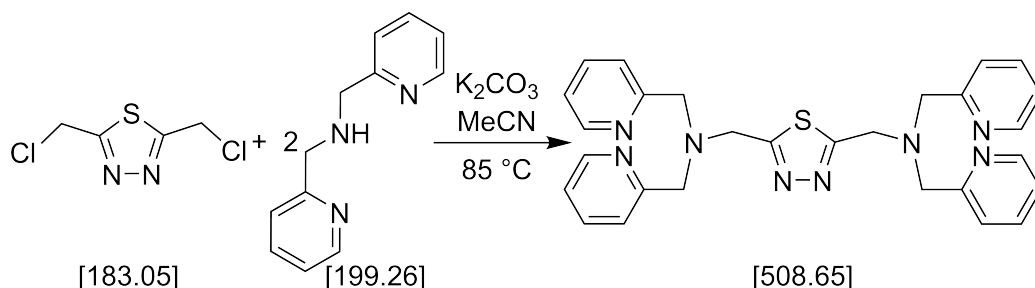
A suspension of bis(picolyl)amine (1.82 g, 9.15 mmol) and potassium carbonate (3,16 g, 22.85 mmol) in acetonitrile (170 mL) was heated to 75 °C. A solution of 2,5-bis(chloro methyl)-1,3,4-thiadiazole (0,84 g, 4.57 mmol) in acetonitrile (30 mL) was added and the reaction mixture heated overnight to 85 °C. The warm reaction mixture was filtered to remove the colorless potassium carbonate and the volume of the filtrate reduced to a volume of 20 mL under reduced pressure. The reaction mixture was left in the refrigerator overnight and the resulting pale solid filtered off and washed with a small amount of cold acetonitrile. The solid was dissolved in water and extracted with dichloromethane. The organic phase was dried with magnesium sulfate and evaporated to dryness under reduced pressure. The pure ligand was isolated as a pale orange solid.

Yield: 1,33 g (2.62 mmol, 57 %).

^{1}H NMR (400 MHz, CDCl$_3$, 25 °C): (figure B.11)

δ = 8.53 (ddd, $^3J_{H,H}$ = 4.89 Hz, 1.70 Hz, 0.85 Hz, 4H, H5-Py), 7.64 (dd, $^3J_{H,H}$ = 7.7 Hz, 1.8 Hz, 4H, H4-Py), 7.50 (td, $^3J_{H,H}$ = 7.8 Hz, 1.1 Hz, 4H, H2-Py), 7.16 (ddd, $^3J_{H,H}$ = 7.5 Hz, 4.9 Hz, 1.2 Hz, 4H, H3-Py), 4.14 (s, 4H, CH$_2$-TDA), 3.91 (s, 8H, CH$_2$-Py).

^{13}C NMR (100 MHz, CDCl3, 25 °C): (figure B.12)

δ = 171.32 (C-TDA), 158.21 (C1-Py), 149.23 (C5-Py), 136.54 (C4-Py), 123.10 (C2-Py), 122.30 (C3-Py), 59.91 (CH$_2$-Py), 52.69 (CH$_2$-TDA) ppm.

Elemental Analysis: (**L6** + 1/6 DCM): calc. C 64.71, H 5.46, N 21.43, S 6.13; found C 64.58, H 5.41, N 21.61, S 6.12.

FD-MS (DMSO): m/z (%) = 508.12 (100) [L6$^+$], 509.11 (39) [L6$^+$], 510.11 (11) [L6$^+$]. (figure E.6)

7.2.2. Complex Syntheses

7.2.2.1. $[Fe_2(\mu\text{-}L2)_2](BF_4)_4 \cdot 2MeCN$ (C1)

The ligand **L2** (106 mg, 0.4 mmol) and $Fe(BF_4)_2 * 6H_2O$ (101 mg, 0.3 mmol) were dissolved in 10 mL methanol. The solution was stored in a diethyl ether diffusion and yellow polycrystalline solid could be obtained after two weeks. The polycrystalline solid was dissolved in acetonitrile and stored in a diethyl ether diffusion, resulting in colorless single crystals of **C1** suitable for X-ray diffraction experiments after 6 days.

Elemental Analysis: ($[Fe_2(\mu\text{-}L2)_2](BF_4)_4 \cdot 1.2MeCN$): calc. C 37.89, H 3.94, N 15.19, S 5.27; found C 37.74, H 3.54, N 15.58, S 5.61.

ESI-MS (MeCN): m/z (%) = 382.1, (38) [2xL2+Fe^{2+}], 429.1 (34) [2xL2+2xFe^{2+}+2xF$^-$], 783.2 (100) [2xL2+Fe^{2+}+F$^-$], 851.3 (32) [2xL2+Fe^{2+}+BF$_4^-$], 877.2 (6) [2xL2+2xFe^{2+}+3xF$^-$], 945.2 (11) [2xL2+2xFe^{2+}+BF$_4^-$+2F$^-$]. (figure E.7)

7.2.2.2. $[Fe_2(\mu\text{-}L2)_2](ClO_4)_4 \cdot 1MeCN+0.75MeOH$ (C2)

The ligand **L2** (53 mg, 0.15 mmol) was dissolved in 3 mL methanol and a solution of $Fe(ClO_4)_2 * xH_2O$ (41 mg, 0.15 mmol) in 4 mL methanol was added. The solution was subjected to vapor diffusion of diethyl ether and yellow polycrystalline solid was obtained after 10 days. The polycrystalline solid was dissolved in acetonitrile and subjected to vapor diffusion of diethyl ether. Colorless single crystals of **C2** suitable for X-ray diffraction experiments were obtained after 11 days.

Elemental Analysis: ($[Fe_2(\mu\text{-}L2)_2](ClO_4)_4 \cdot 0.5MeCN+0.5MeOH$): calc. C 35.89, H 3.81, N 13.95; found C 35.50, H 3.76, N 14.34.

ESI-MS (MeCN): m/z (%) = 382.1, (23) [2xL2+Fe^{2+}], 509.0 (10) [2xL2+2xFe^{2+}+2xClO$_4^-$], 863.1 (100) [2xL2+Fe^{2+}+ClO$_4^-$].(figure E.8)

7.2.2.3. [Fe$_2$(μ-L2)$_2$](F$_3$CSO$_3$)$_4$·2THF (C3)

The ligand **L2** (36 mg, 0.1 mmol) and Fe(F$_3$CSO$_3$)$_2$ (36 mg, 0.1 mmol) were dissolved in 8 mL acetonitrile. 4 mL tetrahydrofuran were added to the solution and daily addition of 1 mL tetrahydrofuran resulted in colorless single crystals of **C3** suitable for X-ray diffraction experiments after 4 days.

Elemental Analysis: ([Fe$_2$(μ-**L2**)$_2$](F$_3$CSO$_3$)$_4$·1.5THF): calc. C 36.23, H 3.70, N 11.02, S 12.61; found C 35.92, H 2.55, N 11.50, S 12.34.

ESI-MS (MeCN): m/z (%) = 382.1, (27) [2xL2+Fe^{2+}], 559.0 (60) [2xL2+2xFe^{2+}+ 2xF$_3$CSO$_3^-$], 709.0 (18) [2xL2+H$^+$], 913.2 (100) [2xL2+Fe^{2+}+F$_3$CSO$_3^-$], 1267.0 (55) [2xL2+2xFe^{2+}+3xF$_3$CSO$_3^-$].(figure E.9)

7.2.2.4. [Fe$_2$(μ-L3)$_2$](BF$_4$)$_4$ (C4)

The ligand **L3** (106 mg, 0.3 mmol) and Fe(BF$_4$)$_2$*6H$_2$O (101 mg, 0.3 mmol) were dissolved in 10 mL acetonitrile and the solution subjected to vapor diffusion of diethyl ether. Light yellow crystals were obtained after two weeks and redissolved in acetonitrile. Vapor diffusion of diethyl ether into the solution yielded the complex as colorless single crystals of **C4** suitable for X-ray diffraction experiments after one week.

Elemental Analysis: ([Fe$_2$(μ-**L3**)$_2$](BF$_4$)$_4$·1.25MeCN): calc. C 37.93, H 3.95, N 15.22; found C 37.67, H 3.72, N 15.47.

ESI-MS (MeCN): m/z (%) = 382.1, (38) [2xL3+Fe^{2+}], 429.1 (47) [2xL3+2xFe^{2+}+2xF$^-$], 783.2 (100) [2xL3+Fe^{2+}+F$^-$], 851.3 (25) [2xL3+Fe^{2+}+BF$_4^-$], 877.2 (14) [2xL3+2xFe^{2+}+ 3xF$^-$], 945.2 (24) [2xL3+2xFe^{2+}+BF$_4^-$+2F$^-$]. (figure E.10)

7.2.2.5. [Fe$_2$(μ-L4)$_2$](BF$_4$)$_4$ (C5)

The ligand **L4** (53 mg, 0.15 mmol) was dissolved in 5 mL ethanol and added to a solution of Fe(BF$_4$)$_2$*6H$_2$O (51 mg, 0.15 mmol) in 5 mL ethanol. This resulted in the immediate precipitation of the desired complex. The solid was separated by filtration

and washed with ethanol. The complex **C5** was isolated in form of a yellow powder.

Elemental Analysis: ([Fe$_2$(μ-**L4**)$_2$](BF$_4$)$_4$·0.5H$_2$O): calc. C 36.74, H 3.85, N 14.28; found C 36.53, H 3.79, N 14.38.

ESI-MS (MeCN): m/z (%) = 355.2 (91) [L4+H$^+$], 382.1 (100) [2xL4+Fe^{2+}], 429.1 (27) [2xL4+2xFe^{2+}+2xF$^-$], 783.3 (21) [2xL4+Fe^{2+}+F$^-$], 851.3 (12) [2xL4+Fe^{2+}+BF$_4^-$]. (figure E.11)

7.2.2.6. [Fe$_2$(μ-**L5**)$_2$](BF$_4$)$_4$ (C6)

The ligand **L5** (97 mg, 0.25 mmol) was dissolved in 5 mL tetrahydrofuran and layered with a tetrahydrofuran/acetonitrile (1:1, 5 mL) separation layer. Fe(BF$_4$)$_2$*6H$_2$O (85 mg, 0.25 mmol) was dissolved in 5 mL acetonitrile and layer on top of the separation layer. Yellow polycrystalline solid was obtained after three weeks and complete diffusion of the solvents.

Elemental Analysis: ([Fe$_2$(μ-**L5**)$_2$](BF$_4$)$_4$·1.5MeCN): calc. C 36.22, H 3.78, N 14.62, S 4.96; found C 36.33, H 3.71, N 14.50, S 5.30.

ESI-MS (MeCN): m/z (%) = 387.2 (22) [L5+H$^+$], 414.1 (97) [2xL5+Fe^{2+}], 847.2 (100) [2xL5+Fe^{2+}+F$^-$], 915.3 (62) [2xL5+Fe^{2+}+BF$_4^-$], 1077.2 (48) [2xL5+2xFe^{2+}+2xBF$_4^-$ +F$^-$]. (figure E.12)

7.2.2.7. [Fe$_2$(μ-**L6**)$_2$(NCE)$_4$] (C7-C9)

[508.65]   +   2 [Fe(NCE)$_2$py$_4$] $\xrightarrow[\text{r.t.}]{\text{MeOH/DCM} \atop \text{N}_2}$
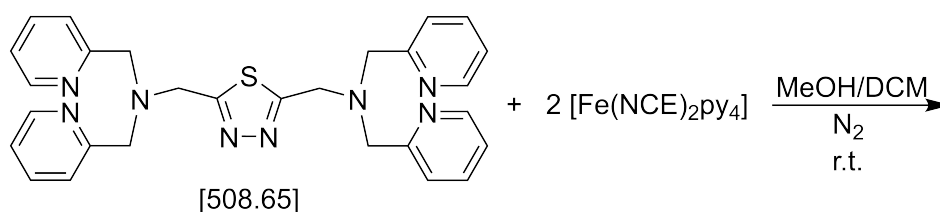
The [Fe(NCE)$_2$py$_4$] precursor was dissolved in 9 mL degassed methanol and filtered through celite. The ligand **L6** was dissolved in 3 mL degassed methanol and 1,5 mL

degassed dichloromethane and added to the iron(II) solution. The desired complex directly precipitated and the reaction mixture was stirred for further 45 minutes in a nitrogen atmosphere. The precipitate was filtered, washed with degassed methanol and dried under high vacuum.

$[Fe_2(\mu\text{-}\mathbf{L6})_2(NCS)_4]$ **C7**

149 mg of $[Fe(NCS)_2py_4]$ (0.3 mmol) and 77 mg of **L6** (0.15 mmol) were used to obtain 24 mg (0.028 mmol, 19 %) of **C7** as a yellow powder.

Elemental Analysis: ($[Fe_2(\mu\text{-}\mathbf{L6})_2(SCN)_4]\cdot$ 1 MeOH + 0.5 H_2O): calc. C 44.35, H 3.72, N 18.18, S 17.94; found C 44.35, H 3.43, N 18.99, S 17.66.

IR(KBr, cm^{-1}): 3444(br), 2359(m), 2061(s), 1604(s), 1441(s), 1384(s), 1156(s), 1053(w), 1019(w), 763(s), 645(w), 490(w).

$[Fe_2(\mu\text{-}\mathbf{L6})_2(NCSe)_4]$ **C8**

116 mg of $[Fe(NCSe)_2py_4]$ (0.2 mmol) and 51 mg of **L6** (0.1 mmol) were used to obtain 39 mg (0.0375 mmol, 38 %) of **C8** as a yellow powder.

Elemental Analysis: ($[Fe_2(\mu\text{-}\mathbf{L6})_2(SeCN)_4]\cdot$ 0.5 H_2O): calc. C 36.63, H 2.79, N 16.02, S 3.06; found C 36.86, H 2.91, N 15.76, S 3.32.

IR(KBr, cm^{-1}): 3443(br), 2921(w), 2354(w), 2326(w), 2066(s), 1652(w), 1646(w), 1635(w), 1625(w), 1605(w), 1437(w), 1385(s), 1162(m), 1094(w), 1072(w), 1054(w), 759(m), 669(w), 560(w), 419(w).

$[Fe_2(\mu\text{-}\mathbf{L6})_2(NCBH_3)_4]$ **C9**

180 mg of $[Fe(NCBH_3)_2py_4]$ (0.4 mmol) and 77 mg of **L6** (0.15 mmol) were used to obtain 34 mg (0.044 mmol, 29 %) of **C9** as a yellow powder.

Elemental Analysis: ($[Fe_2(\mu\text{-}\mathbf{L6})_2(NCBH_3)_4]\cdot$ 1.25 H_2O): calc. C 47.91, H 5.34, N 20.95, S 4.00; found C 48.17, H 5.00, N 20.59, S 4.19

IR(KBr, cm^{-1}): 3421(br), 2343(m), 2186(s), 2075(m), 1605(s), 1474(w), 1444(m), 1386(w), 1157(m), 1119(s), 1054(w), 1019(w), 876(w), 767(s), 647(w), 419(s).

8. Bibliography

[1] D. Trauner, *Beilstein Journal of Organic Chemistry* **2012**, *8*, 870–871.

[2] J. L. Zhang, J. Q. Zhong, J. D. Lin, W. P. Hu, K. Wu, G. Q. Xu, A. T. S. Wee, W. Chen, *Chem. Soc. Rev.* **2015**, *44*, 2998–3022.

[3] C. Simão, M. Mas-Torrent, N. Crivillers, V. Lloveras, J. M. Artés, P. Gorostiza, J. Veciana, C. Rovira, *Nature Chemistry* **2011**, *3*, 359–364.

[4] P. Liljeroth, *Nature Nanotechnology* **2011**, *7*, 5–6.

[5] P. Liljeroth, J. Repp, G. Meyer, *Science* **2007**, *317*, 1203–1206.

[6] E. Coronado, G. M. Espallargas, *Chem. Soc. Rev.* **2013**, *42*, 1525–1539.

[7] N. Song, Y.-W. Yang, *Chem. Soc. Rev.* **2015**, *44*, 3474–3504.

[8] C. Argyo, V. Weiss, C. Bräuchle, T. Bein, *Chem. Mater.* **2014**, *26*, 435–451.

[9] D. N. Woodruff, R. E. P. Winpenny, R. A. Layfield, *Chem. Rev.* **2013**, *113*, 5110–5148.

[10] C. Plenk, J. Krause, M. Beck, E. Rentschler, *Chem. Commun.* **2015**, *51*, 6524–6527.

[11] R. Sessoli, D. Gatteschi, A. Caneschi, M. A. Novak, *Nature* **1993**, *365*, 141–143.

[12] M. Affronte, *J. Mater. Chem.* **2009**, *19*, 1731–1737.

[13] L. R. Piquer, E. C. Sañudo, *Dalton Trans.* **2015**, *44*, 8771–8780.

[14] A. Fihey, A. Perrier, W. R. Browne, D. Jacquemin, *Chem. Soc. Rev.* **2015**, *44*, 3719–3759.

[15] B. K. Pathem, S. A. Claridge, Y. B. Zheng, P. S. Weiss, *Annual Review of Physical Chemistry* **2013**, *64*, 605–630.

[16] J. v. Lintig, K. Vogt, *J. Biol. Chem.* **2000**, *275*, 11915–11920.

[17] W. Ey, Teil II: Sitzungsbericht, Springer-Verlag, **2013**, 301 S.

[18] B. L. Feringa, W. R. Browne, Molecular Switches, John Wiley & Sons, **2011**, 865 S.

[19] S. Venkataramani, U. Jana, M. Dommaschk, F. D. Sönnichsen, F. Tuczek, R. Herges, *Science* **2011**, *331*, 445–448.

[20] S. Thies, C. Bornholdt, F. Köhler, F. Sönnichsen, C. Näther, F. Tuczek, R. Herges, *Chem. Eur. J.* **2010**, *16*, 10074–10083.

[21] M. Dommaschk, M. Peters, F. Gutzeit, C. Schütt, C. Näther, F. D. Sönnichsen, S. Tiwari, C. Riedel, S. Boretius, R. Herges, *J. Am. Chem. Soc.* **2015**, *137*, 7552–7555.

[22] S. Thies, H. Sell, C. Schütt, C. Bornholdt, C. Näther, F. Tuczek, R. Herges, *J. Am. Chem. Soc.* **2011**, *133*, 16243–16250.

[23] M. Dommaschk, C. Schütt, S. Venkataramani, U. Jana, C. Näther, F. D. Sönnichsen, R. Herges, *Dalton Trans.* **2014**, *43*, 17395–17405.

[24] J. Linares, E. Codjovi, Y. Garcia, *Sensors* **2012**, *12*, 4479–4492.

[25] A. Bousseksou, G. Molnár, L. Salmon, W. Nicolazzi, *Chem. Soc. Rev.* **2011**, *40*, 3313–3335.

[26] Y. Garcia, V. Ksenofontov, P. Gütlich, *Hyperfine Interactions* **2002**, *139-140*, 543–551.

[27] L. Cambi, L. Szegö, *Ber. dtsch. Chem. Ges. A/B* **1931**, *64*, 2591–2598.

[28] L. Cambi, L. Szegö, *Ber. dtsch. Chem. Ges. A/B* **1933**, *66*, 656–661.

[29] L. Cambi, L. Malatesta, *Ber. dtsch. Chem. Ges. A/B* **1937**, *70*, 2067–2078.

[30] W. A. Baker, H. M. Bobonich, *Inorg. Chem.* **1964**, *3*, 1184–1188.

[31] K. Madeja, E. König, *Journal of Inorganic and Nuclear Chemistry* **1963**, *25*, 377–385.

[32] R. C. Stoufer, D. H. Busch, W. B. Hadley, *J. Am. Chem. Soc.* **1961**, *83*, 3732–3734.

[33] P. E. Figgins, D. H. Busch, *J. Am. Chem. Soc.* **1960**, *82*, 820–824.

[34] M. A. Robinson, J. D. Curry, D. H. Busch, *Inorg. Chem.* **1963**, *2*, 1178–1181.

[35] A. Hauser in *Spin Crossover in Transition Metal Compounds I*, Topics in Current Chemistry 233, Springer Berlin Heidelberg, **2004**, S. 49–58.

[36] P. Gütlich, Y. Garcia, H. A. Goodwin, *Chem. Soc. Rev.* **2000**, *29*, 419–427.

[37] P. Gütlich, H. A. Goodwin in *Spin Crossover in Transition Metal Compounds I*, Topics in Current Chemistry 233, Springer Berlin Heidelberg, **2004**, S. 1–47.

[38] P. Gütlich, A. Hauser, H. Spiering, *Angew. Chem. Int. Ed. Engl.* **1994**, *33*, 2024–2054.

[39] J. R. Gispert, Coordination Chemistry, Wiley-VCH, **2008**.

[40] J. S. Miller, M. Drillon, Magnetism: Molecules to Materials IV, John Wiley & Sons, **2002**, 512 S.

[41] A. Bhattacharjee, M. Roy, V. Ksenofontov, J. A. Kitchen, S. Brooker, P. Gütlich, *Eur. J. Inorg. Chem.* **2013**, 843–849.

[42] J. Jeftic, R. Hinek, S. C. Capelli, A. Hauser, *Inorg. Chem.* **1997**, *36*, 3080–3087.

[43] P. Gütlich, A. B. Gaspar, Y. Garcia, *Beilstein Journal of Organic Chemistry* **2013**, *9*, 342–391.

[44] Y. Garcia, P. Gütlich in *Spin Crossover in Transition Metal Compounds II*, Topics in Current Chemistry 234, Springer Berlin Heidelberg, **2004**, S. 49–62.

[45] J.-F. Létard, G. Chastanet, P. Guionneau, C. Desplanches in *Spin-Crossover Materials*, John Wiley & Sons Ltd, **2013**, S. 475–506.

[46] J.-F. Létard, J. A. Real, N. Moliner, A. B. Gaspar, L. Capes, O. Cador, O. Kahn, *J. Am. Chem. Soc.* **1999**, *121*, 10630–10631.

[47] S. Decurtins, P. Gütlich, C. P. Köhler, H. Spiering, A. Hauser, *Chemical Physics Letters* **1984**, *105*, 1–4.

[48] I. Lawthers, J. J. McGarvey, *J. Am. Chem. Soc.* **1984**, *106*, 4280–4282.

[49] A. Hauser in *Spin Crossover in Transition Metal Compounds II*, Topics in Current Chemistry 234, Springer Berlin Heidelberg, **2004**, S. 155–198.

[50] J.-F. Létard, *J. Mater. Chem.* **2006**, *16*, 2550–2559.

[51] J.-F. Létard, G. Chastanet, O. Nguyen, S. Marcén, M. Marchivie, P. Guionneau, D. Chasseau, P. Gütlich, *Monatshefte für Chemie* **2003**, *134*, 165–182.

[52] A. B. Gaspar, G. Levchenko, S. Terekhov, G. Bukin, J. Valverde-Muñoz, F. J. Muñoz-Lara, M. Seredyuk, J. A. Real, *Eur. J. Inorg. Chem.* **2014**, 429–433.

[53] A. Bialonska, R. Bronisz, L. Baranowski, *Eur. J. Inorg. Chem.* **2013**, 720–724.

[54] P. Guionneau, *Dalton Trans.* **2013**, *43*, 382–393.

[55] J. Kusz, M. Nowak, P. Gütlich, *Eur. J. Inorg. Chem.* **2013**, 832–842.

[56] L. A. Barrios, E. Peyrecave-Lleixà, G. A. Craig, O. Roubeau, S. J. Teat, G. Aromí, *Eur. J. Inorg. Chem.* **2014**, 6013–6021.

[57] N. Wannarit, O. Roubeau, S. Youngme, S. J. Teat, P. Gamez, *Dalton Trans.* **2013**, *42*, 7120–7130.

[58] E. König, K. Madeja, *Chem. Commun. (London)* **1966**, 61–62.

[59] P. Gütlich, *Z. anorg. allg. Chem.* **2012**, *638*, 15–43.

[60] A. Hauser, R. Hinek, H. Spiering, P. Gütlich, *Chem. Eur. J.* **1996**, *2*, 1435–1439.

[61] M. Sorai, S. Seki, *J. Phys. Soc. Jpn.* **1972**, *33*, 575–575.

[62] M. Sorai, S. Seki, *Journal of Physics and Chemistry of Solids* **1974**, *35*, 555–570.

[63] R. Boca, M. Boca, H. Ehrenberg, H. Fuess, W. Linert, F. Renz, I. Svoboda, *Chemical Physics* **2003**, *293*, 375–395.

[64] R. Kulmaczewski, J. Olguín, J. A. Kitchen, H. L. C. Feltham, G. N. L. Jameson, J. L. Tallon, S. Brooker, *J. Am. Chem. Soc.* **2014**, *136*, 878–881.

[65] H. L. C. Feltham, C. Johnson, A. B. S. Elliott, K. C. Gordon, M. Albrecht, S. Brooker, *Inorg. Chem.* **2015**, *54*, 2902–2909.

[66] J.-F. Létard, P. Guionneau, L. Rabardel, J. A. K. Howard, A. E. Goeta, D. Chasseau, O. Kahn, *Inorg. Chem.* **1998**, *37*, 4432–4441.

[67] G. A. Craig, J. S. Costa, O. Roubeau, S. J. Teat, H. J. Shepherd, M. Lopes, G. Molnár, A. Bousseksou, G. Aromí, *Dalton Trans.* **2013**, *43*, 729–737.

[68] K. S. Murray in *Spin-Crossover Materials*, John Wiley & Sons Ltd, **2013**, S. 1–54.

[69] S. Hayami, Z.-z. Gu, M. Shiro, Y. Einaga, A. Fujishima, O. Sato, *J. Am. Chem. Soc.* **2000**, *122*, 7126–7127.

[70] J.-F. Létard, P. Guionneau, L. Goux-Capes in *Spin Crossover in Transition Metal Compounds III*, Topics in Current Chemistry 235, Springer Berlin Heidelberg, **2004**, S. 221–249.

[71] O. Roubeau, *Chem. Eur. J.* **2012**, *18*, 15230–15244.

[72] B. Weber in *Spin-Crossover Materials*, John Wiley & Sons Ltd, **2013**, S. 55–76.

[73] B. Weber, *Coordination Chemistry Reviews*, Deutsche Forschungsgemeinschaft Molecular Magnetism Research Report **2009**, *253*, 2432–2449.

[74] C. Baldé, W. Bauer, E. Kaps, S. Neville, C. Desplanches, G. Chastanet, B. Weber, J. F. Létard, *Eur. J. Inorg. Chem.* **2013**, 2744–2750.

[75] V. Petrouleas, J. P. Tuchagues, *Chemical Physics Letters* **1987**, *137*, 21–25.

[76] L. Salmon, A. Bousseksou, B. Donnadieu, J.-P. Tuchagues, *Inorg. Chem.* **2005**, *44*, 1763–1773.

[77] J. S. Costa, C. Balde, C. Carbonera, D. Denux, A. Wattiaux, C. Desplanches, J.-P. Ader, P. Gütlich, Jean-François Létard, *Inorg. Chem.* **2007**, *46*, 4114–4119.

[78] M. H. Klingele, B. Moubaraki, J. D. Cashion, K. S. Murray, S. Brooker, *Chem. Commun.* **2005**, 987–989.

[79] M. C. Giménez-López, M. Clemente-León, E. Coronado, F. M. Romero, S. Shova, J.-P. Tuchagues, *Eur. J. Inorg. Chem.* **2005**, 2783–2787.

[80] P. Gütlich, *Eur. J. Inorg. Chem.* **2013**, *2013*, 581–591.

[81] E. W. Müller, H. Spiering, P. Gütlich, *Chemical Physics Letters* **1982**, *93*, 567–571.

[82] E. König, *Coordination Chemistry Reviews* **1968**, *3*, 471–495.

[83] H. Goodwin, E. Kucharski, A. White, *Aust. J. Chem.* **1983**, *36*, 1115–1124.

[84] H. Goodwin, R. Sylva, *Aust. J. Chem.* **1968**, *21*, 83–90.

[85] H. A. Goodwin, *Coordination Chemistry Reviews* **1976**, *18*, 293–325.

[86] R. W. Hogue, R. G. Miller, N. G. White, H. L. C. Feltham, G. N. L. Jameson, S. Brooker, *Chem. Commun.* **2014**, *50*, 1435–1437.

[87] J. Klingele, D. Kaase, M. H. Klingele, J. Lach, *Dalton Trans.* **2012**, *41*, 1397–1406.

[88] N. Moliner, A. B. Gaspar, M. C. Muñoz, V. Niel, J. Cano, J. A. Real, *Inorg. Chem.* **2001**, *40*, 3986–3991.

[89] N. Moliner, M. C. Muñoz, S. Létard, J.-F. Létard, X. Solans, R. Burriel, M. Castro, O. Kahn, J. A. Real, *Inorganica Chimica Acta* **1999**, *291*, 279–288.

[90] H. S. Scott, T. M. Ross, N. F. Chilton, I. A. Gass, B. Moubaraki, G. Chastanet, N. Paradis, J.-F. Lètard, K. R. Vignesh, G. Rajaraman, S. R. Batten, K. S. Murray, *Dalton Trans.* **2013**, *42*, 16494–16509.

[91] S. Zheng, M. A. Siegler, O. Roubeau, S. Bonnet, *Inorg. Chem.* **2014**, *53*, 13162–13173.

[92] M. A. Halcrow in *Spin-Crossover Materials*, John Wiley & Sons Ltd, **2013**, S. 147–169.

[93] J. A. Real, A. B. Gaspar, V. Niel, M. C. Muñoz, *Coordination Chemistry Reviews* **2003**, *236*, 121–141.

[94] M. Sorai, J. Ensling, P. Gütlich, *Chemical Physics* **1976**, *18*, 199–209.

[95] H. Spiering, N. Willenbacher, *J. Phys.: Condens. Matter* **1989**, *1*, 10089.

[96] N. Paradis, G. Chastanet, F. Varret, J.-F. Létard, *Eur. J. Inorg. Chem.* **2013**, *2013*, 968–974.

[97] T. Tayagaki, A. Galet, G. Molnár, M. C. Muñoz, A. Zwick, K. Tanaka, J.-A. Real, A. Bousseksou, *J. Phys. Chem. B* **2005**, *109*, 14859–14867.

[98] M. P. Shores, C. M. Klug, S. R. Fiedler in *Spin-Crossover Materials*, John Wiley & Sons Ltd, **2013**, S. 281–301.

[99] Y. Hasegawa, R. Sakamoto, K. Takahashi, H. Nishihara, *Inorg. Chem.* **2013**, *52*, 1658–1665.

[100] L. J. Kershaw Cook, H. J. Shepherd, T. P. Comyn, C. Balde, O. Cespedes, G. Chastanet, M. A. Halcrow, *Chemistry* **2015**, *21*, 4805–16.

[101] J.-Y. Li, C.-T. He, Y.-C. Chen, M. Zhang, W. Liu, Z.-P. Ni, M.-L. Tong, *J. Mater. Chem. C* **2015**, *3*, 7830–7835.

[102] W. Liu, L. Wang, J. Su, Y.-C. Chen, J. Tucek, R. Zboril, Z.-P. Ni, M.-L. Tong, *Inorg. Chem.* **2015**, *54*, 8711–8716.

[103] N. Nassirinia, S. Amani, S. J. Teat, O. Roubeau, P. Gamez, *Chem. Commun.* **2013**, *50*, 1003–1005.

[104] K. Nakano, N. Suemura, K. Yoneda, S. Kawata, S. Kaizaki, *Dalton Trans.* **2005**, 740–743.

[105] J. A. Kitchen, J. Olguin, R. Kulmaczewski, N. G. White, V. A. Milway, G. N. Jameson, J. L. Tallon, S. Brooker, *Inorganic Chemistry* **2013**, *52*, 11185–99.

[106] C. Köhler, E. Rentschler, *Eur. J. Inorg. Chem.* **2015**, DOI `10.1002/ejic.201501278`.

[107] C.-C. Wu, J. Jung, P. K. Gantzel, P. Gütlich, D. N. Hendrickson, *Inorg. Chem.* **1997**, *36*, 5339–5347.

[108] J. A. Kitchen, N. G. White, G. N. L. Jameson, J. L. Tallon, S. Brooker, *Inorg. Chem.* **2011**, *50*, 4586–4597.

[109] L. Wiehl, G. Kiel, C. P. Koehler, H. Spiering, P. Guetlich, *Inorg. Chem.* **1986**, *25*, 1565–1571.

[110] F. P. Huang, C. Yang, H. Y. Li, P. F. Yao, X. H. Qin, S. P. Yan, M. Kurmoo, *Dalton transactions* **2015**, *44*, 6593–9.

[111] J. J. Amoore, C. J. Kepert, J. D. Cashion, B. Moubaraki, S. M. Neville, K. S. Murray, *Chemistry* **2006**, *12*, 8220–8227.

[112] M. Bartel, A. Absmeier, G. N. L. Jameson, F. Werner, K. Kato, M. Takata, R. Boca, M. Hasegawa, K. Mereiter, A. Caneschi, W. Linert, *Inorg. Chem.* **2007**, *46*, 4220–4229.

[113] L. J. K. Cook, R. Kulmaczewski, O. Cespedes, M. A. Halcrow, *Chem. Eur. J.* **2015**, 1789–1799.

[114] S. Kanegawa, S. Kang, O. Sato, *Eur. J. Inorg. Chem.* **2013**, *2013*, 725–729.

[115]   M. Steinert, B. Schneider, S. Dechert, S. Demeshko, F. Meyer, *Angew. Chem. Int. Ed.* **2014**, *53*, 6135–6139.

[116]   H. Wang, C. Sinito, A. Kaiba, J. S. Costa, C. Desplanches, P. Dagault, P. Guionneau, J.-F. Létard, P. Negrier, D. Mondieig, *Eur. J. Inorg. Chem.* **2014**, 4927–4933.

[117]   A. Lennartson, P. Southon, N. F. Sciortino, C. J. Kepert, C. Frandsen, S. Mørup, S. Piligkos, C. J. McKenzie, *Chem. Eur. J.* **2015**, *21*, 16066–16072.

[118]   V. Niel, J. M. Martinez-Agudo, M. C. Muñoz, A. B. Gaspar, J. A. Real, *Inorg. Chem.* **2001**, *40*, 3838–3839.

[119]   Z. Yan, M. Li, H.-L. Gao, X.-C. Huang, D. Li, *Chem. Commun.* **2012**, *48*, 3960–3962.

[120]   M. Carmen Muñoz, J. Antonio Real in *Spin-Crossover Materials*, John Wiley & Sons Ltd, **2013**, S. 121–146.

[121]   M. M. Dîrtu, C. Neuhausen, A. D. Naik, A. Rotaru, L. Spinu, Y. Garcia, *Inorg. Chem.* **2010**, *49*, 5723–5736.

[122]   O. Kahn, E. Codjovi, *Philosophical Transactions of the Royal Society of London A: Mathematical Physical and Engineering Sciences* **1996**, *354*, 359–379.

[123]   O. Kahn, C. J. Martinez, *Science* **1998**, *279*, 44–48.

[124]   S. Ohta, C. Yoshimura, N. Matsumoto, H. Okawa, A. Ohyoshi, *Bulletin of the Chemical Society of Japan* **1986**, *59*, 155–159.

[125]   A. Real, J. Zarembowitch, O. Kahn, X. Solans, *Inorg. Chem.* **1987**, *26*, 2939–2943.

[126]   J. Olguín, S. Brooker in *Spin-Crossover Materials*, John Wiley & Sons Ltd, **2013**, S. 77–120.

[127]   K. S. Murray, C. J. Kepert in *Spin Crossover in Transition Metal Compounds I*, Topics in Current Chemistry 233, Springer Berlin Heidelberg, **2004**, S. 195–228.

[128]   V. Ksenofontov, H. Spiering, S. Reiman, Y. Garcia, A. B. Gaspar, N. Moliner, J. A. Real, P. Gütlich, *Chemical Physics Letters* **2001**, *348*, 381–386.

[129] J. A. Real, H. Bolvin, A. Bousseksou, A. Dworkin, O. Kahn, F. Varret, J. Zarembowitch, *J. Am. Chem. Soc.* **1992**, *114*, 4650–4658.

[130] J. A. Real, I. Castro, A. Bousseksou, M. Verdaguer, R. Burriel, M. Castro, J. Linares, F. Varret, *Inorg. Chem.* **1997**, *36*, 455–464.

[131] A. B. Gaspar, V. Ksenofontov, H. Spiering, S. Reiman, J. A. Real, P. Gütlich, *Hyperfine Interactions* **2002**, *144-145*, 297–306.

[132] C. Grunert, S. Reiman, H. Spiering, J. Kitchen, S. Brooker, P. Gütlich, *Angewandte Chemie* **2008**, *120*, 3039–3041.

[133] K. Nakano, S. Kawata, K. Yoneda, A. Fuyuhiro, T. Yagi, S. Nasu, S. Morimoto, S. Kaizaki, *Chem. Commun.* **2004**, 2892–2893.

[134] N. Ortega-Villar, A. L. Thompson, M. C. Muñoz, V. M. Ugalde-Saldívar, A. E. Goeta, R. Moreno-Esparza, J. A. Real, *Chem. Eur. J.* **2005**, *11*, 5721–5734.

[135] Y. Hu, C.-Y. Li, X.-M. Wang, Y.-H. Yang, H.-L. Zhu, *Chem. Rev.* **2014**, *114*, 5572–5610.

[136] B. Gierczyk, M. Zalas, *Organic Preparations and Procedures International* **2005**, *37*, 213–222.

[137] Z. Kaleta, B. T. Makowski, T. Soós, R. Dembinski, *Org. Lett.* **2006**, *8*, 1625–1628.

[138] C. Tschierske, D. Girdziunaite, *J. Prakt. Chem.* **1991**, *333*, 135–137.

[139] J. Klingele, D. Kaase, M. H. Klingele, J. Lach, S. Demeshko, *Dalton Trans.* **2010**, *39*, 1689–1691.

[140] M. H. Klingele, B. Moubaraki, K. S. Murray, S. Brooker, *Chem. Eur. J.* **2005**, *11*, 6962–6973.

[141] A. Noble, J. Olguín, R. Clérac, S. Brooker, *Inorganic Chemistry* **2010**, *49*, 4560–4569.

[142] C. J. Schneider, J. D. Cashion, B. Moubaraki, S. M. Neville, S. R. Batten, D. R. Turner, K. S. Murray, *Polyhedron* **2007**, *26*, 1764–1772.

[143] C. J. Schneider, J. D. Cashion, N. F. Chilton, C. Etrillard, M. Fuentealba, J. A. K. Howard, J.-F. Létard, C. Milsmann, B. Moubaraki, H. A. Sparkes, S. R. Batten, K. S. Murray, *Eur. J. Inorg. Chem.* **2013**, 850–864.

[144] D. J. Harding, W. Phonsri, P. Harding, I. A. Gass, K. S. Murray, B. Moubaraki, J. D. Cashion, L. Liu, S. G. Telfer, *Chem. Commun.* **2013**, *49*, 6340–6342.

[145] C. Rajadurai, Z. Qu, O. Fuhr, B. Gopalan, R. Kruk, M. Ghafari, M. Ruben, *Dalton Trans.* **2007**, 3531–3537.

[146] Y. C. Chuang, C. T. Liu, C. F. Sheu, W. L. Ho, G. H. Lee, C. C. Wang, Y. Wang, *Inorganic Chemistry* **2012**, *51*, 4663–4671.

[147] B. A. Leita, S. M. Neville, G. J. Halder, B. Moubaraki, C. J. Kepert, J.-F. Létard, K. S. Murray, *Inorg. Chem.* **2007**, *46*, 8784–8795.

[148] W. Zhang, F. Zhao, T. Liu, M. Yuan, Z.-M. Wang, S. Gao, *Inorg. Chem.* **2007**, *46*, 2541–2555.

[149] B. J. C. Vieira, J. C. Dias, I. C. Santos, L. C. J. Pereira, V. da Gama, J. C. Waerenborgh, *Inorg. Chem.* **2015**, *54*, 1354–1362.

[150] M. Stollenz, C. Große, F. Meyer, *Chem. Commun.* **2008**, 1744–1746.

[151] S. Konar, E. Zangrando, M. G. B. Drew, T. Mallah, J. Ribas, N. R. Chaudhuri, *Inorg. Chem.* **2003**, *42*, 5966–5973.

[152] J. M. Clemente-Juan, C. Mackiewicz, M. Verelst, F. Dahan, A. Bousseksou, Y. Sanakis, J.-P. Tuchagues, *Inorg. Chem.* **2002**, *41*, 1478–1491.

[153] R. L. Carlin, Magnetochemistry, Springer Science & Business Media, **2012**, 339 S.

[154] H. Petzold, S. Heider, *Eur. J. Inorg. Chem.* **2011**, *2011*, 1249–1254.

[155] M. Seredyuk, A. B. Gaspar, V. Ksenofontov, Y. Galyametdinov, J. Kusz, P. Gütlich, *J. Am. Chem. Soc.* **2008**, *130*, 1431–1439.

[156] E. A. Medlycott, G. S. Hanan, T. S. M. Abedin, L. K. Thompson, *Polyhedron* **2008**, *27*, 493–501.

[157] A. Escuer, G. Vlahopoulou, F. Lloret, F. A. Mautner, *Eur. J. Inorg. Chem.* **2014**, *2014*, 83–92.

[158] C. Belle, C. Bougault, M.-T. Averbuch, A. Durif, J.-L. Pierre, J.-M. Latour, L. Le Pape, *J. Am. Chem. Soc.* **2001**, *123*, 8053–8066.

[159] P. Rajakumar, A. Thirunarayanan, S. Raja, S. Ganesan, P. Maruthamuthu, *Tetrahedron Letters* **2012**, *53*, 1139–1143.

[160] W. Q. Tian, Y. A. Wang, *J. Org. Chem.* **2004**, *69*, 4299–4308.

[161] W. A. Gobeze, V. A. Milway, J. Olguín, G. N. L. Jameson, S. Brooker, *Inorg. Chem.* **2012**, *51*, 9056–9065.

[162] D. Zhu, Y. Xu, Z. Yu, Z. Guo, H. Sang, T. Liu, X. You, *Chem. Mater.* **2002**, *14*, 838–843.

[163] C. Liu, J.-H. Chen, J. She, G.-H. Lee, S.-M. Peng, *Journal of Organometallic Chemistry* **2006**, *691*, 3574–3580.

[164] H. Baba, M. Nakano, *Polyhedron* **2009**, *28*, 2087–2091.

[165] O. Kahn, Molecular Magnetism, Wiley, **1993**, 396 S.

[166] F. Himo, T. Lovell, R. Hilgraf, V. V. Rostovtsev, L. Noodleman, K. B. Sharpless, V. V. Fokin, *J. Am. Chem. Soc.* **2005**, *127*, 210–216.

[167] A. Kroll, K. Monczak, D. Sorsche, S. Rau, *Eur. J. Inorg. Chem.* **2014**, *2014*, 3462–3466.

[168] L. Palatinus, G. Chapuis, *Journal of Applied Crystallography* **2007**, *40*, 786–790.

[169] G. M. Sheldrick, *Acta Crystallographica Section C Structural Chemistry* **2015**, *71*, 3–8.

[170] O. V. Dolomanov, L. J. Bourhis, R. J. Gildea, J. A. K. Howard, H. Puschmann, *Journal of Applied Crystallography* **2009**, *42*, 339–341.

[171] N. F. Chilton, R. P. Anderson, L. D. Turner, A. Soncini, K. S. Murray, *J. Comput. Chem.* **2013**, *34*, 1164–1175.

[172] J. C. Cobas, F. J. Sardina, *Concepts Magn. Reson.* **2003**, *19A*, 80–96.

[173] S. Bhattacharya, K. Snehalatha, V. P. Kumar, *J. Org. Chem.* **2003**, *68*, 2741–2747.

A. Abbreviations

SMMs	Single-molecule magnets
LD-CISSS	Light-driven coordination-induced spin-state switching
LS	low-spin
HS	high-spin
SCO	Spin-crossover
Δ	Ligand field splitting
Δ_{crit}	Critical ligand field splitting
P	Spin pairing energy
ΔE_{HL}^0	Zero-point energy difference
ΔG	Gibbs free energy difference
ΔH	Enthalpy difference
ΔS	Entropy difference
$T_{1/2}$	Transition temperature
LIESST	Light-Induced Excited Spin-State Trapping
ST	Spin transition
γ_{HS}	High-spin fraction
$\chi(T)$	Magnetic susceptibility as a function of the temperature
SQUID	Superconducting QUantum Interference Device
phen	1,10-Phenanthroline
NCS	Thiocyanate
NCSe	Selenocyanate
$NCBH_3$	Cyanborohydride
CN^-	Cyanide
OCN^-	Cyanate

$(CN)_2N^-$	Dicyanamide
δ	Isomer shift
ΔE_Q	Quadrupole splitting
Γ	Lorentzian line width
K	Kelvin
DSC	Differential scanning calorimetry
UV/Vis	Ultraviolet/visible
IR	Infrared
cm^{-1}	Wavenumber
PMAT	4-Amino-3,5-bis{[(2-pyridylmethyl)amino]methyl}-4H-1,2,4-triazole
PMAP	3,5-Bis{[(2-pyridylmethyl)amino]methyl}-pyrazole
Σ	Octahedral distortion parameter
NMR	Nuclear magnetic resonance
ppm	Parts per million (10^{-6})
ESI-MS	Electrospray ionization mass spectrometry
FD-MS	Field desorption mass spectrometry
MeOH	Methanol
DMSO	Dimethylsulfoxide
DMF	N,N-Dimethylformamide
MeCN	Acetonitrile
THF	Tetrahydrofuran
m/z	Mass-to-charge ratio
g-value	Landé factor
J	Exchange parameter
D	Zero-field splitting parameter
TIP	Temperature independent paramagnetism
py	pyridine

B. NMR Spectra
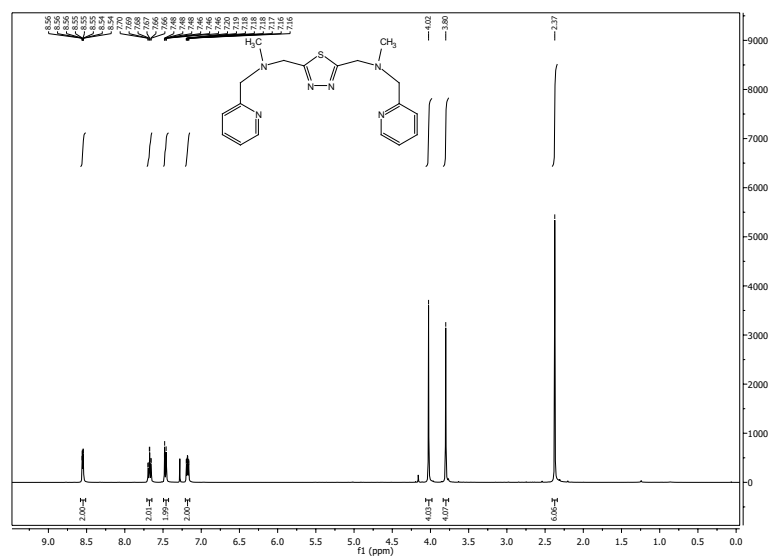
Figure B.1.: ^1H-NMR spectrum of **L2** (2,5-Bis[N-methyl-N-(2-pyridylmethyl)-aminomethyl]-1,3,4-thiadiazole).
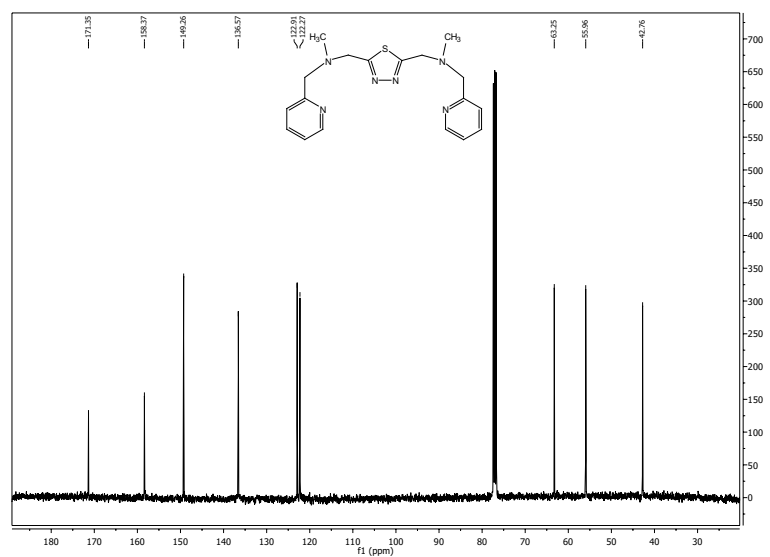
Figure B.2.: ^13C-NMR spectrum of **L2** (2,5-Bis[N-methyl-N-(2-pyridylmethyl)-aminomethyl]-1,3,4-thiadiazole).
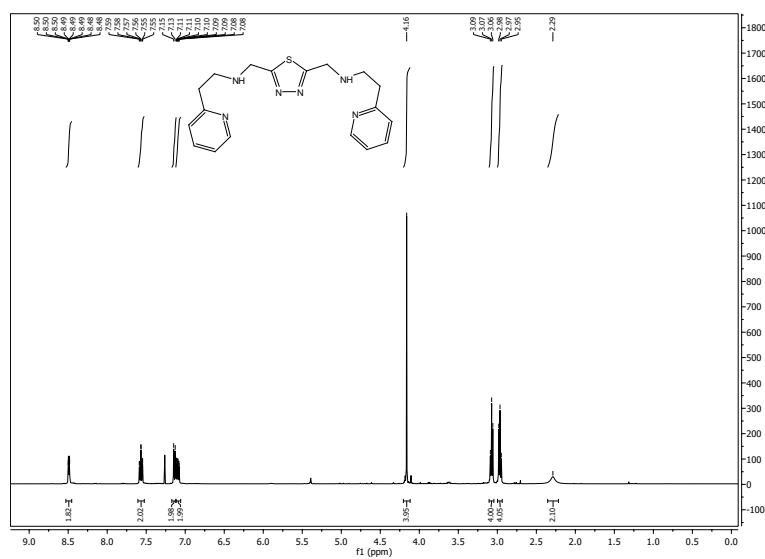
Figure B.3.: ^{1}H-NMR spectrum of **L3** (2,5-Bis[(2-pyridylethyl)aminomethyl]-1,3,4-thiadiazole).
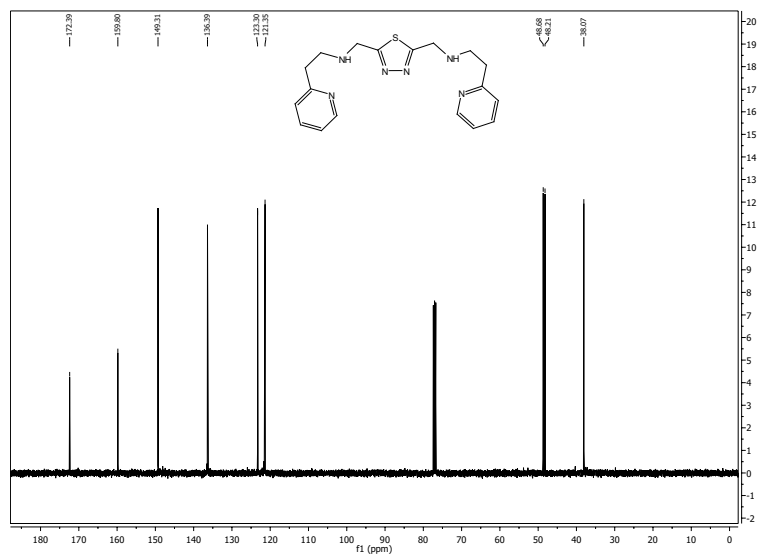
Figure B.4.: ^{13}C-NMR spectrum of **L3** (2,5-Bis[(2-pyridylethyl)aminomethyl]-1,3,4-thiadiazole).
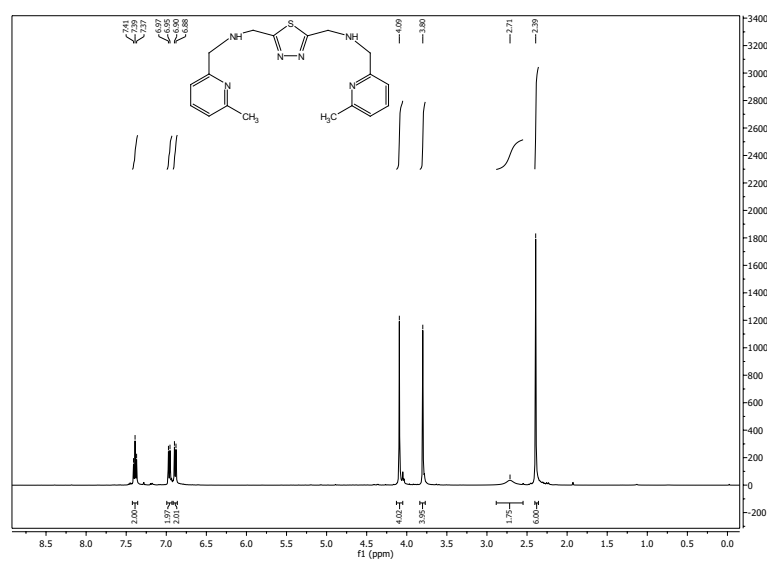
Figure B.5.: ^{1}H-NMR spectrum of **L4** (2,5-Bis[(2-(6-methyl-pyridyl)methyl)-aminomethyl]-1,3,4-thiadiazole).
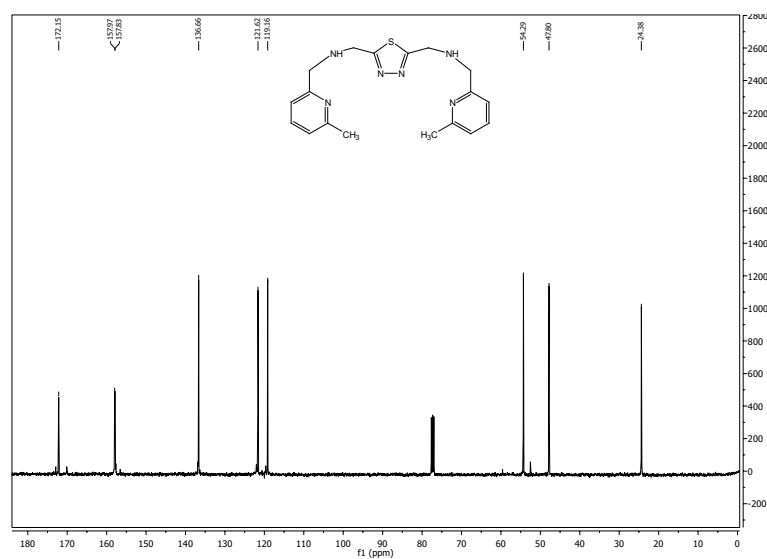
Figure B.6.: ^{13}C-NMR spectrum of **L4** (2,5-Bis[(2-(6-methyl-pyridyl)methyl)-aminomethyl]-1,3,4-thiadiazole).
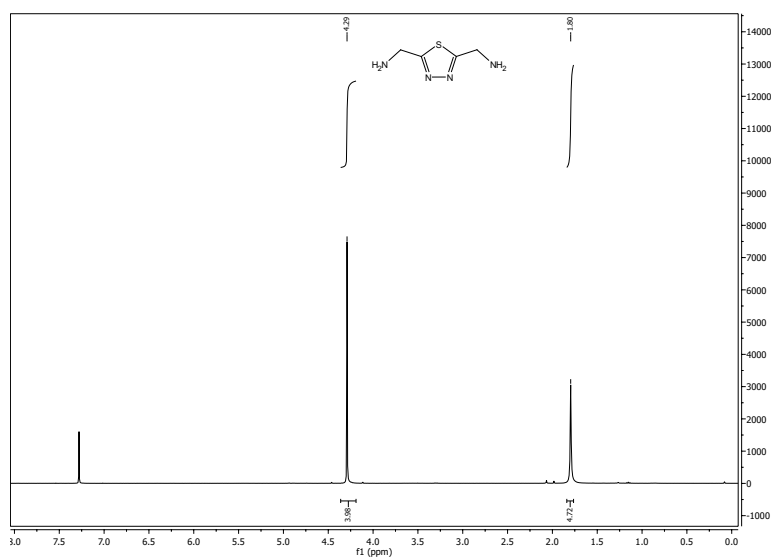
Figure B.7.: ^{1}H-NMR spectrum of 2,5-Bis(aminomethyl)-1,3,4-thiadiazole.
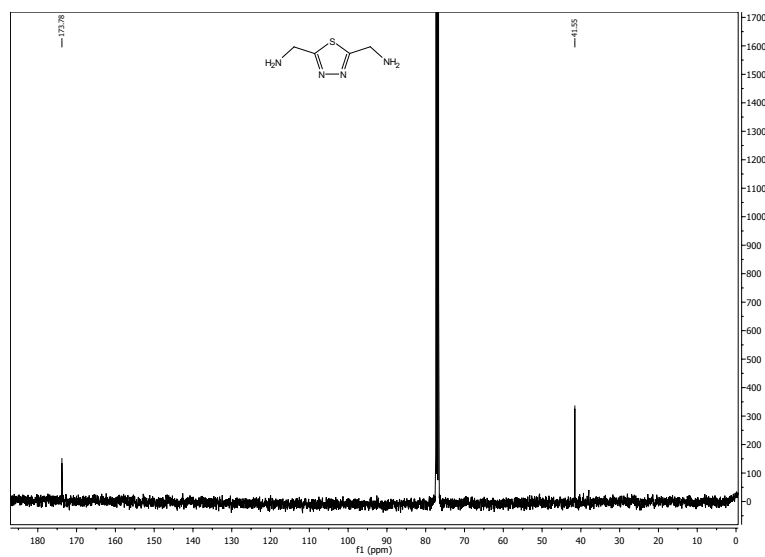
Figure B.8.: ^{13}C-NMR spectrum of 2,5-Bis(aminomethyl)-1,3,4-thiadiazole.
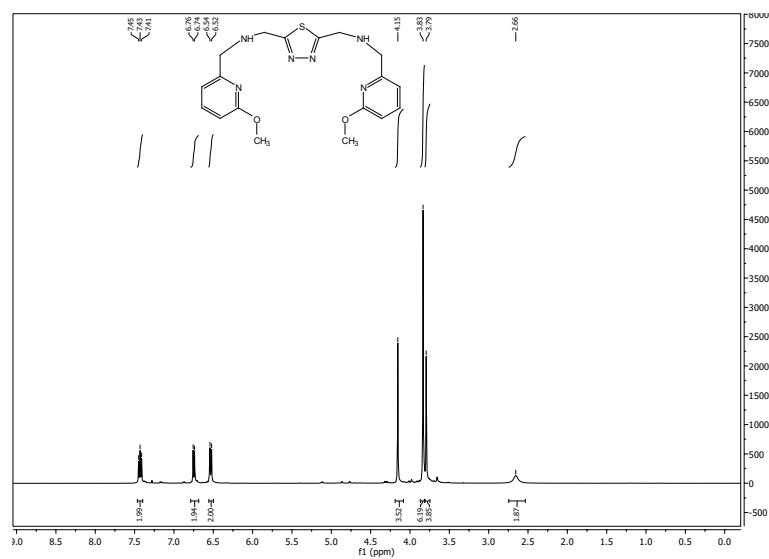
Figure B.9.: ^{1}H-NMR spectrum of **L5** (2,5-Bis[(2-(6-methoxy-pyridyl)methyl)-aminomethyl]-1,3,4-thiadiazole).
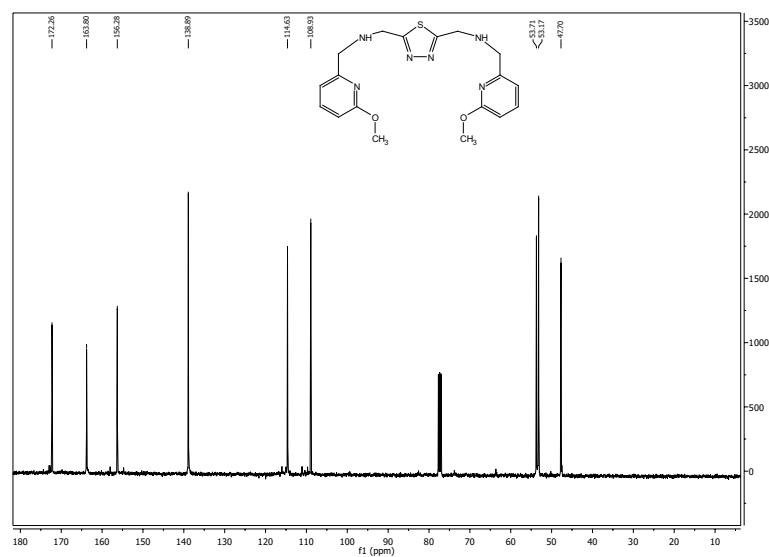
Figure B.10.: ^{13}C-NMR spectrum of **L5** (2,5-Bis[(2-(6-methoxy-pyridyl)methyl)-aminomethyl]-1,3,4-thiadiazole).
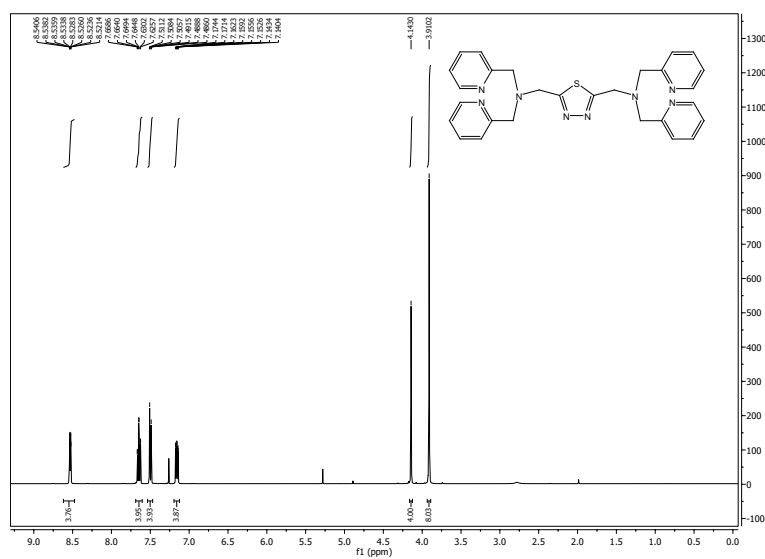
Figure B.11.: ^{1}H-NMR spectrum of **L6** (2,5-Bis[N,N-bis(2-pyridylmethyl)aminomethyl]-1,3,4-thiadiazole).
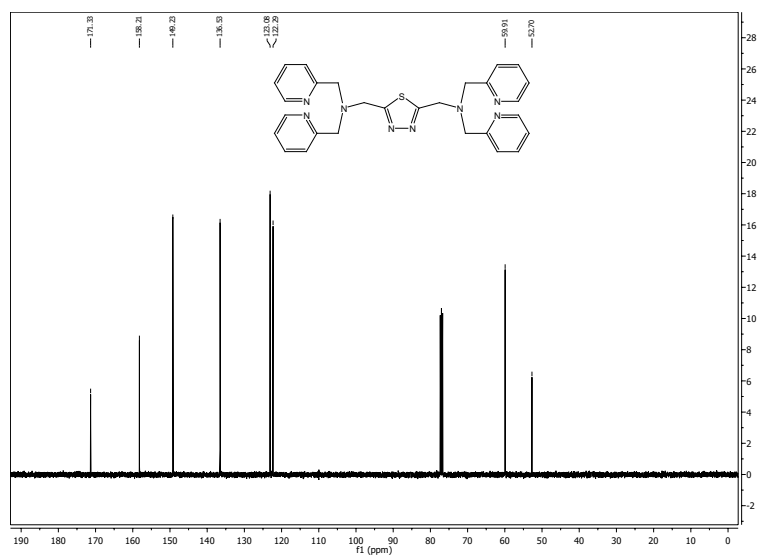
Figure B.12.: ^{13}C-NMR spectrum of **L6** (2,5-Bis[N,N-bis(2-pyridylmethyl)aminomethyl]-1,3,4-thiadiazole).

C. Crystallographic Data
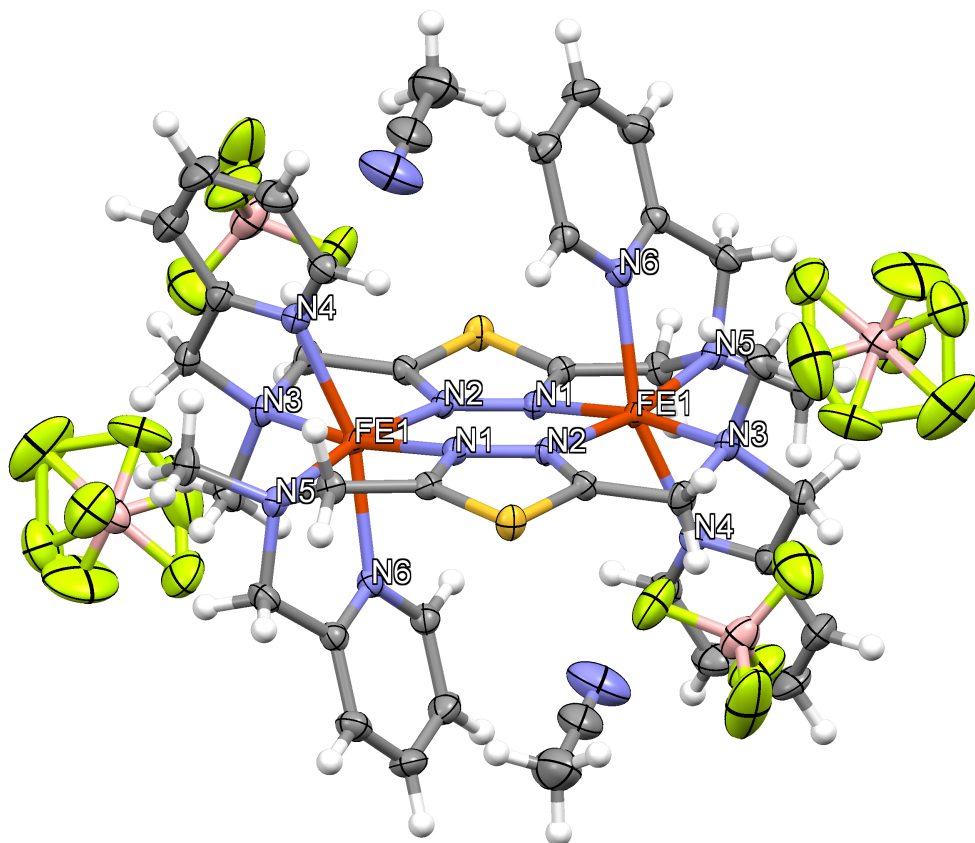
Figure C.1.: Molecular structure of **C1** ([Fe$_2$(μ-**L2**)$_2$](BF$_4$)$_4$·2MeCN) with thermal ellipsoids at 50 % probability level. Color scheme: dark red - Fe(II), yellow - S, blue - N, red - O, pink - B, green - F, grey - C, white - H.
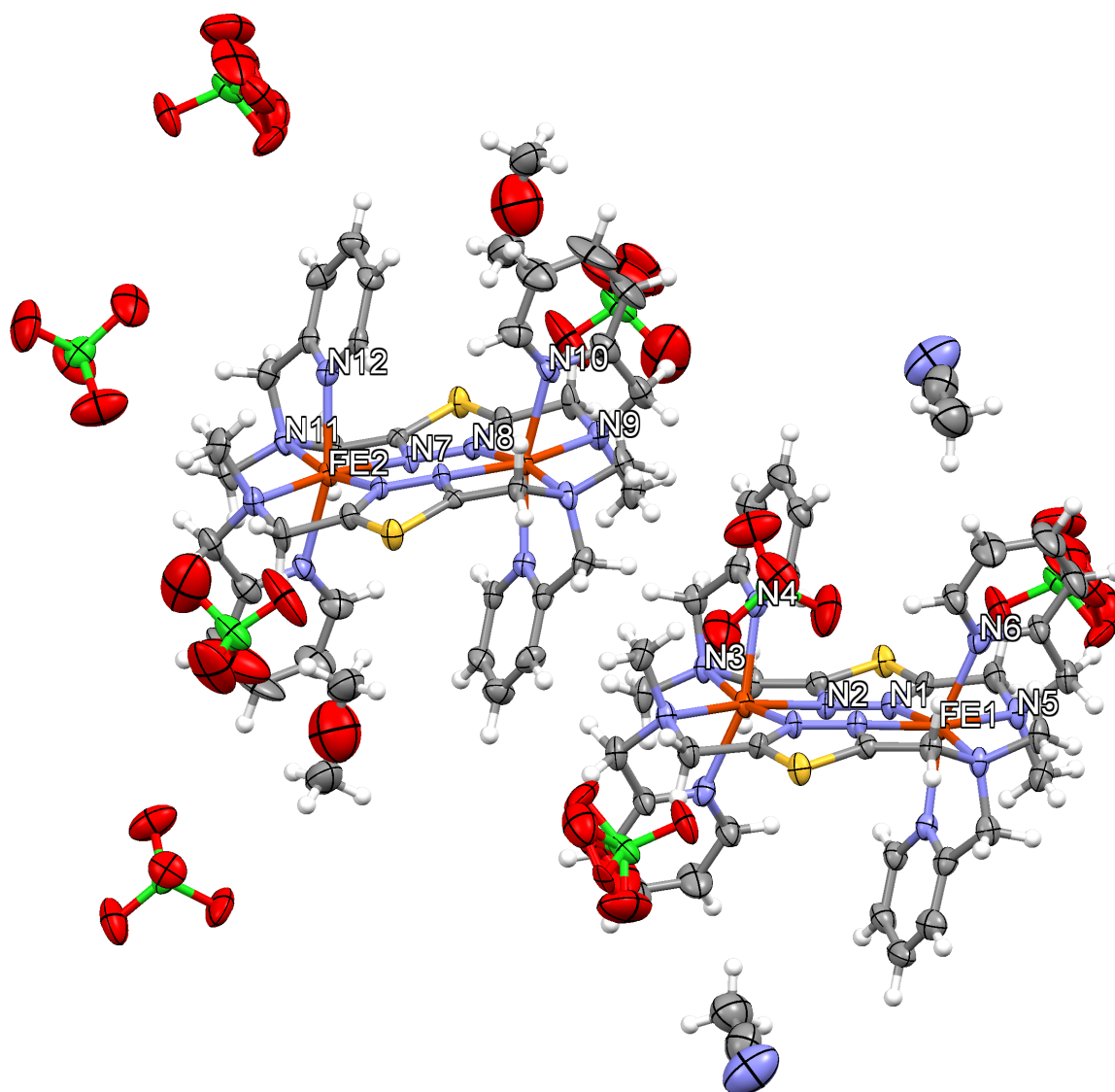
Figure C.2.: Molecular structure of **C2** (2([Fe$_2$(μ-**L2**)$_2$](ClO$_4$)$_4$)·2MeCN+1.5MeOH) with thermal ellipsoids at 50 % probability level. Color scheme: dark red - Fe(II), yellow - S, blue - N, red - O, green - Cl, grey - C, white - H.
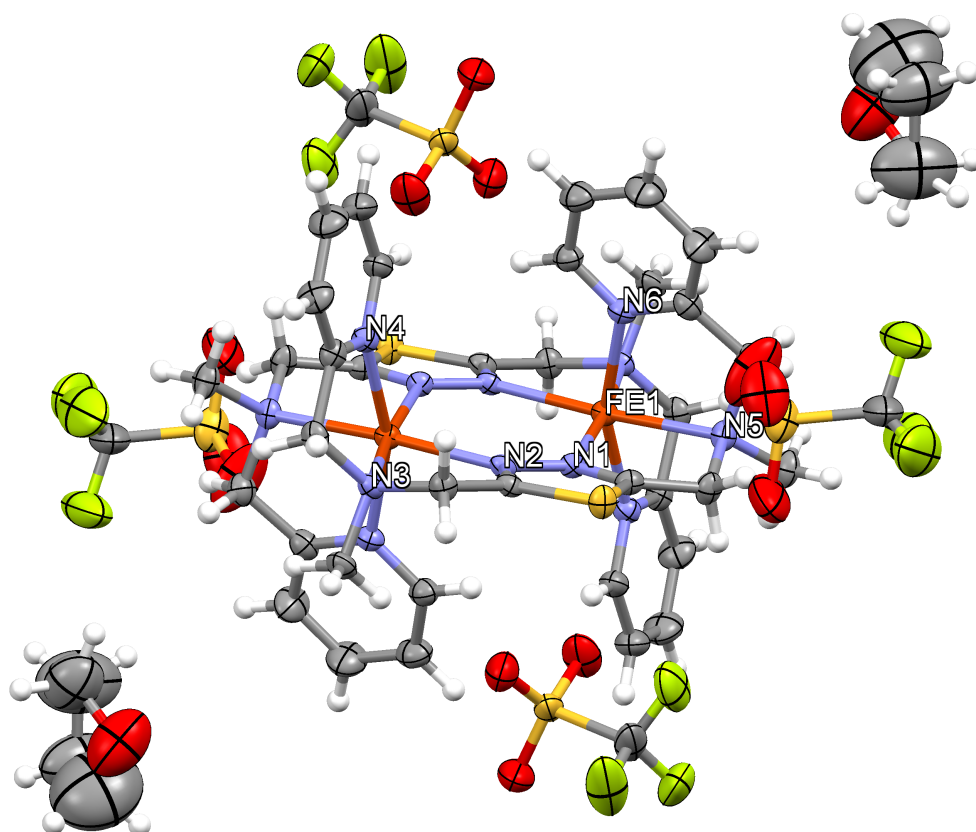
Figure C.3.: Molecular structure of **C3** ($[Fe_2(\mu\text{-}\mathbf{L2})_2](F_3CSO_3)_4 \cdot 2THF$) with thermal ellipsoids at 50 % probability level. Color scheme: dark red - Fe(II), yellow - S, blue - N, red - O, light green - F, grey - C, white - H.

C.1. Crystallographic Parameters

	C1	C2	C3
formula	$C_{40}H_{50}Fe_2B_4$ $F_{16}N_{14}S_2$	$C_{38.38}H_{48.12}Fe_2Cl_4$ $O_{16.38}N_{13}S_2$	$C_{48}H_{60}Fe_2O_{14}$ $F_{12}N_{12}S_6$
formula weight	1250.00	1271.14	1561.14
crystal system	triclinic	triclinic	triclinic
space group	$P\bar{1}$	$P\bar{1}$	$P\bar{1}$
a /Å	10.7111(7)	10.8303(17)	10.8636(8)
b /Å	10.8581(8)	12.1905(19)	13.1593(9)
c /Å	12.5456(9)	21.541(4)	13.8106(10)
α /°	98.934(2)	97.153(4)	62.6749(16)
β /°	109.3640(19)	104.545(4)	67.0049(19)
γ /°	104.2791(19)	107.343(4)	71.5319(18)
V /Å^3	1288.39(16)	2565.8	1591.7(2)
Z	1	2	1
T /K	173	173	173
$\rho_{calcd.}$ [g/cm^3]	1.611	1.645	1.629
μ [mm^{-1}]	0.750	0.937	0.758
R(int)	0.0340	0.1064	0.0567
S	1.025	0.811	0.920
R1 (I > 2σ(I))	0.0439	0.0617	0.0558
wR2 (all data)	0.1111	0.1521	0.1462
av. Fe-N	2.211	2.207/2.208	2.210
Σ	124.73	125.10/126.54	123.84

C.2. Selected Bond Lengths and Angles

Table C.1.: Selected bond lengths (Å) and angles (°) for compound of **C1**.

Fe-N bond lengths		N-Fe-N angles	
Fe1-N1	2.174(2)	N1-Fe1-N2	96.16(7)
Fe1-N2	2.180(2)	N1-Fe1-N3	170.14(6)
Fe1-N3	2.240(2)	N1-Fe1-N4	99.08(7)
Fe1-N4	2.141(2)	N1-Fe1-N5	77.47(7)
Fe1-N5	2.362(2)	N1-Fe1-N6	86.75(7)
Fe1-N6	2.171(2)	N2-Fe1-N3	76.83(7)
		N2-Fe1-N4	102.88(7)
		N2-Fe1-N5	170.13(7)
		N2-Fe1-N6	95.35(7)
		N3-Fe1-N4	76.10(7)
		N3-Fe1-N5	110.37(7)
		N3-Fe1-N6	100.68(7)
		N4-Fe1-N5	85.72(7)
		N4-Fe1-N6	160.07(7)
		N5-Fe1-N6	76.92(7)

Table C.2.: Selected bond lengths (Å) and angles (°) for compound of **C2**.

Fe-N bond lengths		N-Fe-N angles	
Fe1-N1	2.185(5)	N1-Fe1-N2	95.93(17)
Fe1-N2	2.171(5)	N1-Fe1-N3	169.92(17)
Fe1-N3	2.367(5)	N1-Fe1-N4	95.35(18)
Fe1-N4	2.156(5)	N1-Fe1-N5	76.96(17)
Fe1-N5	2.238(5)	N1-Fe1-N6	103.65(18)
Fe1-N6	2.126(5)	N2-Fe1-N3	77.63(17)
		N2-Fe1-N4	87.03(18)
		N2-Fe1-N5	170.32(18)
		N2-Fe1-N6	99.55(19)
		N3-Fe1-N4	76.73(17)
		N3-Fe1-N5	110.28(17)
		N3-Fe1-N6	85.22(18)
		N4-Fe1-N5	100.05(19)
		N4-Fe1-N6	159.04(19)
		N5-Fe1-N6	76.14(19)
Fe2-N7	2.183(5)	N7-Fe2-N9	170.25(18)
Fe2-N8	2.182(5)	N7-Fe2-N11	77.31(17)
Fe2-N9	2.236(5)	N7-Fe2-N8	96.02(17)
Fe2-N10	2.138(5)	N7-Fe2-N10	100.27(19)
Fe2-N11	2.342(5)	N7-Fe2-N12	84.88(17)
Fe2-N12	2.167(5)	N8-Fe2-N9	76.45(17)
		N8-Fe2-N10	102.33(18)
		N8-Fe2-N11	169.00(16)
		N8-Fe2-N12	93.99(17)
		N9-Fe2-N10	75.7(2)
		N9-Fe2-N11	111.06(17)
		N9-Fe2-N12	101.64(18)
		N10-Fe2-N11	87.58(18)
		N10-Fe2-N12	162.19(18)
		N11-Fe2-N12	76.85(17)

Table C.3.: Selected bond lengths (Å) and angles (°) for compound of **C3**.

Fe-N bond lengths		N-Fe-N angles	
Fe1-N1	2.169(3)	N1-Fe1-N2	96.35(11)
Fe1-N2	2.178(3)	N1-Fe1-N3	172.07(10)
Fe1-N3	2.243(3)	N1-Fe1-N4	102.45(11)
Fe1-N4	2.154(3)	N1-Fe1-N5	77.40(10)
Fe1-N5	2.360(3)	N1-Fe1-N6	85.45(11)
Fe1-N6	2.156(3)	N2-Fe1-N3	76.62(11)
		N2-Fe1-N4	101.04(11)
		N2-Fe1-N5	170.43(11)
		N2-Fe1-N6	95.18(11)
		N3-Fe1-N4	75.71(11)
		N3-Fe1-N5	110.05(11)
		N3-Fe1-N6	98.69(11)
		N4-Fe1-N5	87.49(10)
		N4-Fe1-N6	160.95(12)
		N5-Fe1-N6	77.25(11)

D. Magnetic Measurements
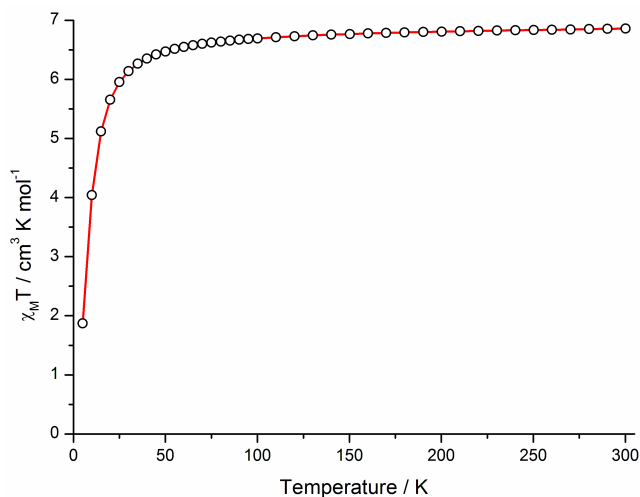
Figure D.1.: $\chi_M T$ vs. T data for the compounds **C1**. The experimental data is presented in circles and the fit of the magnetic data as a red line. g = 2.137, J = -0.430 cm^{-1}, $|D|$ = 5.90 cm^{-1} and TIP = 2·10^{-4} cm^{3}mol^{-1}
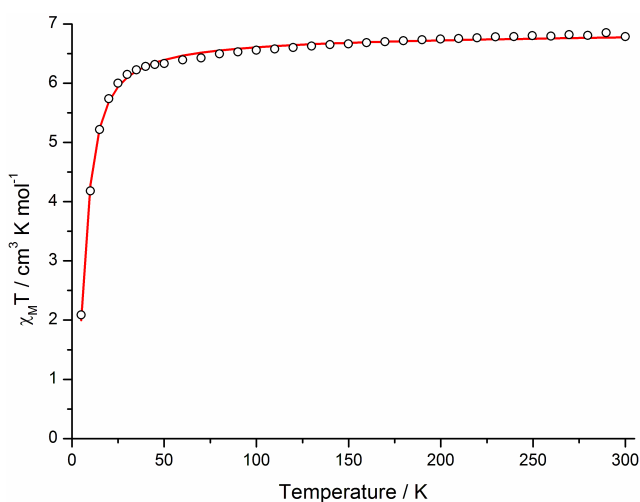
Figure D.2.: $\chi_M T$ vs. T data for the compounds **C2**. The experimental data is presented in circles and the fit of the magnetic data as a red line. g = 2.094, J = -0.479 cm^{-1}, $|D|$ = 3.83 cm^{-1} and TIP = 2·10^{-4} cm^{3}mol^{-1}
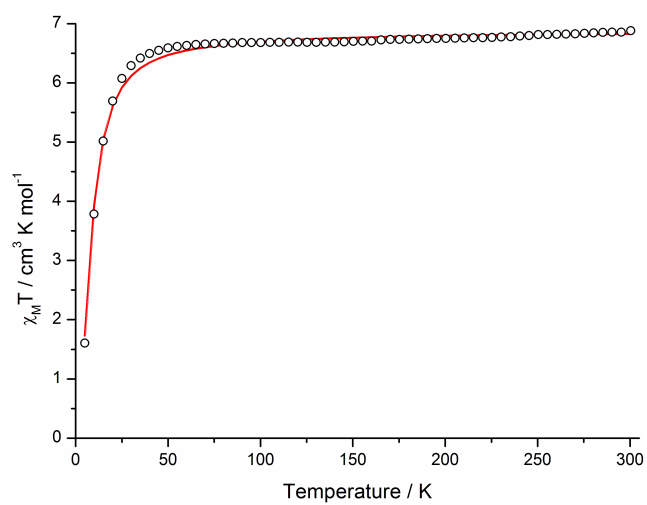
Figure D.3.: χ_MT vs. T data for the compounds **C3**. The experimental data is presented in circles and the fit of the magnetic data as a red line. g = 2.137, J = -0.452 cm^{-1}, $|D|$ = 5.96 cm^{-1} and *TIP* = 2·10^{-4} cm^{3}mol^{-1}

E. Mass Spectrometry
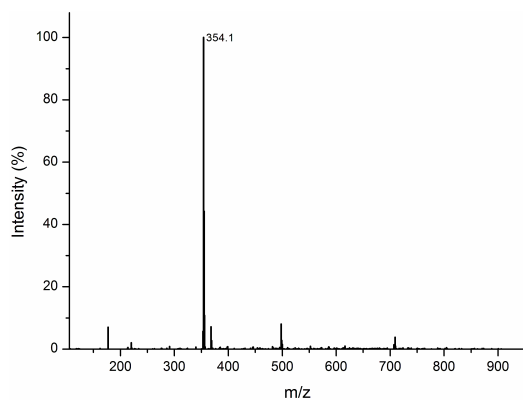
Figure E.1.: FD-MS spectrum of **L2** (2,5-Bis[N-methyl-N-(2-pyridylmethyl)-aminomethyl]-1,3,4-thiadiazole).
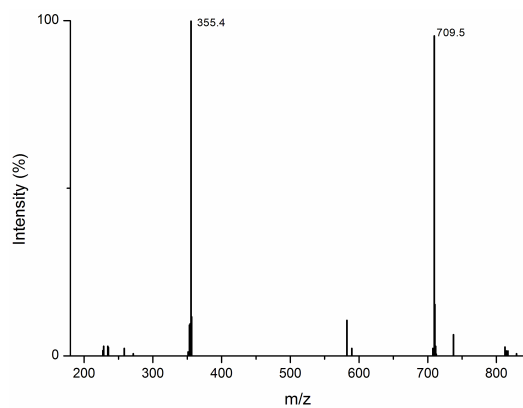
Figure E.2.: FD-MS spectrum of **L3** (2,5-Bis[(2-pyridylethyl)aminomethyl]-1,3,4-thiadiazole).
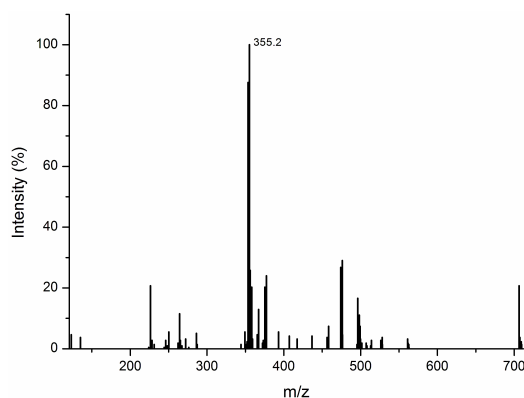
Figure E.3.: ESI-MS spectrum of **L4** (2,5-Bis[(2-(6-methyl-pyridyl)methyl)aminomethyl]-1,3,4-thiadiazole).
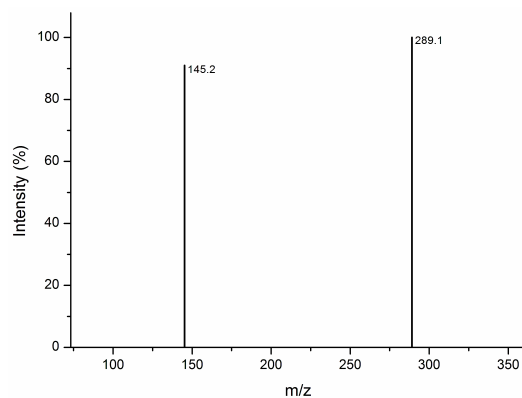
Figure E.4.: FD-MS spectrum of 2,5-Bis(aminomethyl)-1,3,4-thiadiazole.
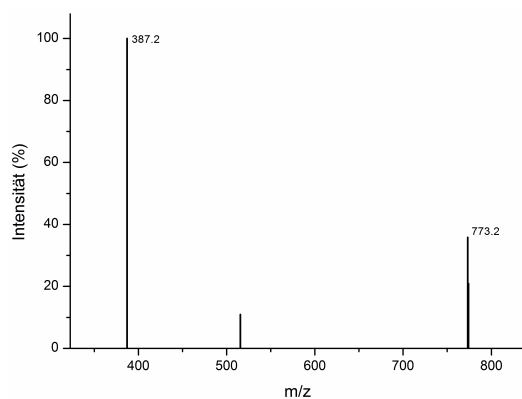
Figure E.5.: FD-MS spectrum of **L5** (2,5-Bis[(2-(6-methoxy-pyridyl)methyl)-aminomethyl]-1,3,4-thiadiazole).
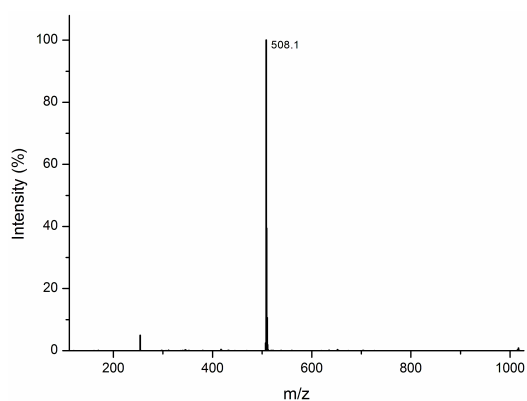
Figure E.6.: FD-MS spectrum of **L6** (2,5-Bis[N,N-bis(2-pyridylmethyl)aminomethyl]-1,3,4-thiadiazole).
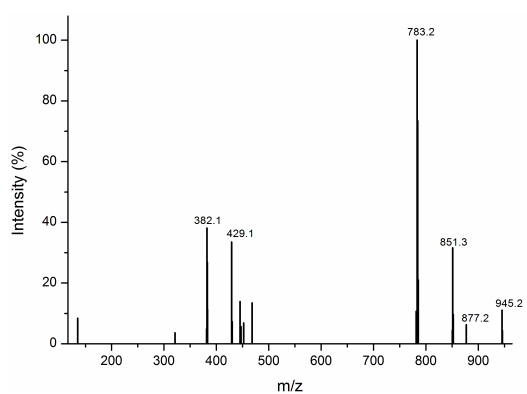
Figure E.7.: ESI-MS spectrum of **C1** [Fe$_2$(μ-**L2**)$_2$](BF$_4$)$_4$·2MeCN.
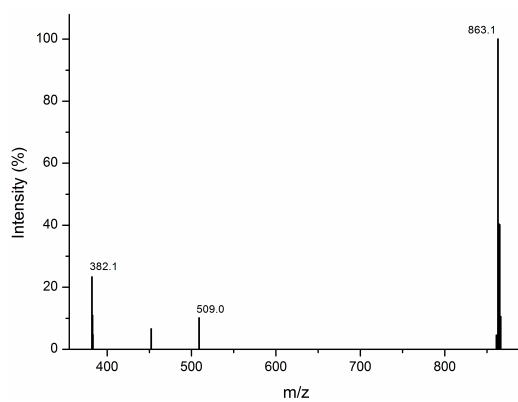
Figure E.8.: ESI-MS spectrum of **C2** [Fe$_2$(μ-**L2**)$_2$](ClO$_4$)$_4$·1MeCN+0.75MeOH.
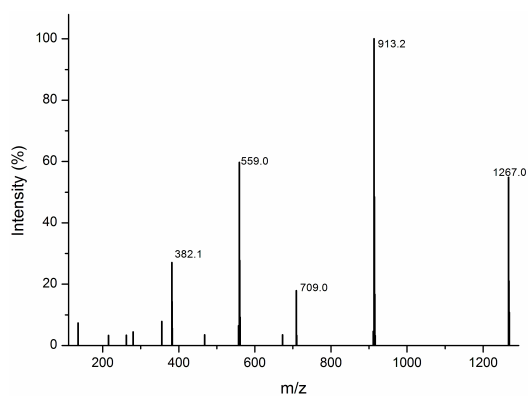
Figure E.9.: ESI-MS spectrum of **C3** $[Fe_2(\mu\text{-}\textbf{L2})_2](F_3CSO_3)_4 \cdot 2THF$.
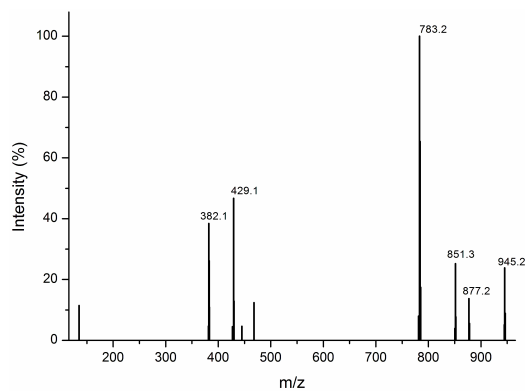
Figure E.10.: ESI-MS spectrum of **C4** $[Fe_2(\mu\text{-}\textbf{L3})_2](BF_4)_4$.
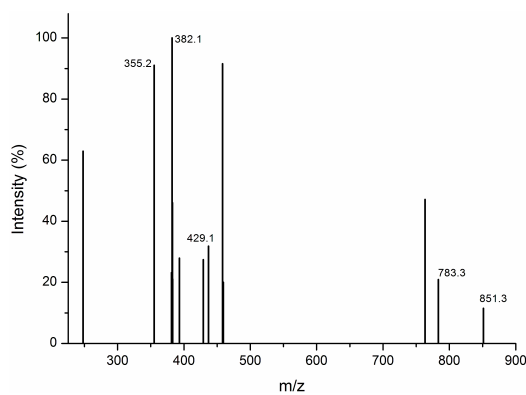
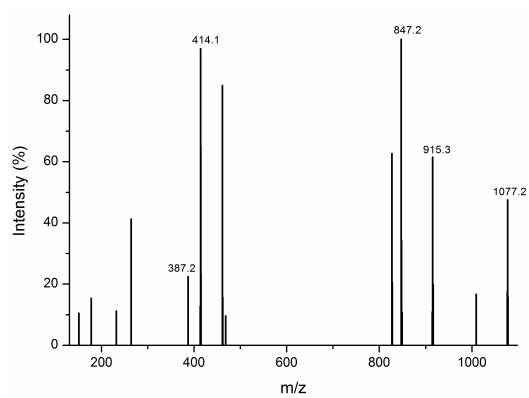Figure E.11.: ESI-MS spectrum of **C5** $[Fe_2(\mu\text{-}\textbf{L4})_2](BF_4)_4$.

Figure E.12.: ESI-MS spectrum of **C6** [Fe$_2$(μ-**L5**)$_2$](BF$_4$)$_4$.

F. Infrared Spectra
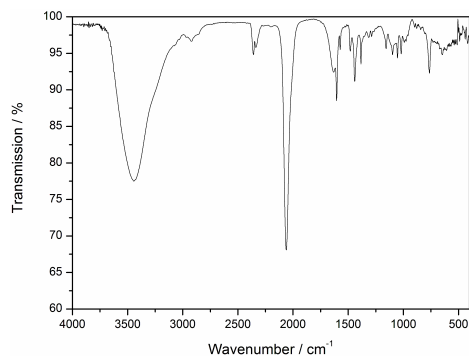
Figure F.1.: IR spectrum of **C7** [Fe$_2$(μ-**L6**)$_2$(NCS)$_4$].
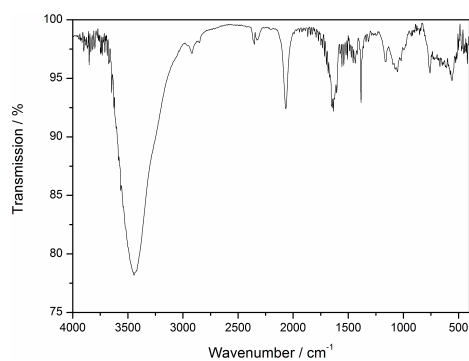
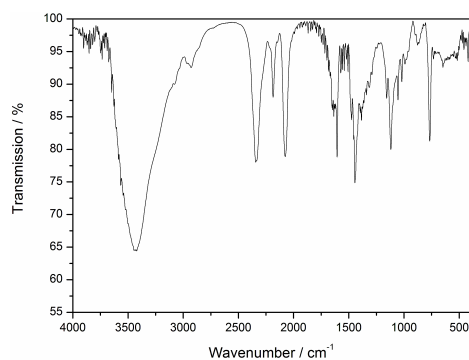Figure F.2.: IR spectrum of **C8** [Fe$_2$(μ-**L6**)$_2$(NCSe)$_4$].

Figure F.3.: IR spectrum of **C9** [Fe$_2$(μ-**L6**)$_2$(NCBH$_3$)$_4$].

G. Curriculum Vitae

Name:

Date of Birth:

Birthplace:

Education:

02/2013 - present	**Doctoral Studies in Chemistry**
	Doctoral Studies in the group of Prof. Dr. Eva Rentschler at the Institute of Inorganic and Analytical Chemistry at the Johannes Gutenberg University Mainz.
	Topic of the Dissertation:
	'Spin-Crossover Systems based on 1,3,4-Thiadiazoles'
10/2014 - 02/2015	**Research Visit**
	To the group of Prof. Sally Brooker at the University of Otago in Dunedin, New Zealand.
	With financial support of a DAAD ('German Academic Exchange Service') PhD scholarship.
04/2007 - 12/2012	**Chemistry Studies**
	At the Johannes Gutenberg University Mainz.
	Degree: Chemistry Diplom (1.6)

04/2012 - 12/2012   Diploma thesis in the group of Prof. Dr. Eva Rentschler

Topic of the Diploma thesis: 'Semichinoidic Bridging-ligands'

04/2006 - 12/2012   **Alternate Civilian Service**

'Geschwister de Haye'sche Stiftung Altenzentrum', Koblenz

08/1997 - 03/2006   **School**

Allgemeine Hochschulreife, Priv. Johannes-Gymnasium,

Lahnstein

Publications:

06/2015   'A Family of Dinuclear Iron(II) SCO Compounds Based on a
                     1,3,4-Thiadiazole Bridging Ligand' by Christian F. Herold, Luca
                     M. Carrella and Eva Rentschler.
                     (Including the Cover-Picture of Issue 22/2015)
                     European Journal of Inorganic Chemistry **2015**, 3632-3636

01/2016   'Solvent-depending SCO behavior of dinuclear iron(II)
                     complexes with a 1,3,4-thiadiazole bridging ligand'
                     by Christian F. Herold, Sergii I. Shylin and Eva Rentschler
                     Inorganic Chemistry (submitted)